A COMPARISON OF TWO FINITE ELEMENT MODELS FOR THE PREDICTION OF PERMAFROST TEMPERATURES

J. P. Gosink
T. E. Osterkamp
K. Kawasaki

Geophysical Institute
University of Alaska
Fairbanks, Alaska

FINAL REPORT

Alaska Department of Transportation and Public Facilities

Agreement 82IP361

1986

TABLE OF CONTENTS

LIST OF FIGURES

Research Recommendations

This report presents the results of tests involving two computer models for the ground thermal regime, the Goodrich model (Goodrich, 1978) and the Guymon/Hromadka model (Guymon and Hromadka, 1977). The Geodyn model (Resource Management Associates) was also assessed informally, primarily for comparison with various features of the Goodrich and the Guymon/Hromadka models.

A general conclusion of this investigation is that all three models contain limitations which require resolution before use as a general purpose engineering design tool. In this section, we list specific improvements, tests and comparisons for all three models which should help to clarify their relative merits and establish their usefulness as engineering design tools.

1) Long term testing of Geodyn - Long term (20 year) comparisons of calculated and analytic temperatures are presented in this report for both the Goodrich and the Guymon/Hromadka models. These two models use direct solution techniques which preclude the introduction of convergence errors. Geodyn uses a Newton-Raphson iterative technique which is subject to convergence errors over long terms. It is necessary to assess the long-term growth of convergence errors in the Geodyn model.

2) The Guymon/Hromadka model presently lacks a surface heat balance simulation for determining boundary conditions. This modification is necessary before the Guymon/Hromadka model could be used for general engineering design purposes. Note that there are several surface heat balance simulations through a snow cover, already coded and in use, which could be adapted to the Guymon/Hromadka model. These include the surface heat balance simulations in the Goodrich model, in the Geodyn model, and in DYRSMICE - a reservoir model developed by us (Gosink, Osterkamp and Hoffman, 1983).

3) Both the Guymon/Hromadka model and the Geodyn model are difficult to use in cases involving freeze and thaw of unsaturated soils because of the need for user-specification of soil properties related to moisture transport and hydraulic conductivity. We recommend a comparison between the calculated solutions of these two models against field data for a complex case with freezing and thawing of unsaturated soil and for a case with a transverse gradient in overburden.

4) Our experience with currently available data sets shows that a complete data set including the thermal and hydrological regimes and measurements of all model parameters is urgently required to test numerical models of heat and mass transport.

5) Presently the Guymon/Hromadka model requires the solution of Richards equation for moisture transport for all cases of freezing and thawing; consequently this requires the specification of pressure boundary conditions and the five Gardner constants: A_k, A_θ, n_k, n_θ and E. For cases involving freezing or thawing in saturated soils, a simpler approach may be warranted. Therefore a useful modification to the Guymon/Hromadka model for saturated soils would be the capability to solve the heat transport equation only with empirical relations between soil moisture and temperature. However, the predictions should be carefully tested against field data. This modification clearly would simplify the Guymon/Hromadka model, making it easier to use, but whether it would be an improvement could only be ascertained by comparison with field data.

6) The application of these models or any other numerical methods for investigating heat and mass transfer in permafrost for engineering design progress requires specification of the thermal and hydrological

parameters of the permafrost. It is presently possible to predict some thermal parameters (e.g., thermal conductivity) to within ± 50% or so given the necessary soil information. However, most of the permafrost in Interior Alaska exists within a few degrees of its melting temperature. At these temperatures, unfrozen water effects dominate the behavior of the thermal and hydrological parameters. Unfortunately, there are practically no measurements on these parameters within a degree or two of the melting temperature. It should also be noted that none of the three models under discussion includes a full unfrozen water content formulation. Specifically, the models do not contain the provision for a general unfrozen water vs. temperature function prescribed by the user for the particular soil being studied. We have developed a modification of the Guymon model which includes this provision; however, there are no data available with which to test this formulation. We recommend that a research program be initiated to measure the thermal and hydrological parameters of natural permafrost samples at temperatures very close to the melting point and, in particular, to determine the effects of unfrozen water on these properties. The modified program which we have developed could then be tested against these data.

7) No available thermal model, including the three discussed in this report, has the capability to predict the thermal regime of soils with substantial dissolved salts during freezing and thawing. Dissolved salts in relatively high concentrations (about 3 ppt) have been detected in the soils of the Fairbanks area in recent studies (Osterkamp, unpublished data). These concentrations would be expected to increase substantially with the increased use of salt for melting ice on highways and airport runways. Salt concentrations are of course still higher

near coastal locations. Therefore, a reliable thermal model for Alaskan applications should be developed containing an accurate simulation of the effects of salt transport including salt segregation, salt redistribution and freezing point depression.

FINAL REPORT

Thermal Analysis of Roadways and Airstrips

Introduction

The thermal regime of freezing soils is of concern to scientists and engineers interested in a wide range of problems. For highway and airport planning and construction in northern regions, there is a need to be able to predict the soil temperatures, freeze front positions, ice segregation and frost heave over long periods of time. For these projects, the surface boundary conditions will be altered by construction, for example, or by removal of the vegetative mat and by changes in surface elevation, slope and exposure. The soils, fill and various embankment and construction materials used for these projects will have a wide range of thermal and hydraulic properties. In addition, the effects of construction will be non-uniform, implying that the required analysis must be at least two-dimensional, and in some cases, three-dimensional. All these changes to the local terrain will irrevocably alter the ground thermal and hydraulic regimes, thereby affecting the long-term stability of the soil.

In permafrost areas, the analysis of soil thermal and hydraulic regimes is complicated by phase change effects and by moisture migration. During freezing, mobile soil moisture is drawn toward the freezing front, increasing the available latent heat; therefore, it is critical particularly in unsaturated soils, that moisture transport and soil water phase change be

correctly simulated. The moisture transport is affected by soil moisture tension and hydraulic conductivity, as well as by soil thermal regime, implying that moisture transport and soil temperatures are strongly coupled. The analysis of ground thermal regime is therefore extremely complex, involving coupled heat and moisture transport, changing surface boundary conditions, and soil thermal and hydraulic properties which vary both spatially and temporally with freezing. No analytic solutions exist for the coupled problem of moisture and heat transport in a freezing soil. The only feasible method of analysis for these types of problems involves the use of state-of-the-art computer modeling.

This report presents the results of tests involving two computer models for the ground thermal regime, the Goodrich model (Goodrich, 1978) and the Guymon/Hromadka model (Guymon and Hromadka, 1977). These computer models were identified in a preliminary report (Kawasaki, Osterkamp and Gosink, 1982) as being the most accessible and generally the most sophisticated of the models examined. Capabilities and limitations of the models emphasizing particularly useful features and their application to long-term permafrost problems are discussed. Where feasible they have been tested against analytic models. Furthermore, in Appendix A, detailed information is listed for the Guymon/Hromadka model including input data file directions, previously unavailable, and subjective comments by the report authors. Finally, the importance of specific problems, such as moisture migration, long time scales, and overburden effects, to reliable calculation of ground thermal regime is discussed.

General Discussion of the Models

Both the Goodrich and the Guymon/Hromadka models are finite element simulations of the heat transport equation with phase change. It is widely

accepted that finite element models are better suited to geophysical simulations involving complex geometries or boundaries than are finite difference models. Finite element models also have other advantages including greater versatility in the order of the approximation (linear, parabolic, etc.), a banded matrix form with the availablity of well-established direct solution techniques, procedures and a structure particularly well-suited both for surface flux boundary conditions and phase front movement. Both the Guymon/Hromadka and the Goodrich models use direct rather than iterative solution techniques to solve the governing matrix equations. This implies that both models should be free of convergence type errors, although they may be subject to round-off errors.

It is important to distinguish between the numerical model and the mathematical model. We have determined that both the Goodrich and the Guymon/Hromadka numerical models appear to be stable, convergent, correctly formulated and generally efficient. The finite element solution techniques employed, including setting up of the "stiffness" and "mass" matrices, as well as the implementation of the boundary conditions, are error-free as far as can be ascertained. The important questions, then, concern the mathematical models. Do the mathematical models correctly formulate the critical physical processes involved? Are the equations used to specify these physical processes realistic and consistent? What processes are not modeled, and how serious to the thermal predictions is the exclusion of these processes? Finally, do the models correctly simulate the physical mechanisms of heat transport in permafrost terrain over the long time scales required for roadway development in Alaska?

In the following sections, we will attempt to assess both the numerical and the mathematical models. The approach used to assess the numerical

models is direct, involving test cases, long-term calculations, comparisons with analytic solutions, and in some instances, step-by-step evaluation of computer codes, and comparison with "standard" or existing finite element matrix generation and solver routines (e.g., Smith, 1982 and Pinder and Gray, 1977). The evaluation of the mathematical models involves test cases, and in addition, discussion of the physical processes particularly relevant to permafrost.

The Simulation of Moisture Transport

Any unsaturated flow model must correctly simulate the moisture transport. Free soil moisture is always drawn toward the freezing front; this effect creates a similarity between drying and freezing of soils and implies that accurate simulation of phase change and temperature regime in soils depends strongly upon accurate prediction of moisture migration. There are at least two major approaches for simulating coupled moisture and heat transport in soils. The first, which might be called an algebraic method, uses empirical relations defining soil moisture and/or moisture diffusivity in terms of temperature, resulting in the reduction of two coupled partial differential equations for temperature and moisture or pore pressure into a single partial differential equation. This method implicitly assumes that rates and gradients and particularly boundary conditions of moisture and temperature are similar or at least of comparable order of magnitude (Hromadka, Guymon and Berg, 1981). Since soil-water diffusivity is a sensitive function of moisture content, varying over 3 orders of magnitude (see e.g., Jame, 1978), it may be expected that for a given moisture flux condition, the associated moisture gradient can also vary sharply. Thermal diffusivity of soils, on the other hand, varies less sharply; hence variations in temperature gradients are not as marked as those in moisture gradients.

The second method also employs empirical relations for various soil parameters. However, the two partial differential equations governing temperature and moisture or pore pressure are solved separately, thus releasing some numerical restraints required by the first method. Furthermore, in the first method a zero boundary flux condition of one variable (say zero moisture flux) and a simultaneous non-zero boundary flux condition of another variable (say non-zero geothermal heat flux) cannot both be easily accommodated. This is particularly relevant to problems involving overburden. If a non-uniform distribution of pressure exists as a surface boundary condition, then lateral variations in pore pressure must exist which will change the dynamics of moisture migration. This effect can only be gauged by separate solution of the equations for temperature and pore pressure. Consequently, the second method is more versatile than the first, and particularly suitable for soils undergoing freezing. Finally, other methods also exist which do not even consider moisture migration or require the model-user to prescribe a constant moisture transport velocity. These simple methods do not adequately define the complex physical dynamics of freezing soils. An example to illustrate this deficiency will be given in a later section.

The Goodrich model is an example of the first method, containing several user-selected empirical formulations for soil properties. The Guymon/Hromadka model is an example of the second method containing partial differential equations for both heat transport and pressure potential, Darcy's law for moisture migration, and empirical relations (e.g., linking hydraulic conductivity with soil moisture and ice content). The Geodyn model of Resource Management Associates is an example of a third method, containing user-prescribed moisture transport velocities. These velocities are set to zero whenever ice is encountered.

Guymon/Hromadka Model

FROST2B, the version of the Guymon/Hromadka model used in these comparisons, is a two-dimensional finite element model of coupled heat and moisture transport in a freezing soil. This version incorporates an apparent heat capacity approximation with an "isothermal" phase change of soil water. The isothermal phase change method used in this model is empirical. Temperatures are forced to remain at the freezing point as long as unfrozen water is present in the soil. This is in contrast to data which indicate that a "freezing fringe" exists in which substantial fractions of unfrozen water can be found in soil at temperatures below the freezing point (Anderson and Morgenstern, 1973; Anderson and Tice, 1972). The model further sharpens the frozen-unfrozen front by using a numerical algorithm at the freeze front known as the "lumped-mass" method. This algorithm, which alters the matrix coefficients at nodes undergoing freezing, has the effect of slowing the rate of temperature change until all the unfrozen water changes phase. This method appears to provide an appropriate balance of heat flux across the freezing zone, but without point-by-point accuracy of temperature and unfrozen water content in the freezing fringe.

In the general freezing case, total water content is not conserved, allowing ice in excess of soil porosity to form; the excess ice results in frost heave. Mathematically, this is totally appropriate; there is no reason to assume conservation of soil moisture during freezing since moisture may be drawn from the water table at depth during this process. However, the availability of this moisture is limited by the magnitude of the hydraulic conductivity, the calculated pressure gradients, and the Gardner equations, i.e., the assumed relation between pore pressure and hydraulic con-

ductivity, and between pore pressure and unfrozen water content. The computation of the pressure gradient is accomplished by the solution of a form of Richard's equation. The first two test cases below examine the numerical scheme for the solution of both Richard's equation and the heat transport equation; the third test case examines the appropriateness of the Gardner equations.

Numerical Comparisons

Test cases of the Guymon/Hromadka model were run for a series of problems with existing closed form or analytic solutions. It is expected that any reliable model should be able to accurately predict simple transient diffusion of heat in a soil system with constant and well-defined properties and with scales representative of Alaskan conditions. These test cases are a necessary first step in the evaluation of any numerical model, permitting assessment of the long term stability and accuracy of the model. In particular, the calculated solution should match the exact solution for extended periods; therefore, a calculation period of twenty years was adopted. As a test of the accuracy of the model, one-dimensional boundary conditions were imposed on a two-dimensional grid. This procedure determines the existence of inaccuracies associated with grid position and size.

Test Case 1.

The same grid consisting of a long vertical strip 15 meters deep and 2 meters wide (see Figure 1) was used for both test cases 1 and 2. Grid points were concentrated in the near surface area to better resolve the temperature gradients which were expected to be steeper in this zone. Variable grid spacing is of course, a distinct advantage of the finite element method over the finite difference method. Note that three grid points are defined at each vertical level (at each value of y). When uniform boundary conditions are

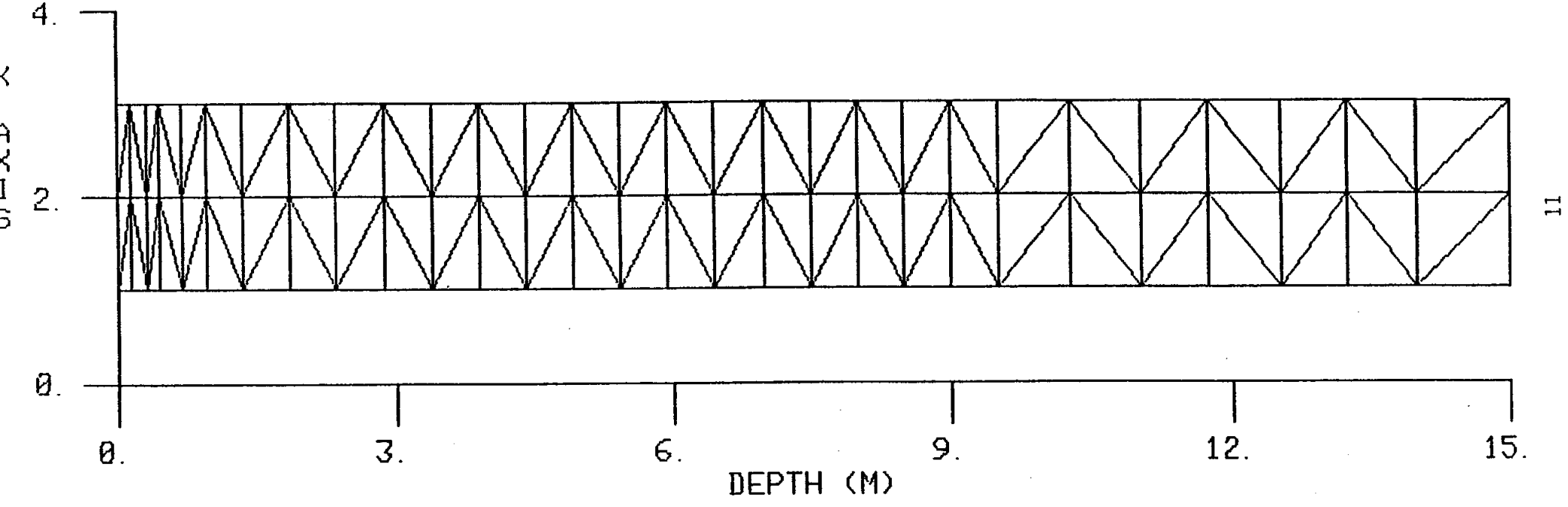

Figure 1. The finite element grid used for test cases 1, 2 and 7. An expanded version of this grid was used for tests cases 3, 4 and 5.

prescribed at y = 0.0 and y = 15.0 m, and zero horizontal flux or "natural boundary conditions" ($\partial T/\partial x = 0.0$ for x = 1.0 and 3.0 m) are prescribed at the lateral boundaries, then the calculated temperatures and freeze-front position should be independent of horizontal position, x. The maintenance of one-dimensionality throughout the calculations provides an evaluation of the accuracy of the numerical scheme.

Initial and boundary conditions for test case 1 are:

$$T\ (x,y,0) = 0.0\ C$$

$$T\ (x,0,t>0) = 1.0\ C$$

$$\partial T/\partial y\ (x,15.0,t>0) = 0.0\ C\ m^{-1}$$

$$\partial T/\partial x\ (x = 1.0 \text{ and } x = 3.0,\ y,\ t>0) = 0.0\ C\ m^{-1}$$

The calculated numerical and analytic temperatures (see Osterkamp, 1983, for the analytical method) after one, five, ten and twenty years are depicted in Figures 2, 3, 4 and 5, respectively. The thermal diffusivity appropriate for silts (κ) is uniform throughout the depth and equal to $2.39 \times 10^{-7}\ m^2\ s^{-1}$, implying a time constant ($\tau = y^2/4\kappa$) equal to 7.46 years. These calculations demonstrate that the Guymon model is exceedingly stable, and capable of maintaining excellent agreement with the exact solution for extended periods of time. Note that the calculated temperatures at each depth actually represent three values (for x = 1, 2, 3; see Figure 1). These three values are sufficiently close to appear to be plotted as one point at every depth and throughout the calculation period, indicating accuracy of the numerical scheme.

This case tests the modeling of both the governing equations, i.e., the convective-diffusive equation for heat transport (the energy equation) and the convective-diffusive equation for soil potential (the moisture transport equation or Richards' equation), since the assembly of coefficients

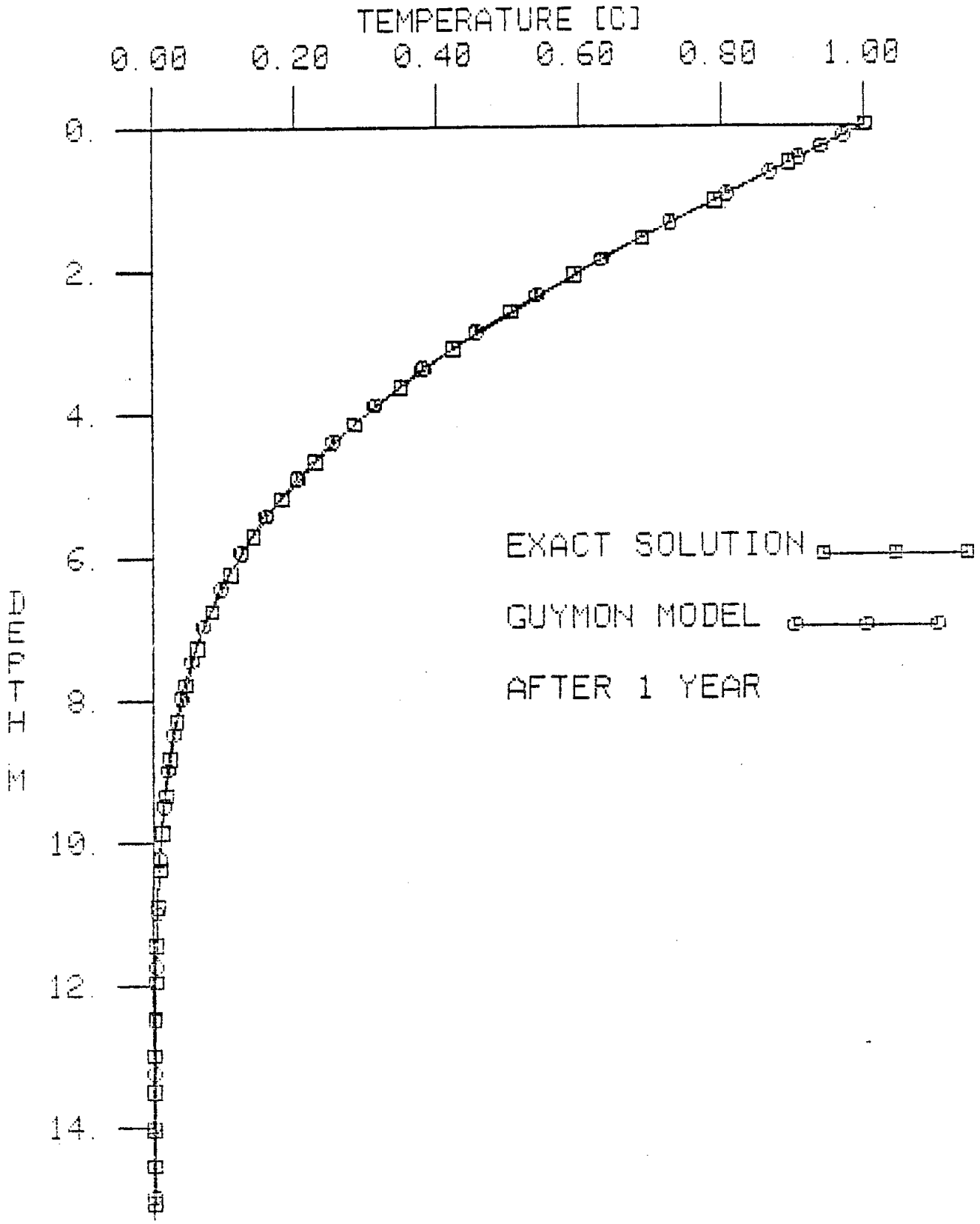

Figure 2. Comparison of exact and calculated (Guymon model) temperatures for test case 1 after one year.

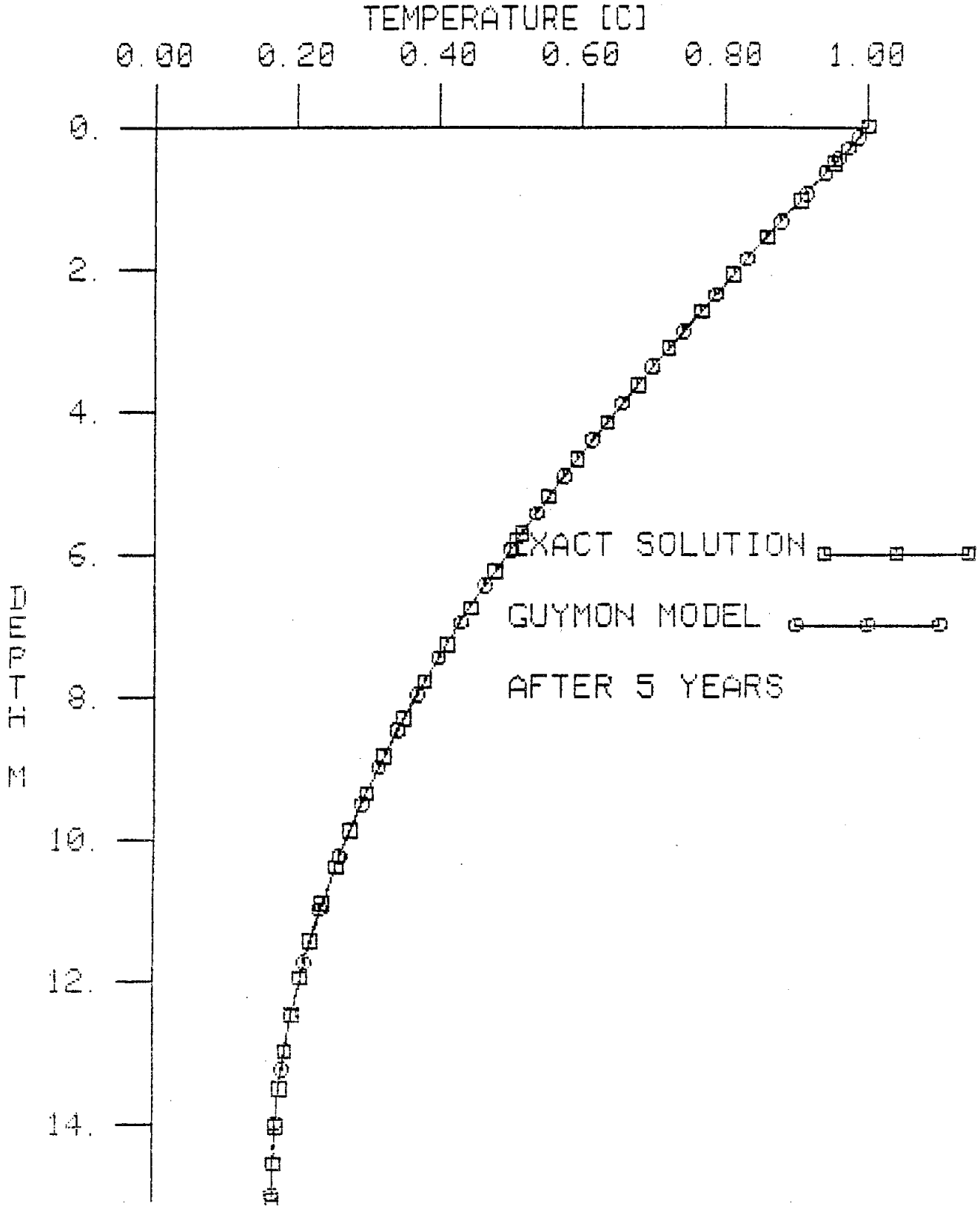

Figure 3. Comparison of exact and calculated (Guymon moel) temperatures for test case 1 after five years.

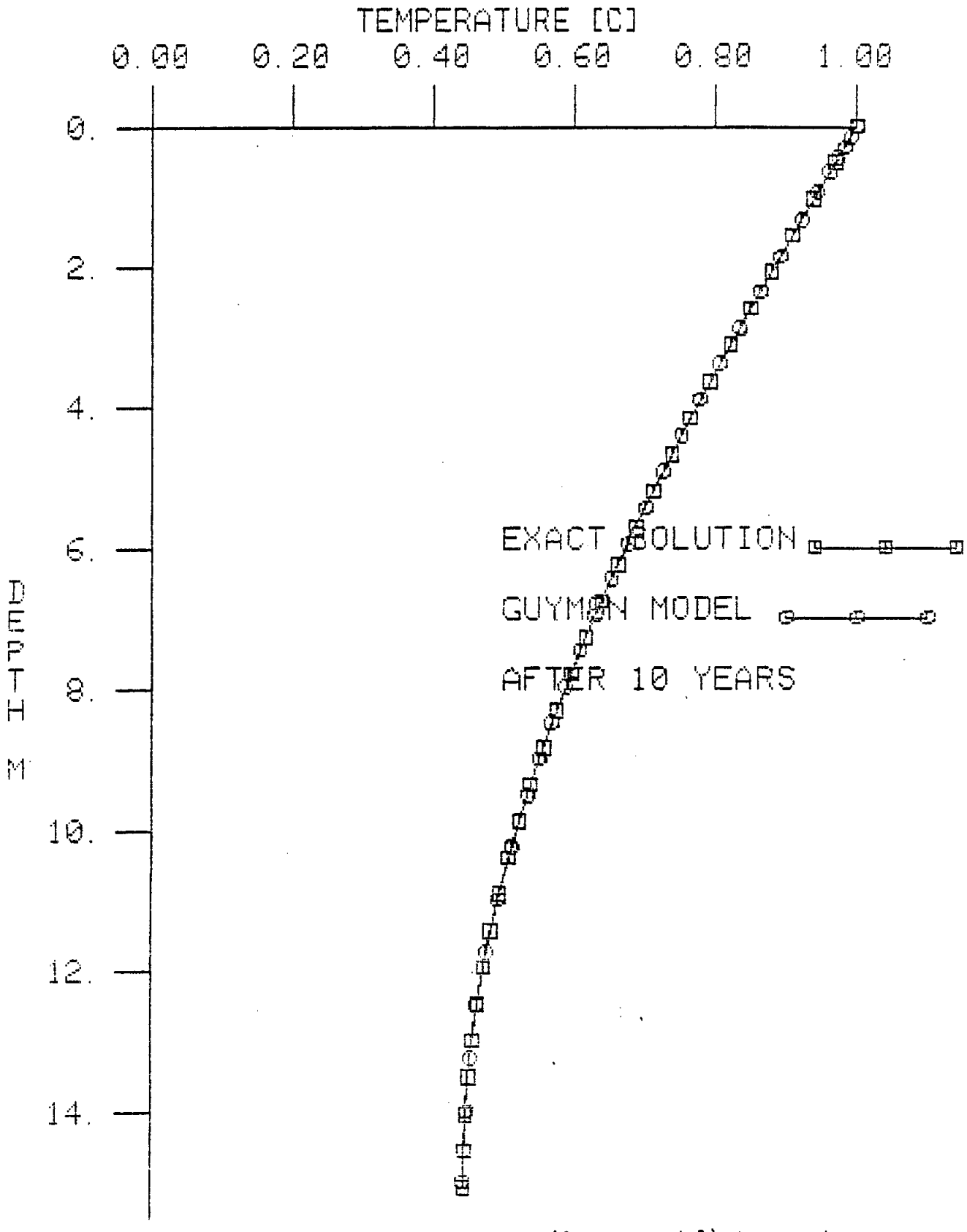

Figure 4. Comparison of exact and calculated (Guymon model) temperatures for test case 1 after ten years.

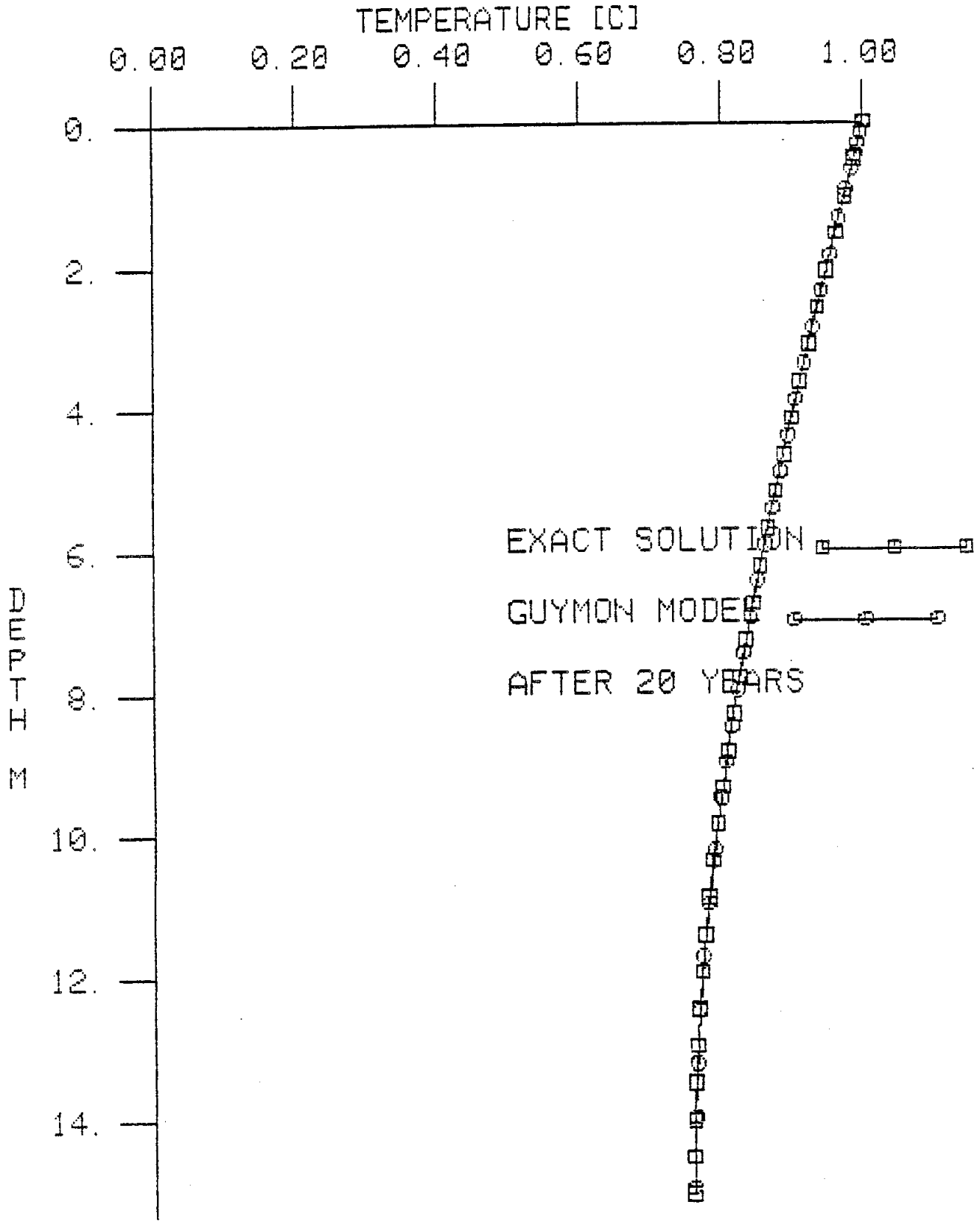

Figure 5. Comparison of exact and calculated (Guymon model) temperatures for test case 1 after twenty years.

for the matrix system is identical for the two equations. Therefore, it may be expected that, for these simple boundary conditions, an imposed and constant surface temperature and/or soil potential with no phase change and constant soil properties, the Guymon and Hromadka numerical models for both soil temperature and moisture transport are accurate and stable near the time and space scales important for highway and airport studies.

Test Case 2

The grid again was the 15 meter deep and 2 meter wide strip depicted in Figure 1. This case involves transient surface boundary conditions and tests the response of the numerical model to variable boundary conditions. In particular, a sinusoidally varying temperature is imposed at the surface simulating seasonal change in air temperature; these conditions, with a zero flux condition at depth, imply an analytic solution known as the trumpet or whiplash curve for soil temperatures.

Initial and boundary conditions for test case 2 are:

$T(x,y,0) = .5\ (1 + e^{-\gamma y} \cos \gamma y)$ C

$T(x,0,t>0) = .5\ (1 + \cos \omega t)$ C

$T(x,15.0,\ t>0) = .5\ (1 + e^{-15\gamma} \cos (\omega t - 15\gamma))$ C

$\partial T/\partial x\ (x=1.0 \text{ and } x=3.0,\ y,\ t>0) = 0.0$

where $\gamma = \sqrt{\omega\kappa}/2$, $\kappa = 7.65 \times 10^{-2}$ m^2 day^{-1}, appropriate for coarse gravels, and $\omega = 2\pi/366$ day^{-1}. The calculated and analytic temperatures after 1.0, 5.25, 10.5 and 19.75 years are depicted in Figures 6, 7, 8 and 9, respectively. The particular timing was chosen to eliminate duplication in the figures, since the analytic solution is periodic.

As in test case 1, the numerical solution reliably tracks the analytic solution throughout the long calculation period. There is very little variation in the three calculated temperatures at the same depth, indicating

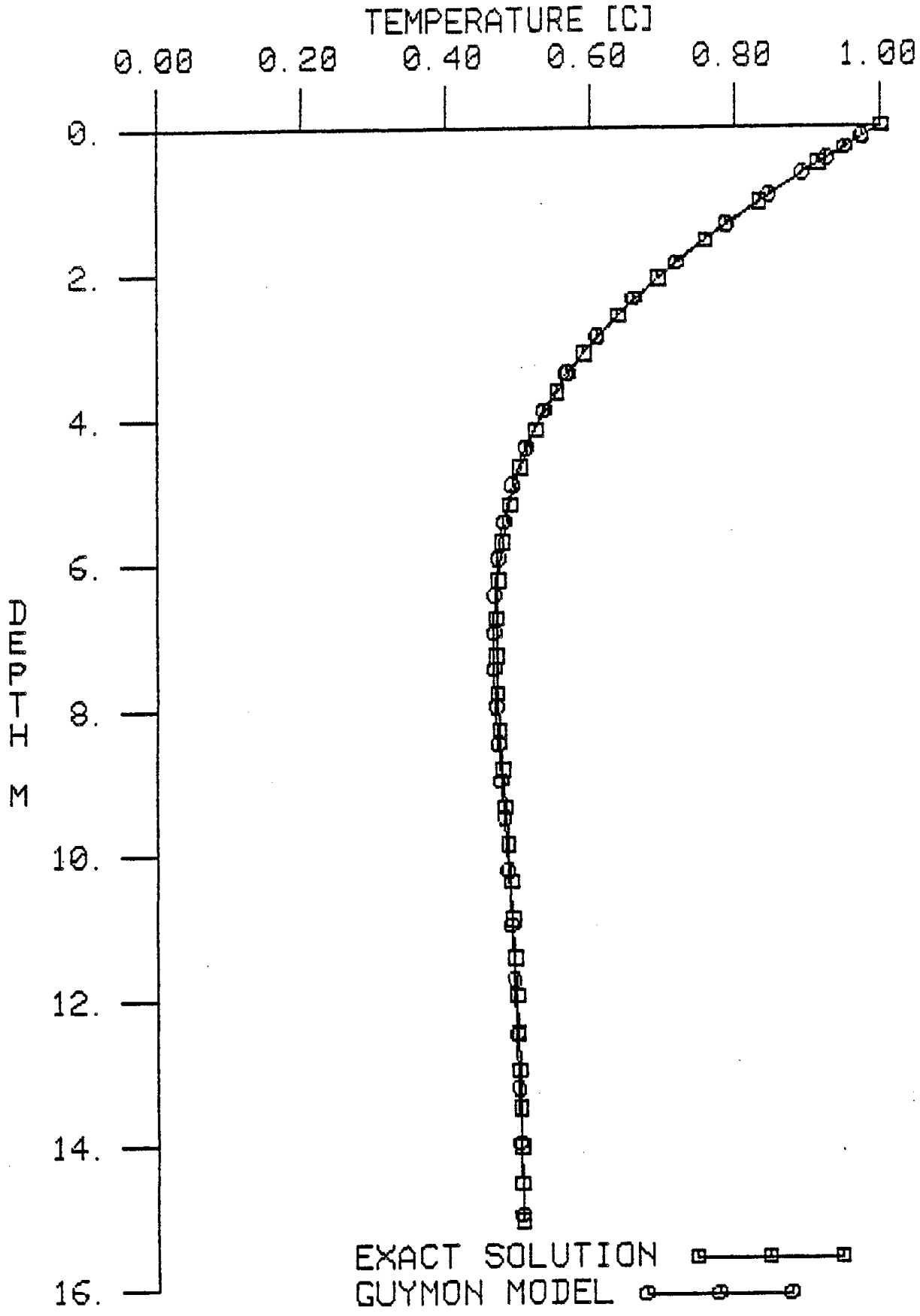

Figure 6. Comparison of exact and calculated (Guymon model) temperatures for test case 2 after one year.

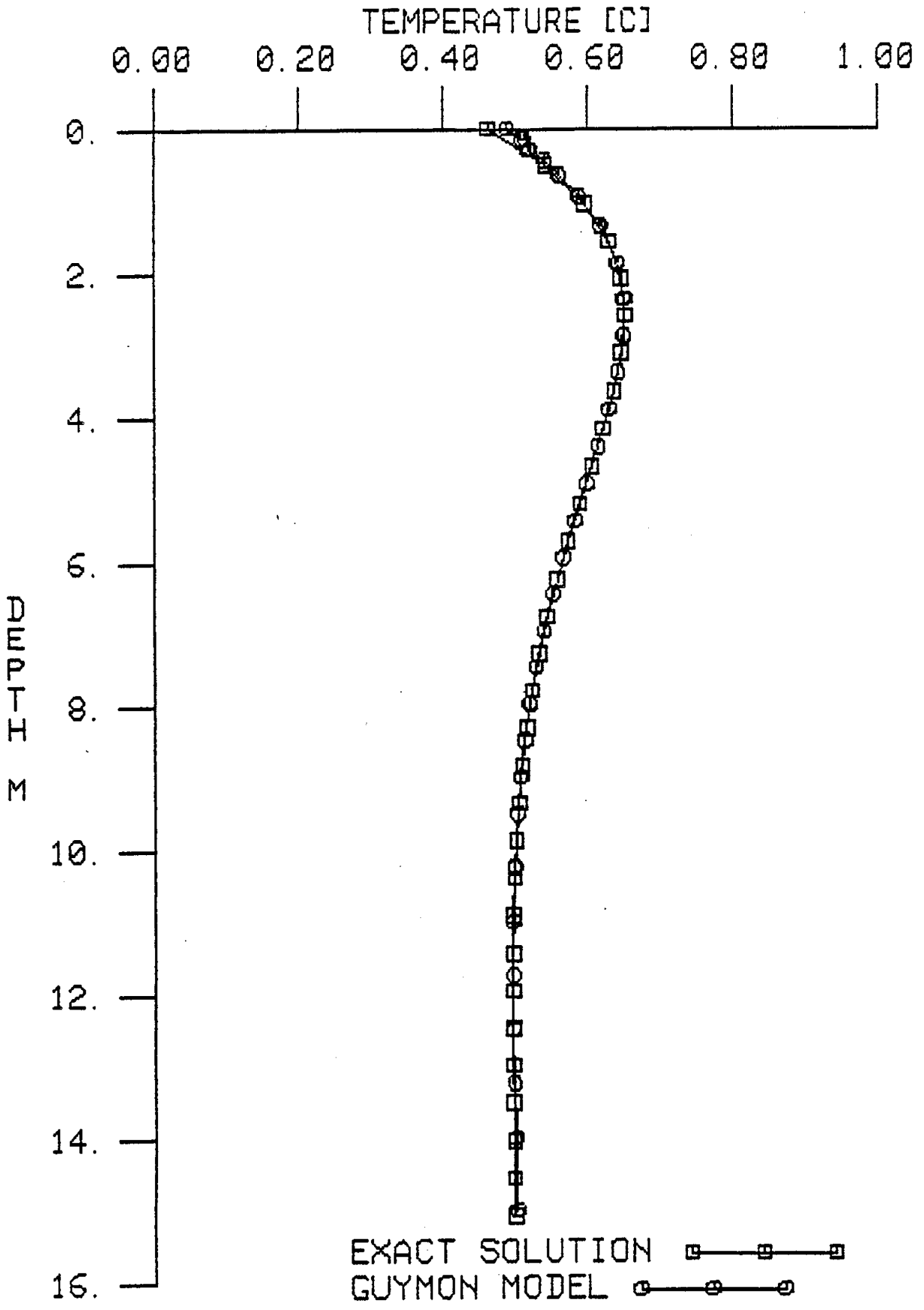

Figure 7. Comparison of exact and calculated (Guymon model) temperatures for test case 2 after 5.25 years.

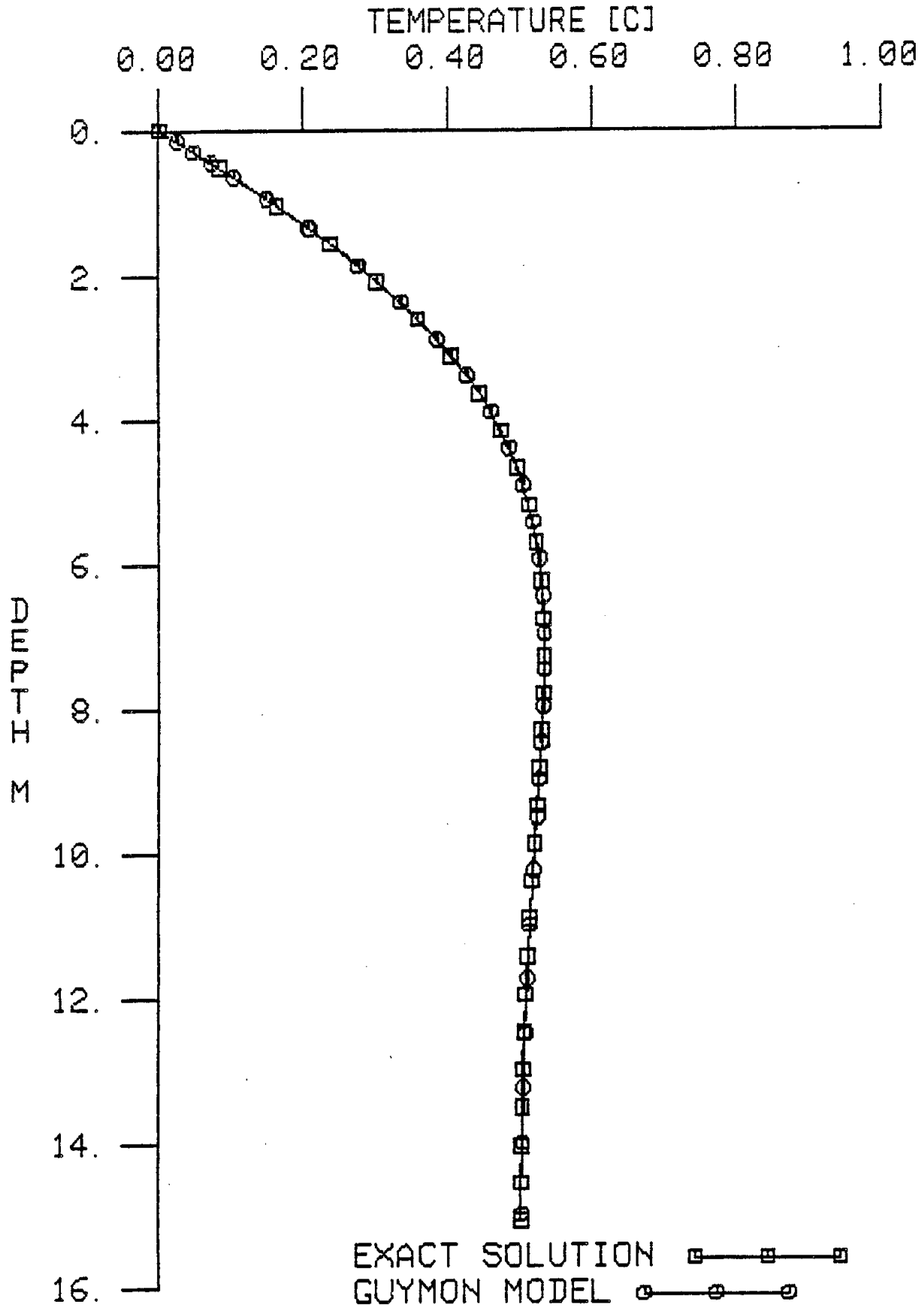

Figure 8. Comparison of exact and calculated (Guymon model) temperatures for test case 2 after 10.5 years.

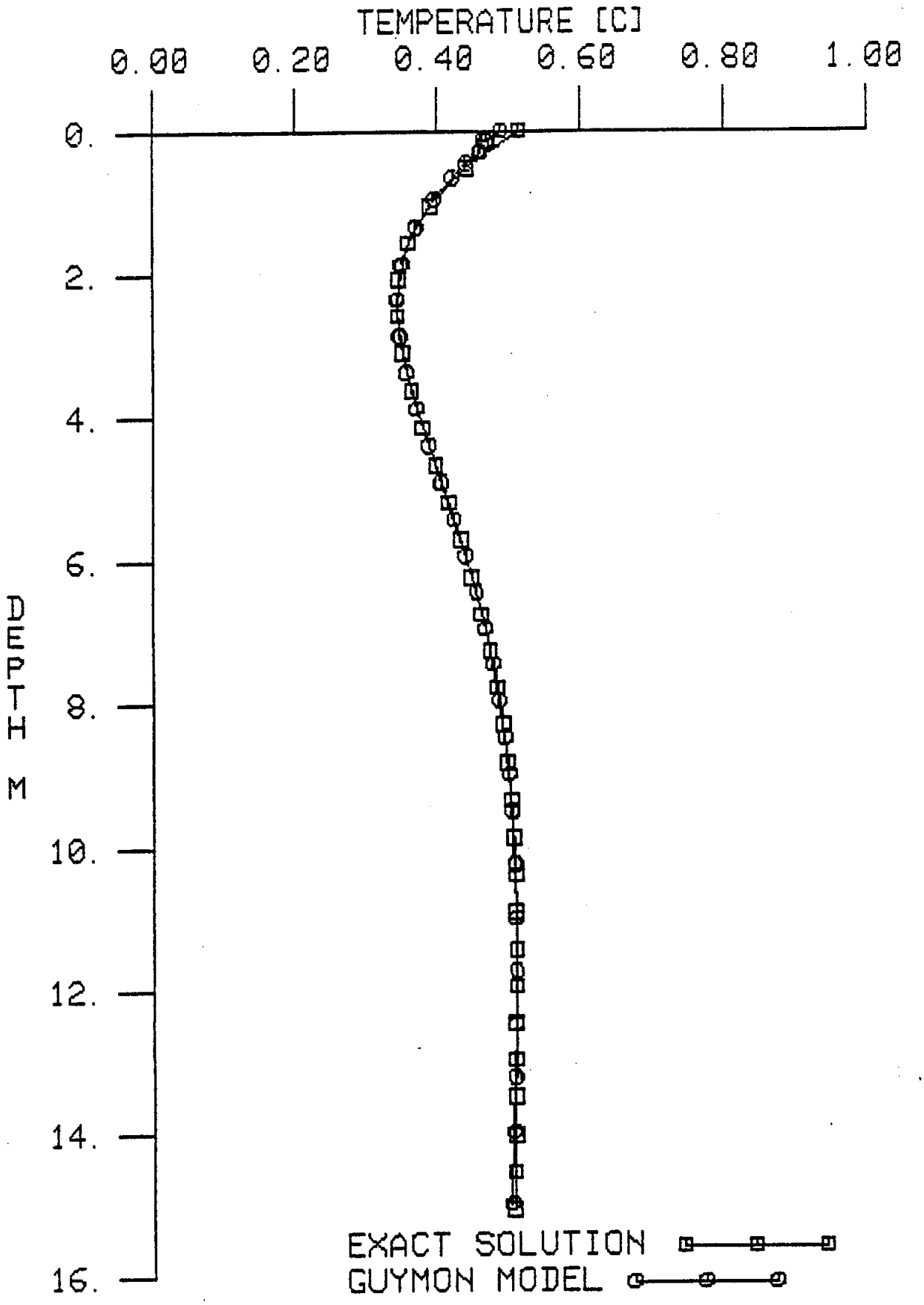

Figure 9. Comparison of exact and calculated (Guymon model) temperatures for test case 2 after 19.75 years.

good accuracy. Some discrepancy between the calculated and the analytic solutions may be noted near the surface at t = 5.25 and 19.75 years. This is due to a deviation or lag between the real time for the analytic solution and the calculation time for the model solution. For this test case, a time step of 6 days was chosen, so that the calculated temperatures define the average temperature within ± 3 days. Note that the analytic surface temperature is changing most rapidly at a time one-fourth and three-fourths through the annual cycle; therefore, the maximum deviation between calculated and analytic surface temperatures also occurs then, as suggested by Figures 7 and 9.

Test Case 3

This test case includes the effects of freezing. Since the freeze front position in sandy gravels after 20 years would be near 15 m, the grid spacing was increased in the vertical direction by a factor of about 4. Both the temperature and the pore pressure equations are solved whenever moisture is present, and moisture is drawn toward the freeze front by tension, simulating the physics of soil moisture migration during freezing. The amount of water drawn toward the freeze front critically influences its position because of the latent heat carried with this moisture flux. Guymon et al., (1980) explains the semi-empirical method used to define hydraulic conductivity and unfrozen water in terms of soil potential; the details of this explanation can be found in the latter and other references (Gardner, 1958; Guymon and Luthin, 1974; Taylor and Luthin, 1978).

The semi-empirical formulations of hydraulic conductivity and unfrozen water content have the effect of making the model more difficult to use, but at the same time, of ensuring versatility and adaptability in the model as more data and understanding of these complex phenomena become available. Guymon

(personal communication) has supplied a listing of four of the empirical coefficients for these formulations; this listing is attached as Appendix B. A fifth parameter, called the hydraulic conductivity exponent adjustment factor and referred to hereafter as E, is not listed in the empirical data. In effect E is a free parameter which is to be determined by model calibration either with known solutions or with laboratory tests of the type of soil under investigation. The calculated solutions are sensitive to the value of E and this sensitivity will be discussed subsequently.

Initial boundary conditions for test case 3 are:

$T(x,y,0) = 1.0$ C

$T(x,0,t>0) = -10.0$ C

$\partial T/\partial y\ (x,58.0,t>0) = 0.0$ C m^{-1}

$\partial T/\partial x\ (x=1.0$ and $x=3.0,\ y,\ t>0) = 0.0$ C m^{-1}

An exact solution does not exist for this problem (the Stefan solution is not applicable due to the zero flux boundary condition at y = 58 m). However, the Stefan solution is a reasonably good approximation to this test case, since it can be shown that for the soil parameters used in the problem, $\partial T/\partial y < .01$ C m^{-1} at y = 58 m and t < 20 years. For the Stefan problem applied to sandy gravels, appropriate soil diffusivities in thawed and frozen ground are:

$\kappa_t = 8.88 \times 10^{-7}\ m^2\ sec^{-1}$

$\kappa_f = 2.19 \times 10^{-6}\ m^2\ sec^{-1}$

This implies a freezing rate parameter, $\lambda \approx 0.27$ (see Carslaw and Jaeger, page 285).

The parameters used in the semi-empirical formulation of unfrozen water content and hydraulic conductivity (e.g., see eq. 4 and 5

in Guymon and Luthin, 1974) appropriate for sandy gravels (from Appendix B) are:

$A_\theta = 1.320$

$n_\theta = 0.166$

$A_k = 2.681$

$n_k = 1.026$

Note that n_θ and n_k are dimensionless exponents of pore pressure in the Gardner (1958) expressions for unfrozen water content and hydraulic conductivity, respectively. In earlier studies, it was assumed that both of these exponents were equal to three in any soil. More recent investigations (Guymon, personal communication) indicate that these exponents vary considerably. As previously stated, measured values of these exponents and the coefficients, A_θ and A_k, are given in Appendix B. The dimensions of the coefficients, A_θ and A_k, vary according to the value of the exponents such that

$$[A_\theta] = [cm^{-n_\theta}] \text{ and } [A_k] = [cm^{-n_k}]$$

If units other than cgs are to be used, the appropriate transformations for A_θ and A_k must be prescribed. Other soil parameters used in the temperature calculations are:

saturated volumetric moisture content, $\theta_o = 0.336$

thermal conductivity of dry soil, $k_s = 64.8$ [cal cm^{-1} hr^{-1} C^{-1}]

volumetric heat capacity of dry soil, $c_s = 0.445$ [cal cm^{-3} C^{-1}]

residual water content value in soil, $r = 0.05$

saturated, unfrozen hydraulic conductivity, $K_H = 5.5$ [cm hr^{-1}]

hydraulic conductivity exponent adjustment factor, $E = 30.0$

The calculated and exact (Stefan) temperatures after 1, 5, 10 and 20 years are depicted in Figures 10, 11, 12 and 13, respectively. The agreement is quite good especially over the first ten years, when the maximum temperature deviation appears to be about 0.2 C. At twenty years the temperature deviation has increased to about 0.4 C near y = 58 m. Agreement between calculated and "exact" solutions is not expected at this depth since the boundary conditions for calculated and "exact" solutions are different. The deviation, in sense but not in quantity, is appropriate. This is because the Stefan solution, which does not specify $\partial T/\partial y = 0.0$, permits heat flux from depths below 58 m to enter the domain. This heat flux could be reduced to zero by choosing a larger grid (depth). The temperature gradient at depth for the Stefan solution may be easily calculated and has a range $0 < \partial T/\partial y \,|_{y = 58} < .009$ C m^{-1}. If we assume that the average heat flux entering from the bottom during twenty years is, $F = | k_t \, \partial T/\partial y | \approx (0.4$ cal m^{-1} sec^{-1} $C^{-1})$ $(.0045$ C $m^{-1})$ or $F = 1.8 \cdot 10^{-3}$ cal m^{-2} sec^{-1}, then this heat flux, integrated over time, can be compared to the "apparent" heat deficit of the lower layer, i.e., the temperature difference between the calculated and Stefan temperatures. F integrated over 20 years is $F \, \Delta t \cong 10^6$ cal m^{-2}. The apparent heat deficit of the lower layer is proportional to the triangular area in Figure 13 between the depths of 25 and 55 m and with maximum height of 0.4 C. With a volumetric specific heat, C, of about 0.63 cal cm^{-3} C^{-1}, the apparent heat deficit is

$$C \int T \, dy \approx (0.63 \cdot 10^6 \text{ cal } m^{-3} \, C^{-1})(.2C)(30 \text{ m})$$

or $$C \int T \, dy \approx 3.78 \cdot 10^6 \text{ cal } m^{-2}$$

Therefore, the calculated total discrepancy in heat is about $3.78 \cdot 10^6$ cal m^{-2} while the Stefan solution accounts for only about 10^6 cal m^{-2}. This

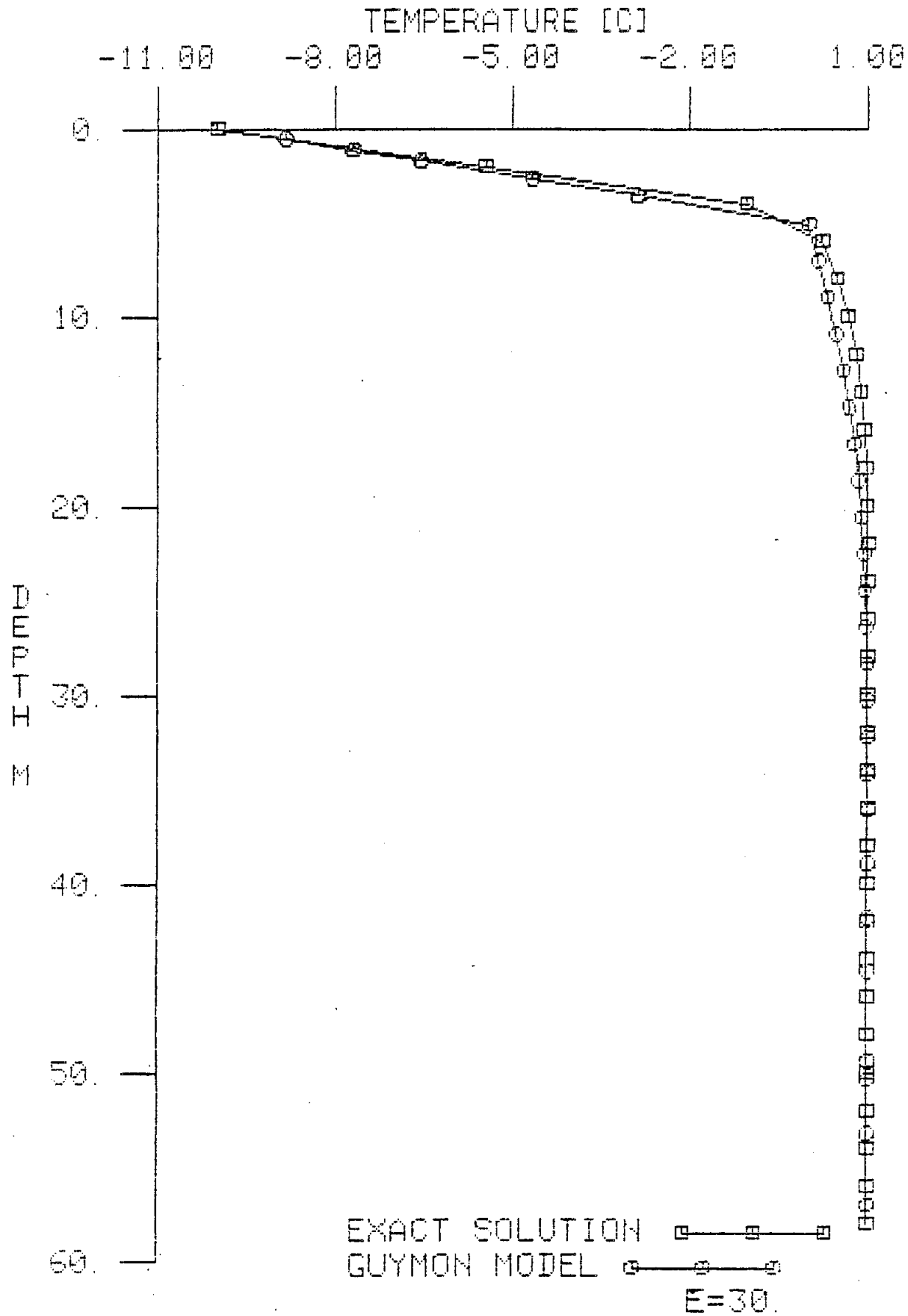

Figure 10. Comparison of exact and calculated (Guymon model) temperatures for test case 3 aftr one year.

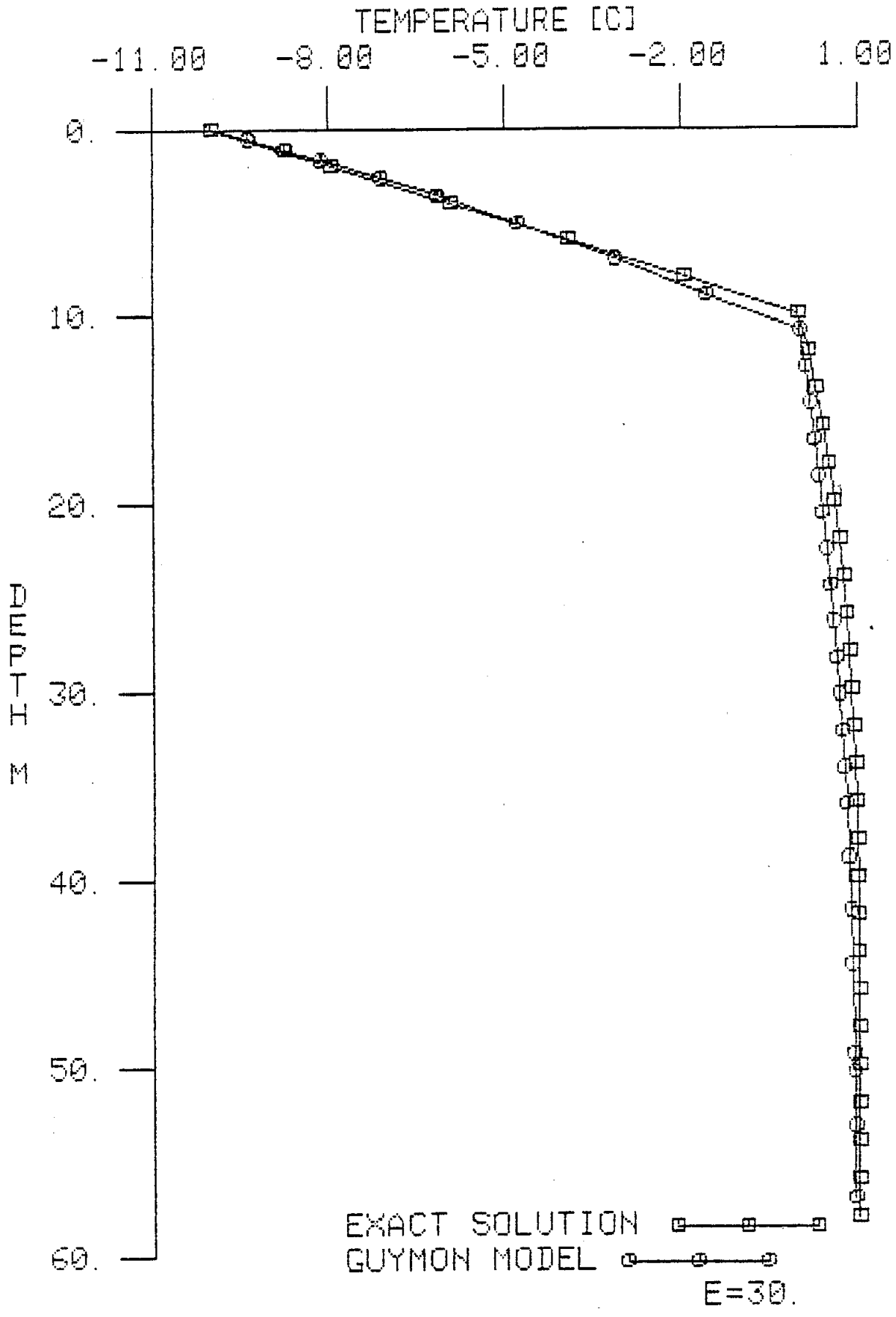

Figure 11. Comparison of exact and calculated (Guymon model) temperatures for test case 3 after five years.

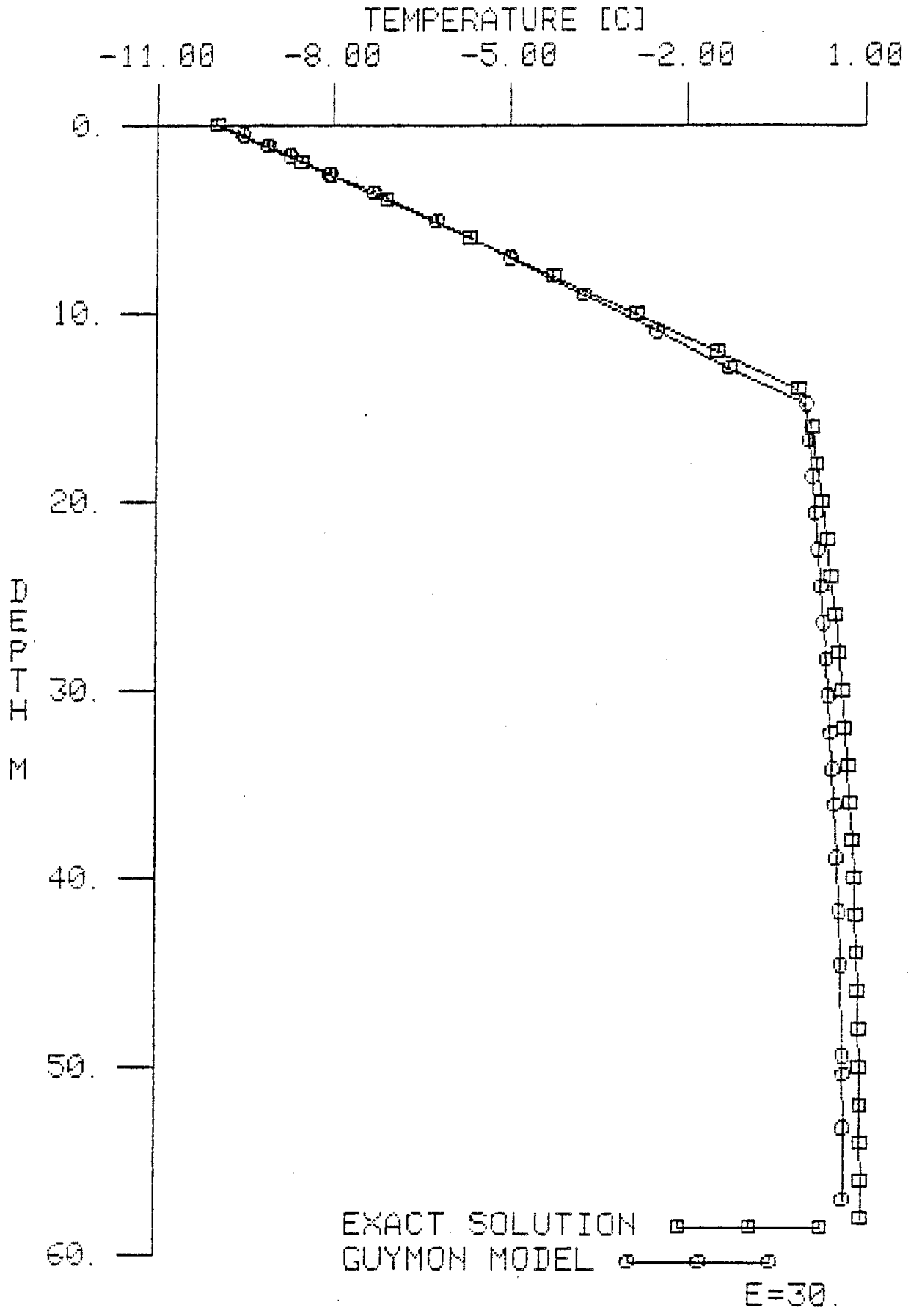

Figure 12. Comparison of exact and calculated (Guymon model) temperatures for test case 3 after ten years.

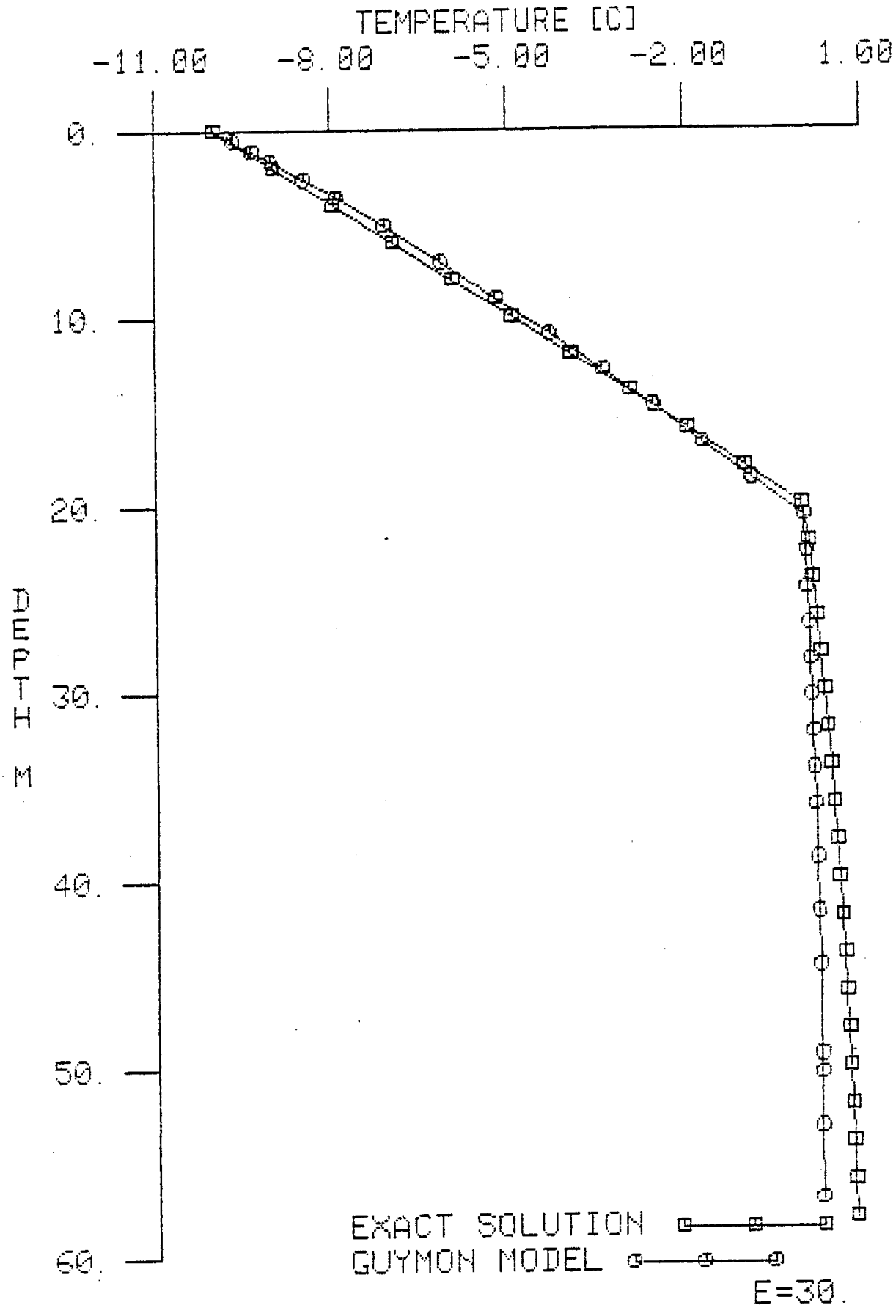

Figure 13. Comparison of exact and calculated (Guymon model) temperatures for test case 3 after twenty years.

implies that the discrepancy between the Stefan solution and the calculated temperatures at y = 58 m is only partially due to the difference in bottom boundary conditions, and partially due to the uncertainties in the selection of soil parameters. The Guymon/Hromadka model cannot be compared directly to the analytic solutions, since the soil parameters including volumetric heat content, thermal conductivity and hydraulic conductivity are computed internally in terms of unfrozen moisture content and ice content, with both moisture and ice content calculated from Gardner type expressions. It should be remembered, however, that the modeling of soil parameters in the Stefan approximation (two values of diffusivity, conductivity and specific heat - one each in the thawed and frozen layers) is extremely simplistic and unrealistic in Alaskan soils. What is demonstrated in this test case is that, given a set of empirically determined coefficients for sandy gravel, the Guymon model produces realistic temperatures and freeze front progression which compare well with a similar, but not identical, Stefan problem.

Variations in E

The determination of virtually all soil parameters in test case 3 including A_θ, n_θ, A_k, n_k and K_H follows directly from the experimental values which are summarized in Appendix B. The parameter E, however, is not tabulated in Appendix B. There is very little information regarding the determination of E. In Table 2 of one report (Guymon, et al., 1981), E was determined by model calibration for Fairbanks silt (E = 8) and West Lebanon gravel (E = 20). In Table 6 of another report (Guymon, et al., no date) E takes on values of 10, 15, 20 and 30 for "remolded" soils, two types of uniform field soils and nonuniform field soils.

E is the exponent in a hydraulic conductivity attenuation factor:

$$K_H = K(\Psi) \cdot 10^{-E\theta_i}$$

where K_H is the actual hydraulic conductivity, $K(\Psi)$ is the hydraulic conductivity in unsaturated, unfrozen soil (which is a function of pore pressure, Ψ), and θ_i is volumetric ice content. Details can be found in the reference by Guymon et al. (1980), with additional information in Taylor and Luthin (1978) and Jame (1978). Basically E becomes a strong attenuation factor for moisture migration whenever ice content is large. For example, if $E = 30$, and $\theta_i = 0.1$, then $10^{-E\theta_i} = 10^{-3}$, and if $\theta_i = 0.35$, then $10^{-E\theta i} = 10^{-11}$. The importance of E on ground temperature predictions is that attenuation of hydraulic conductivity implies attenuation of moisture transport and, consequently, reduction of the associated latent heat. Therefore, if E is large, it should be expected that the soil will freeze more readily as less moisture is transported to the freeze front. Conversely, if E is small, hydraulic conductivity remains large, more moisture can be transferred to the freeze front, and freeze front penetration is diminished.

In order to assess the quantitative effect of variations in E, several test cases were run using the same soil parameters as in test case 3 but with E varying. The calculated and Stefan solution temperatures after 5 years for E = 0, 20, and 100 are depicted in Figures 14, 15, and 16, respectively, while the case for E = 30 has been shown previously in Figure 11. Note that if E = 0 (Figure 14) the calculated freeze front is near 3 m, while the Stefan freeze front is approaching 9 m. Clearly too much latent heat in the form of moisture transport is directed to the upper layers inhibiting freezing. If E = 100 (Figure 16) the calculated freeze front is near 15 m indicating too little available latent heat is transported by moisture

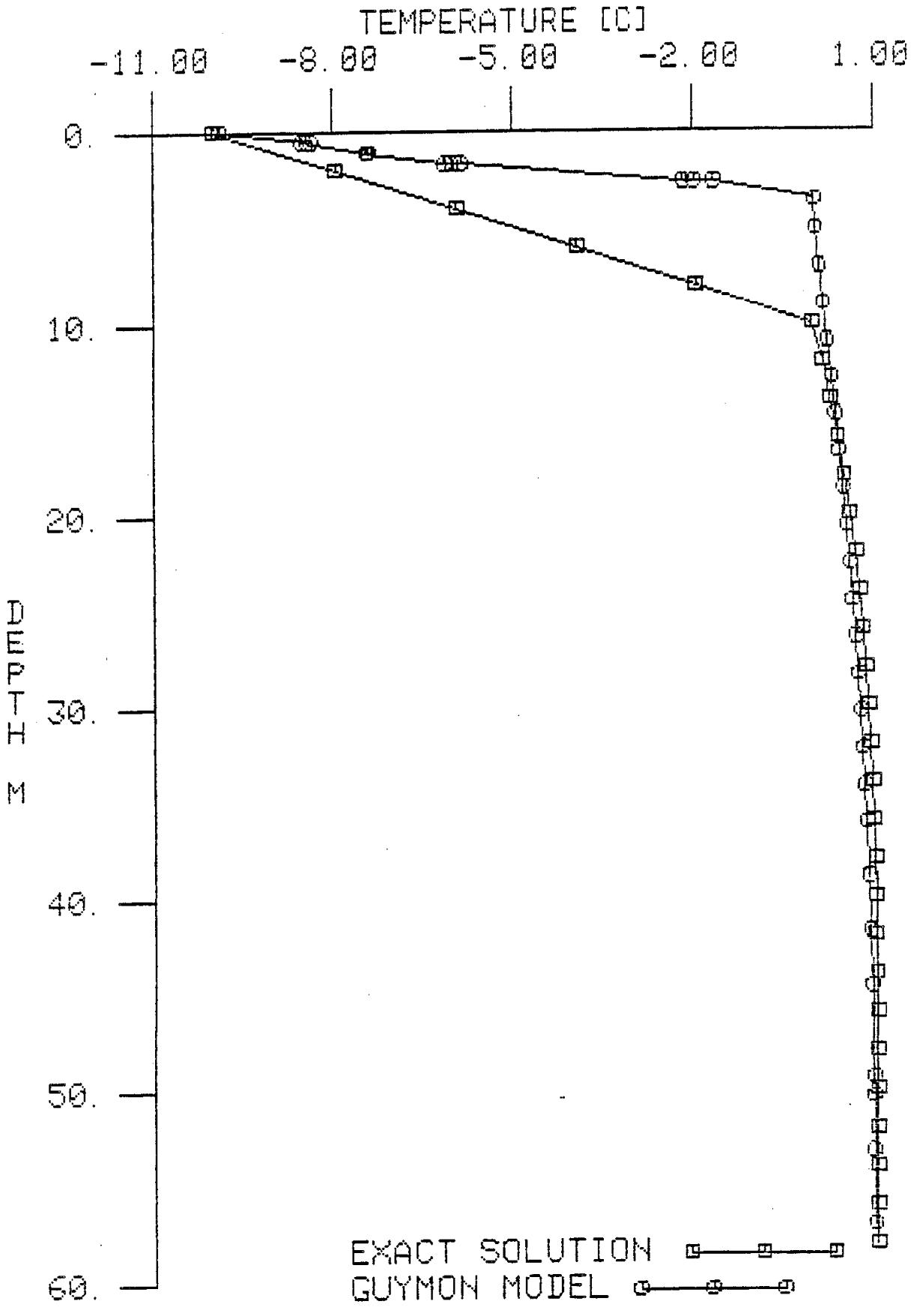

Figure 14. Comparison of exact and calculated (Guymon model) temperatures for test case 3 after five years. E = 0.0.

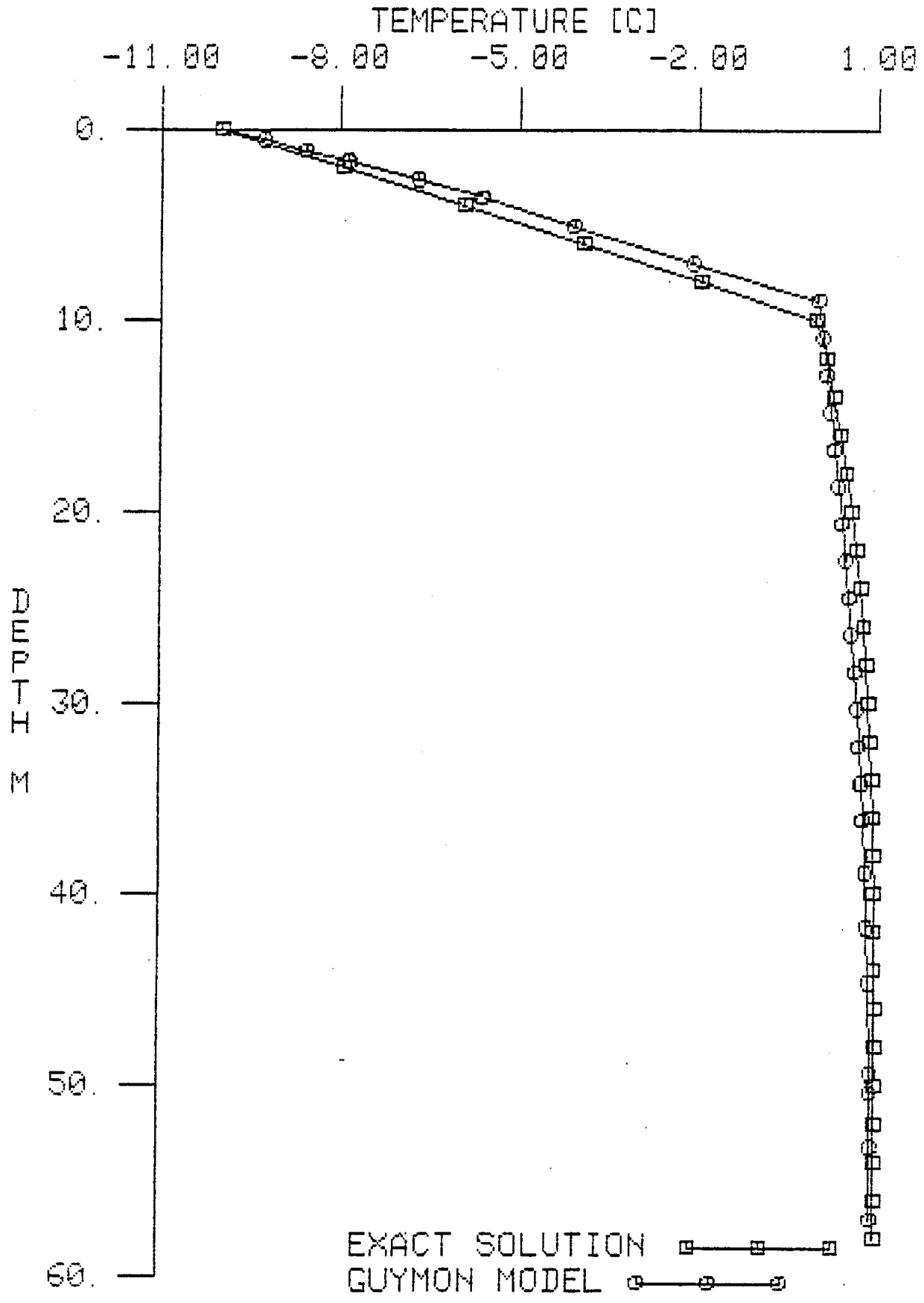

Figure 15. Comparison of exact and calculated (Guymon model) temperatures for test case 3 after five years. E = 20.0.

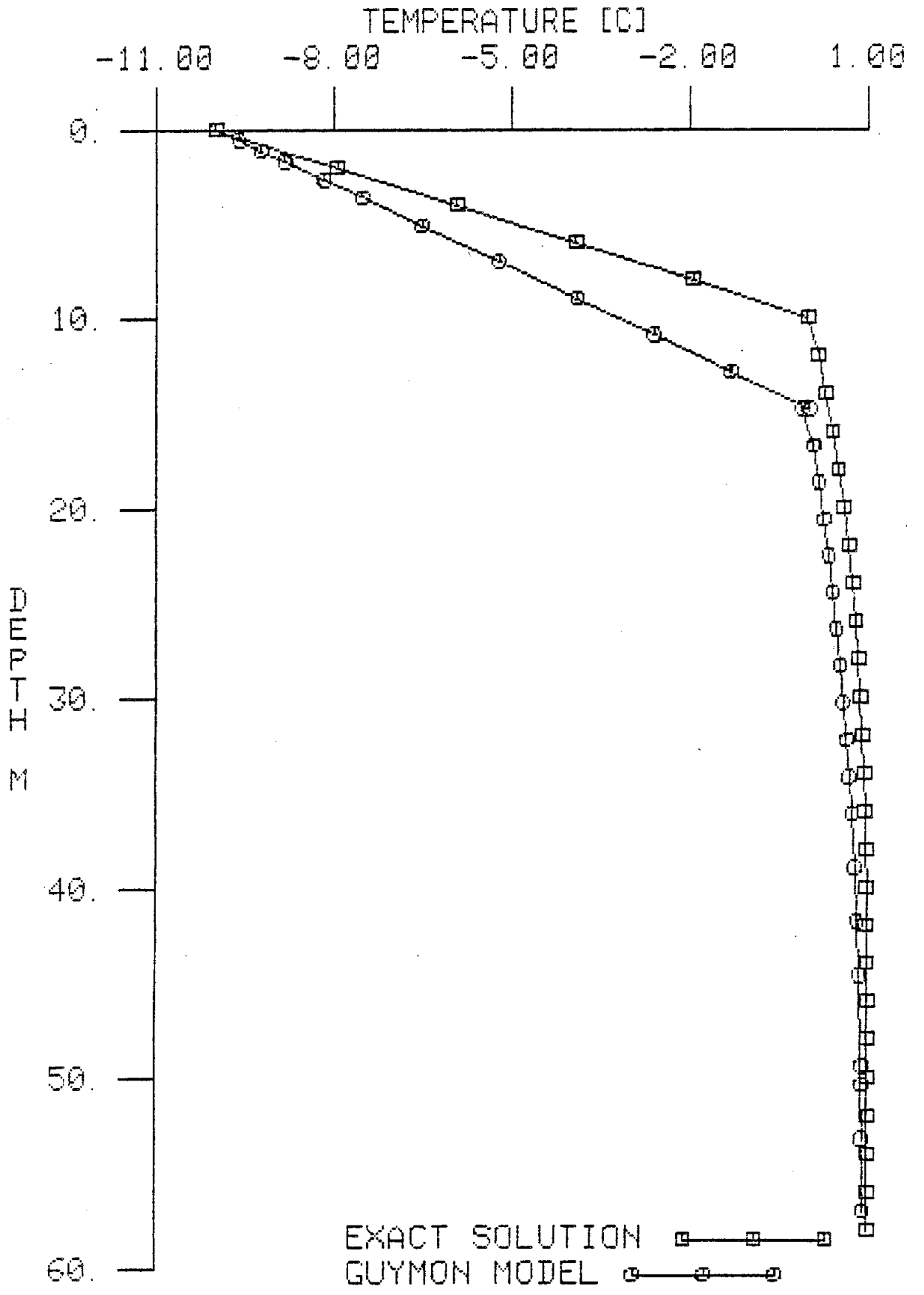

Figure 16. Comparison of exact and calculated (Guymon model) temperatures for test case 3 after five years. E = 100.0.

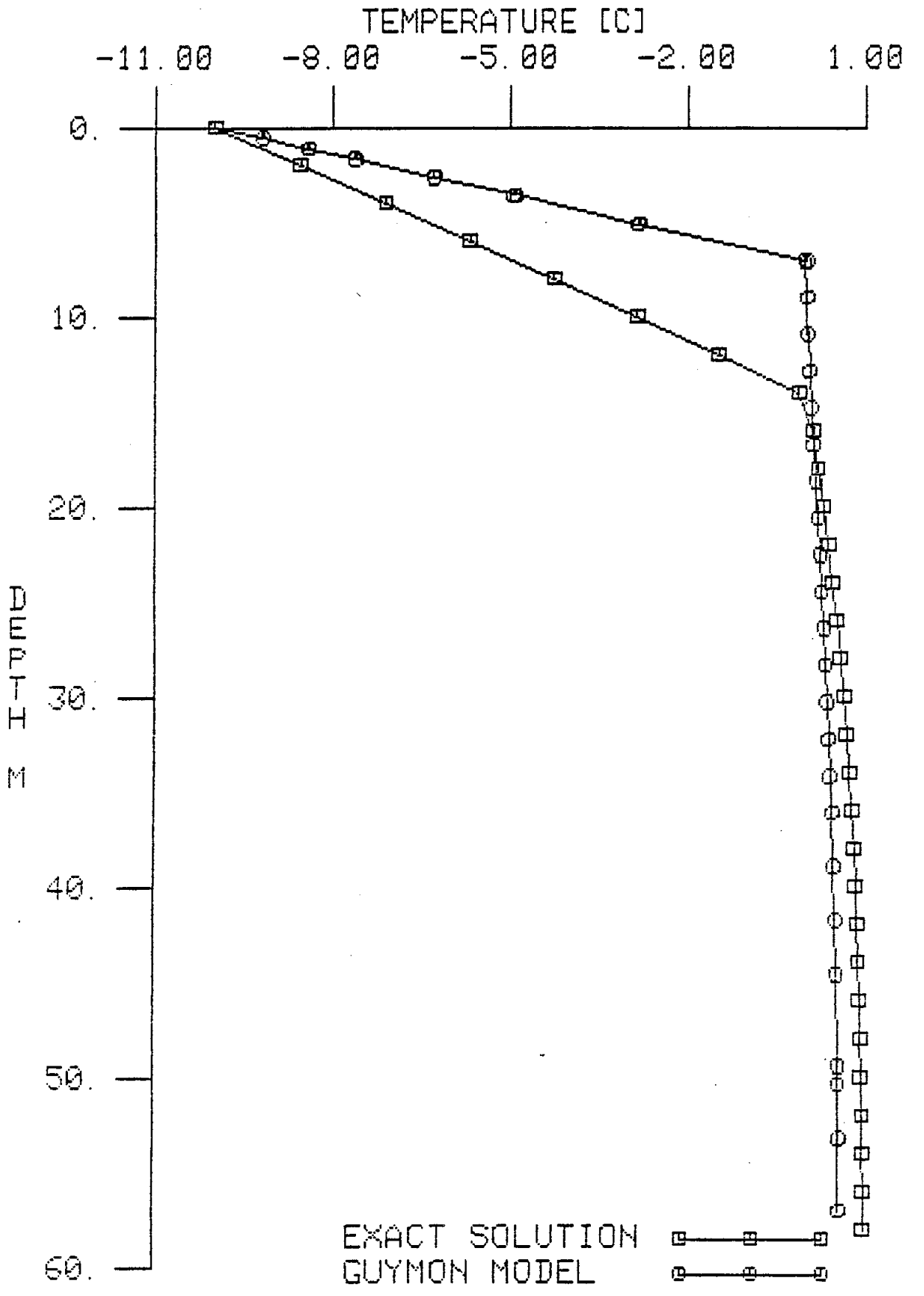

Figure 17. Comparison of exact and calculated (Guymon model) temperatures for test case 3 after ten years. A_k = 1.34.

migration. For E = 20 (Figure 15) and E = 30 (Figure 11), available latent heat is about right, with the calculated freeze front in one case slightly above, and in the second case slightly below the Stefan predictions.

There does not appear to be an a priori method for selecting values of E. Guymon (private communication) recently claimed to have found a relation between E and K_H. As suggested by the references, E seems to vary most frequently between 10 and 30 with the higher values more typical of coarser and more heterogeneous soils. Ideally, at a given site or for a given soil type, a series of laboratory and numerical experiments could be performed to optimize the selection of E. As a pragmatic recourse, we recommend values of E near 10-15 for silts and near 20-30 for gravels.

This example demonstrates the dynamic effect that moisture migration can have on prediction of soil freezing. E effectively controls hydraulic conductivity, which is to say, it effectively controls the moisture flow velocity. "Third method" numerical techniques may require the user to define flow velocity (equivalent to stating E = 0 and K_H = a constant) or may state flow velocity is zero whenever ice is present (equivalent to stating E = 0 if $\theta_i \leq 0$ and E = ∞ if $\theta_i > 0$). Figures 14 and 16 clearly demonstrate that this recourse is unreliable. Note that the Geodyn model is a third method numerical technique, which requires user-specification of moisture flux velocity in unsaturated soils, and internally enforces zero velocity wherever ice is present. Physically, it is not reasonable to expect that the moisture flux velocity goes abruptly from a prescribed value to zero as the soil freezes; instead, we expect a gradual decrease in moisture flux velocity as the ice content in the surrounding soil increases. The specification of E as a hydraulic conductivity attenuation factor matches the intuitive expectation for moisture flux near a freezing front.

Variation in other soil parameters

The Gardner formulations for hydraulic conductivity, $K(\Psi)$, and unfrozen water content, $\theta(\Psi)$, as functions of soil potential, Ψ, are as follows:

$$K(\Psi) = K_H/(A_k|\Psi|^{n_k} + 1)$$

and

$$\theta(\Psi) = \theta_o/(A_\theta|\Psi|^{n_\theta} + 1)$$

where K_H and θ_o are the saturated hydraulic conductivity and moisture content (porosity) respectively. These formulae are applicable only when $\Psi < 0$, i.e., when soil tension exists due to freezing effects. For $\Psi \geq 0$, $K(\Psi) \equiv K_H$ and $\theta(\Psi) \equiv \theta_o$.

The above Gardner expressions have the effect of reducing hydraulic conductivity and moisture content as soil tension increases in magnitude. Both expressions therefore reduce the transport of moisture and associated latent heat to the freeze front as soil tension increases. In fact any increase in either of the denominators in the above expressions decreases the available latent heat transported to the freeze front, and consequently, accelerates the freezing. Conversely, any decrease in either of the denominators decelerates the progression of the freeze front. Examination of Appendix B reveals that the experimental values of A_k and A_θ tend to be somewhat larger for gravels than for sands and silty sands. However, experimental values of n_θ and n_k tend to be somewhat smaller for gravels than for sands and silty sands. Therefore, no clear tendency distinguishing gravels from sands and silty sands can be noted in the Gardner formulations.

The expressions also demonstrate the dynamic effect that differences in pore pressure can have on moisture migration. For example, if excess overburden

exists on only a portion of the calculation domain, we would expect higher subsurface pressures to exist below the overburden. This would imply a transverse pressure gradient, and associated with it, moisture migration away from the high pressure zone toward lower pressures. Ultimately this means faster freezing below the overburden. This effect can only be analyzed with a "second method" model containing equations for both temperature and pressure. Geodyn, a "third method" model, does not calculate pore pressure. As previously stated, the model-user prescribes the flow velocity in unfrozen soil. There is no allowance in Geodyn for a dynamic velocity field changing with time due to overburden variations, freeze front motion or continuity constraints.

Using test case 3 as a standard, two additional test runs were made varying the parameters A_k and A_θ. In Figure 17, the value of A_k has been reduced from the standard 2.681 to 1.340. This figure, depicting the temperature regime and freeze front position after 10 years, may be compared both with the Stefan solution and the standard case in Figure 12. Since A_k has been reduced, we expect that $K(\Psi)$ is relatively larger, and that consequently more moisture and associated latent heat have been transported to the freeze front, reducing the freeze rate of the soil. This is verified by the calculated temperatures.

In Figure 18, the value of A_θ has been reduced from the standard 1.32 to 0.66. Again, we see the same effect, an increase of available moisture and latent heat, resulting in a decrease in freeze front progression.

Finally, a comparison was made between the standard case and an analogous case with different thermal conductivity. The Guymon/Hromadka model uses a simplified form of the DeVries (1952) expression for thermal conductivity:

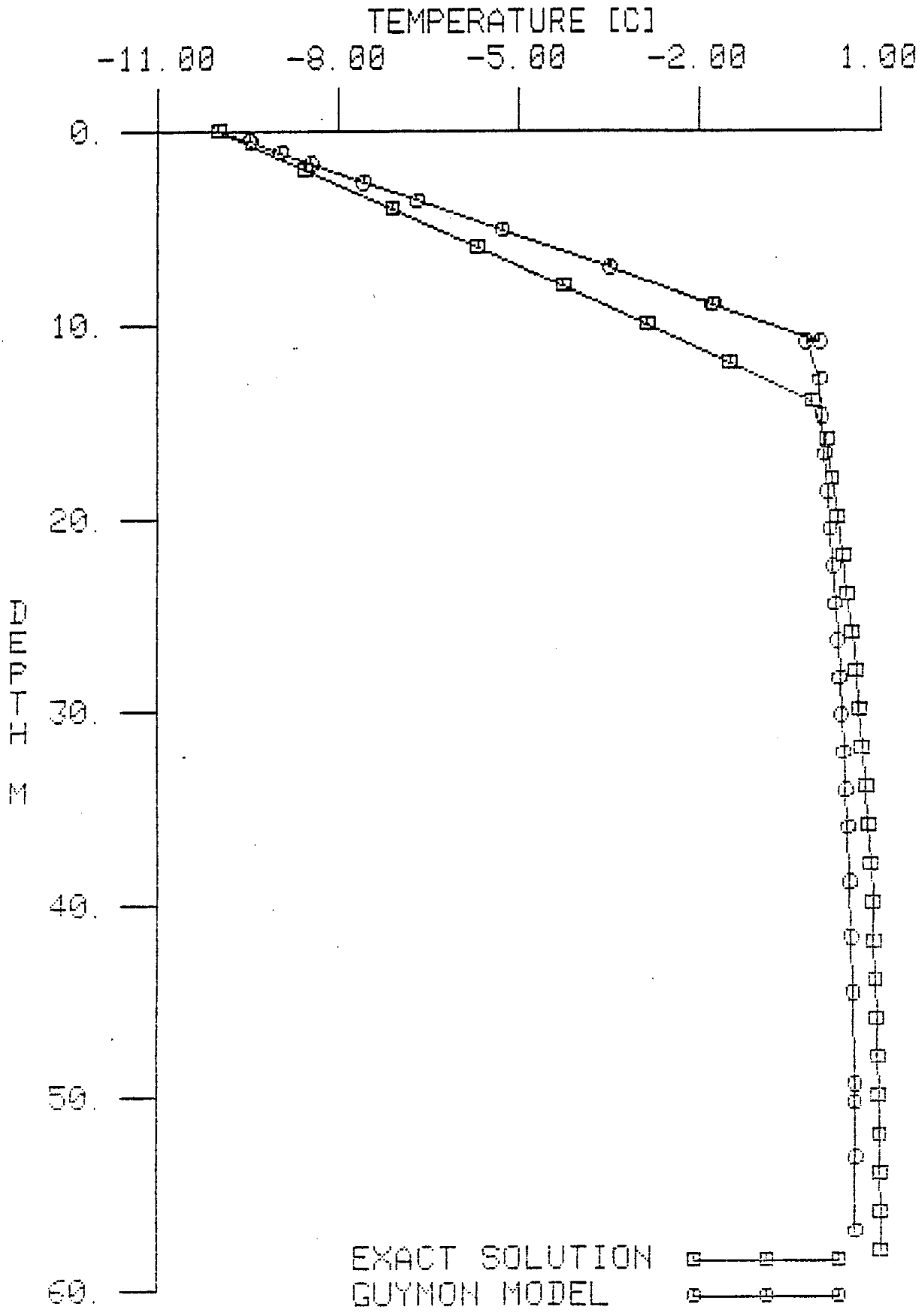

Figure 18. Comparison of exact and calculated (Guymon model) temperatures for test case 3 after ten years. A_θ =0.66.

$$k = \theta_u k_w + \theta_i k_i + (1 - \theta_u - \theta_i) k_s$$

where θ_u is unfrozen water content, k_w is thermal conductivity of water, θ_i is ice content, k_i is thermal conductivity of ice, and k_s is thermal conductivity of dry soil. In the standard case, k_s was taken as 64.8 cal cm^{-1} hr^{-1} C^{-1}. In the test case depicted in Figure 19, k_s is 32.4 cal cm^{-1} hr^{-1} C^{-1}. Reduction of the thermal conductivity implies a reduction in the rate of heat transport. For this example of ground freezing, a reduction in thermal conductivity requires a reduction in the rate of ground cooling, hence the calculated temperatures in Figure 19 are greater than those in the standard case in Figure 12.

Other test cases

A single test case was run for the highway embankment geometry described by Zarling, Connor and Goering (1984). The identical soil conditions as defined in test case 3 were adopted for this problem. The grid for the embankment is depicted in Figure 20a and an expanded view of the grid surrounding the heat dissipation pipe is shown in Figure 20b. The initial conditions were prescribed as follows:

$$T\ (x,\ y < 4.8\ m,\ 0) = 0.0\ C$$

$$T\ (x,\ y > 4.8\ m.\ 0) = 10.0\ C$$

For times greater than zero, the temperature of the exposed terrain or top surface of the highway and embankment and the surface of the pipe are set to 0.0 C. For this test case freezing is not considered; the problem is one of transient heat conduction only. Since neither an analytic solution nor experimental data exist for this problem, no comparisons can be made between exact or measured temperatures and calculated temperature distributions.

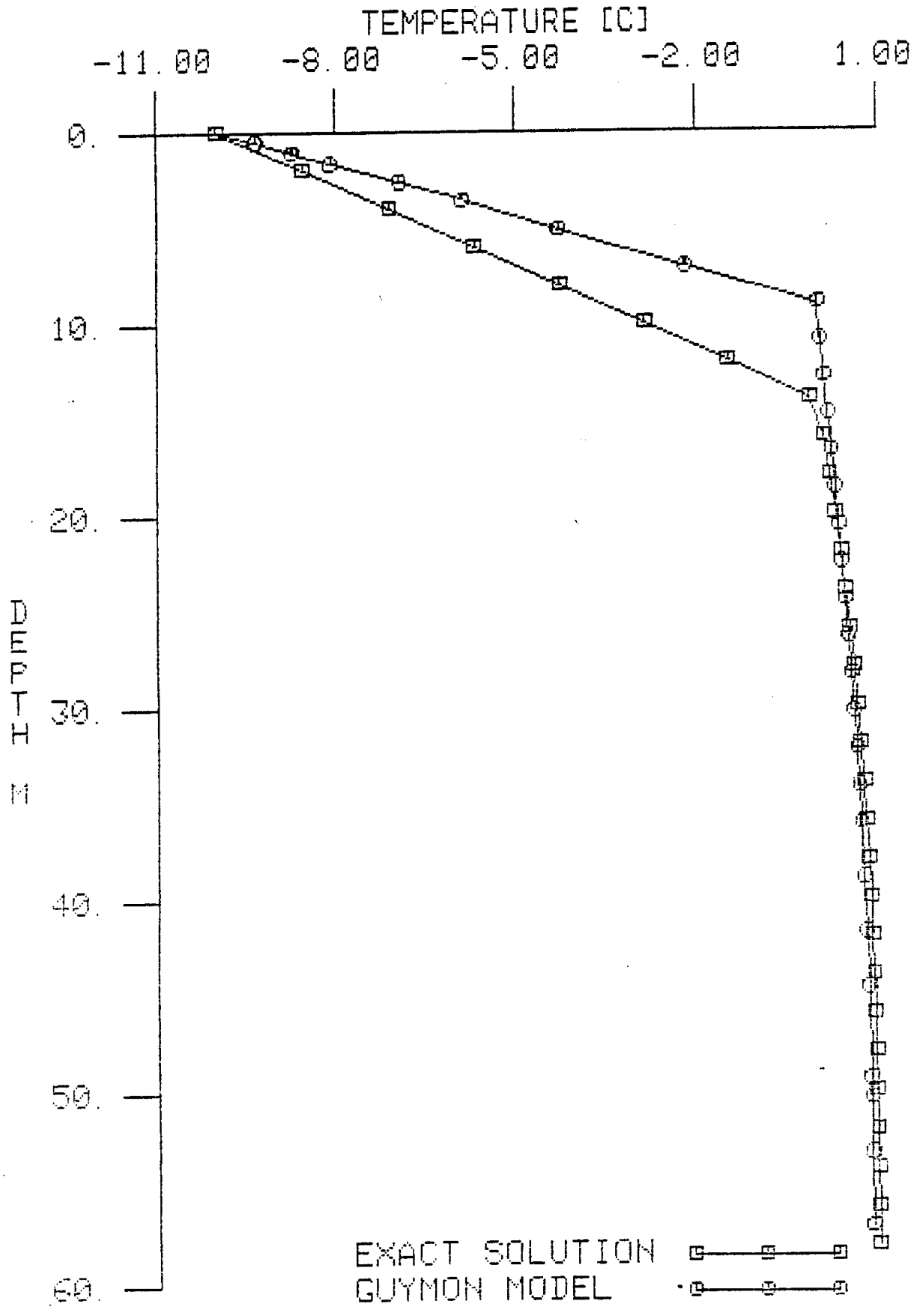

Figure 19. Comparison of exact and calculated (Guymon model) temperatures for test cast 3 after ten years. k_s = 32.4.

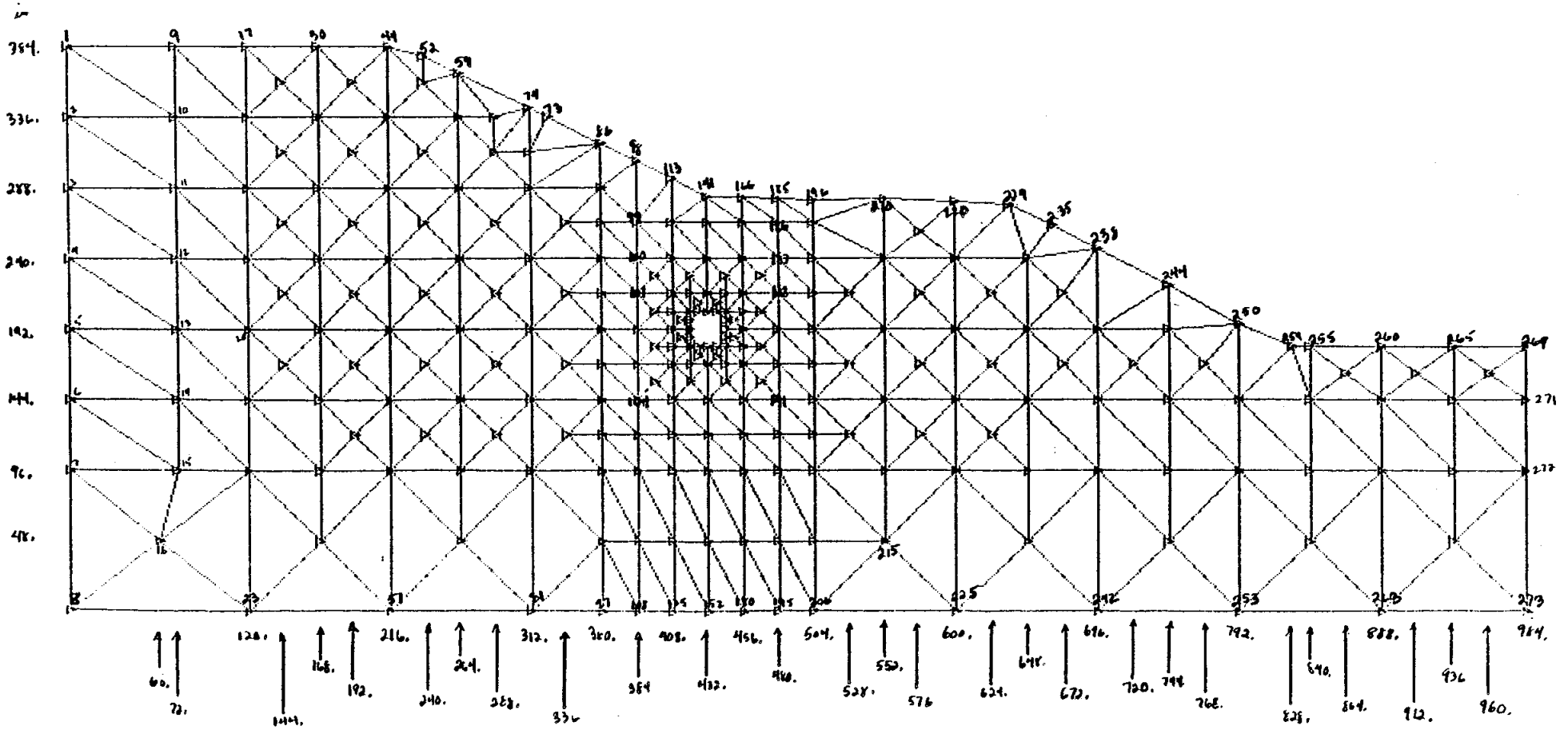

Figure 20a. Highway embankment grid.

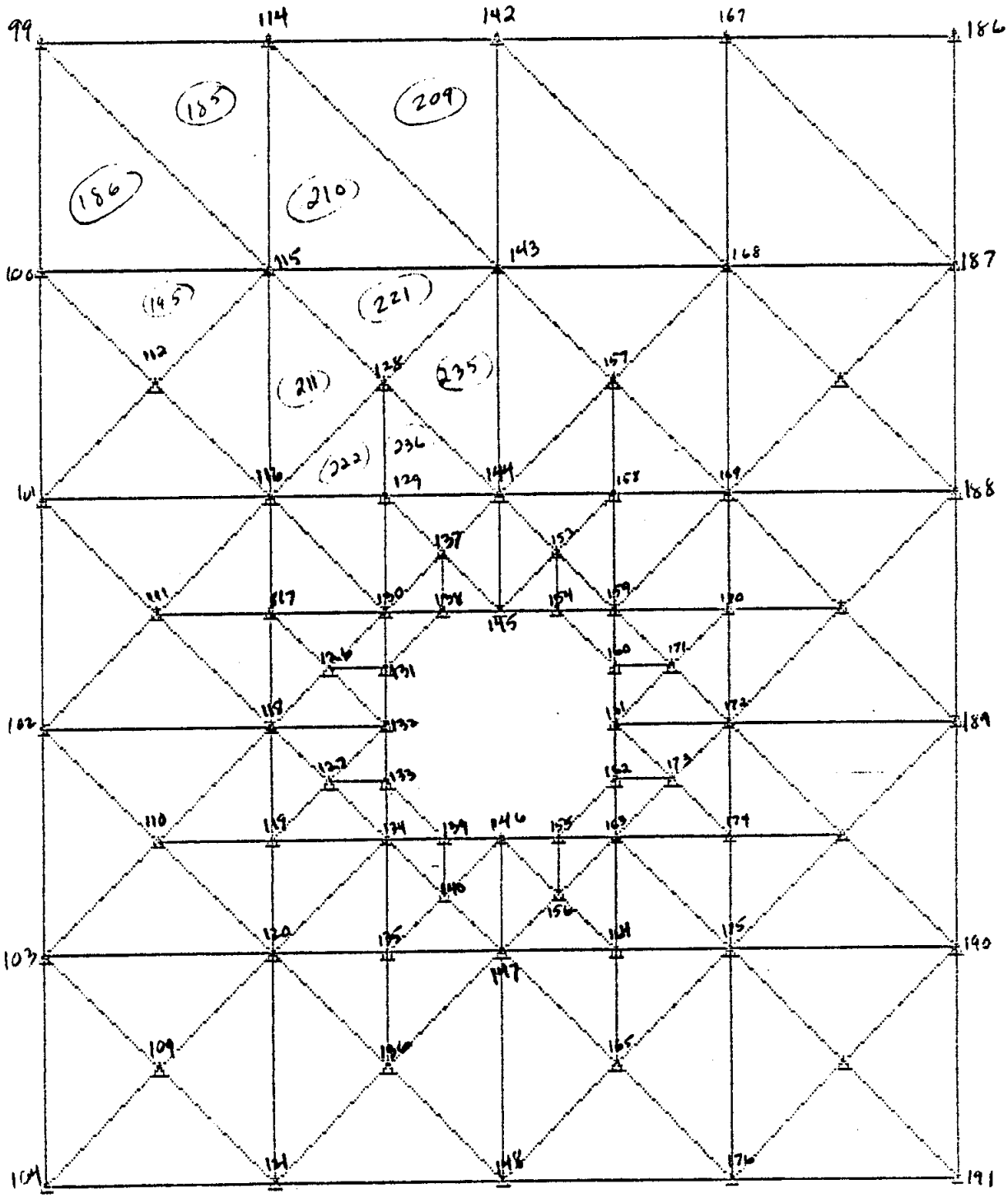

Figure 20b. Grid geometry near the culvert.

This suggests that, at best, the present test case can only provide an indication of the reasonableness of the calculated temperatures. For this reason, only one test case was attempted with the highway embankment geometry. No attempt was made to simulate snow cover or varying surface and/or pipe temperatures.

Calculated temperature distributions after 20 days and 60 days are depicted in Figures 21 and 22 respectively. The figures clearly demonstrate the gradual adjustment to the imposed surface temperature. Note that the time scale ($\tau = y^2/4\kappa$) for the upper layer is about 20 days, which suggests that the temperature of the central core under the highway will have decreased by the factor e^{-1} in about that time. This indicates that the general trend of the calculated solution appears to be correct.

Goodrich Model

T1D, the Goodrich model (Goodrich, 1978), is a sophisticated one-dimensional model containing a great number of user specifiable options including: snow cover with a snow thermal conductivity which is a function of snow density; flux boundary conditions with a surface heat balance; empirical formulas (De Vries, Kersten, Anderson) for determining unfrozen water content, conductivity and diffusivity. The Goodrich model is also well documented and reasonably easy to use and both stable and accurate; unfortunately, it is only one-dimensional.

Numerical Comparisons

The first three test cases used for the Guymon model were also run with the Goodrich model, with the equivalent one-dimensional grid and over the same twenty year period. The grid is not depicted here, since it is calculated internally in the computer model following a geometric progression.

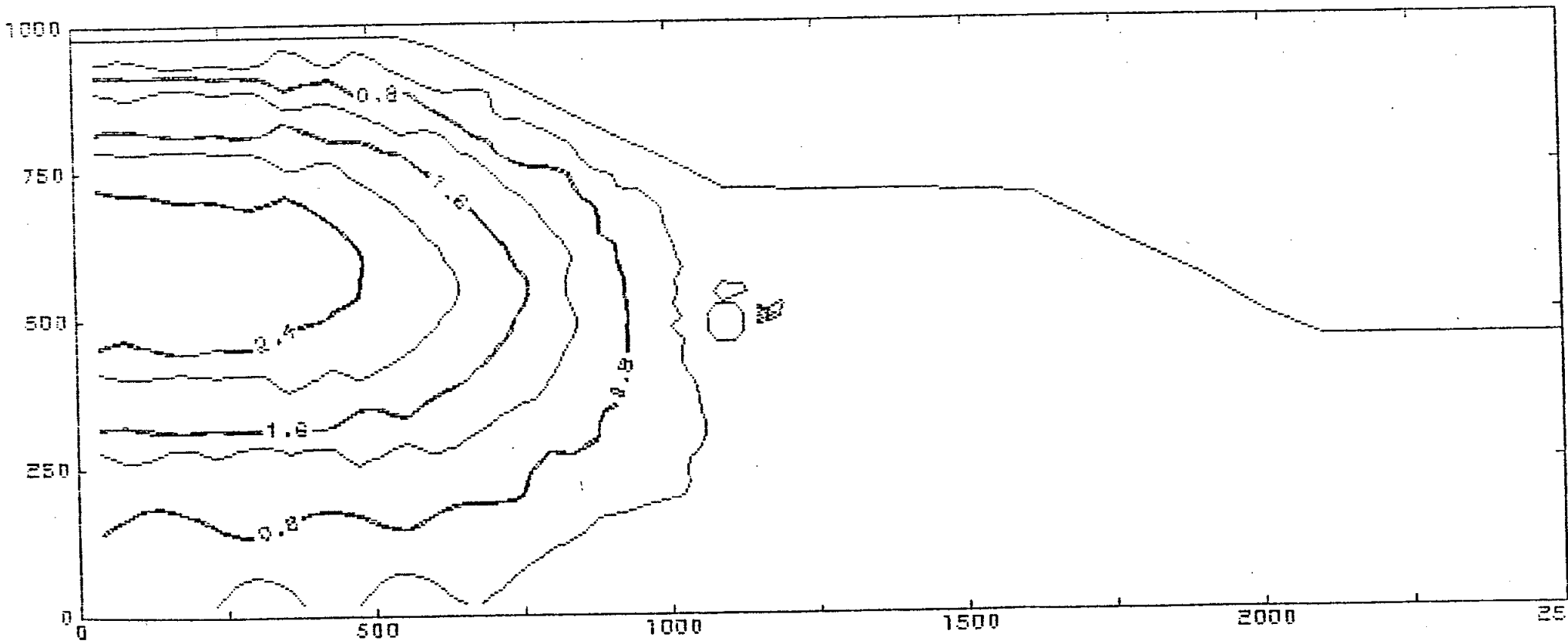

Figure 21. Calculated isotherms in the highway embankment after 20 days.

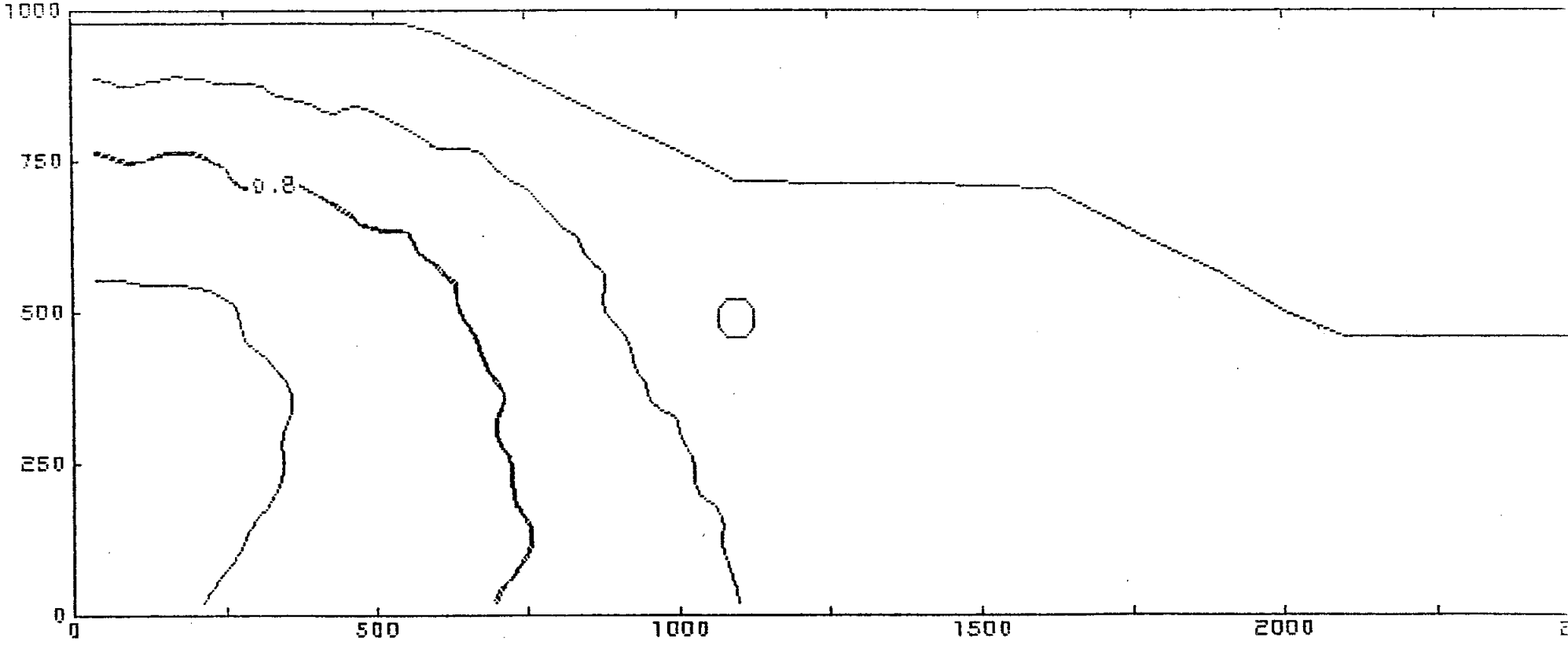

Figure 22. Calculated isotherms in the highway embankment after 60 days.

Test Case 4

Initial and boundary conditions are:

$T(y,0) = 0.0$ C

$T(0,t>0) = 1.0$ C

$\partial T/\partial y\ (15,t>0) = 0.0$ C m^{-1}

The calculated and analytic temperatures after one, five, ten and twenty years are depicted in Figures 23, 24, 25 and 26, respectively. Identical soil parameters for fine silts as used in the comparable Guymon Test Case 1 were employed.

The calculated temperatures are virtually identical to the analytic solution throughout the 20 year simulation period, indicating the excellent stability and accuracy of the numerical scheme. Recall that both the Guymon and the Goodrich numerical scheme use direct solution techniques to solve the governing matrix equations. This feature eliminates the possibility of introducing covergence errors into long-term calculations, which is a potential problem with numerical schemes calling for iterative solution techniques. In contrast Geodyn uses the Newton-Raphson iteration technique to solve the system of equations for nodal temperature. The Newton-Raphson method converges slowly if the initial estimate is substantially different from the final solution. It would be interesting to compare long term solutions (for times greater than 20 years) generated by the Geodyn model with the exact solution for various test cases.

Test Case 5

This is the trumpet curve solution for coarse gravels described previously as the Guymon model test case 2. For these one-dimensional calculations a time step of one day was used.

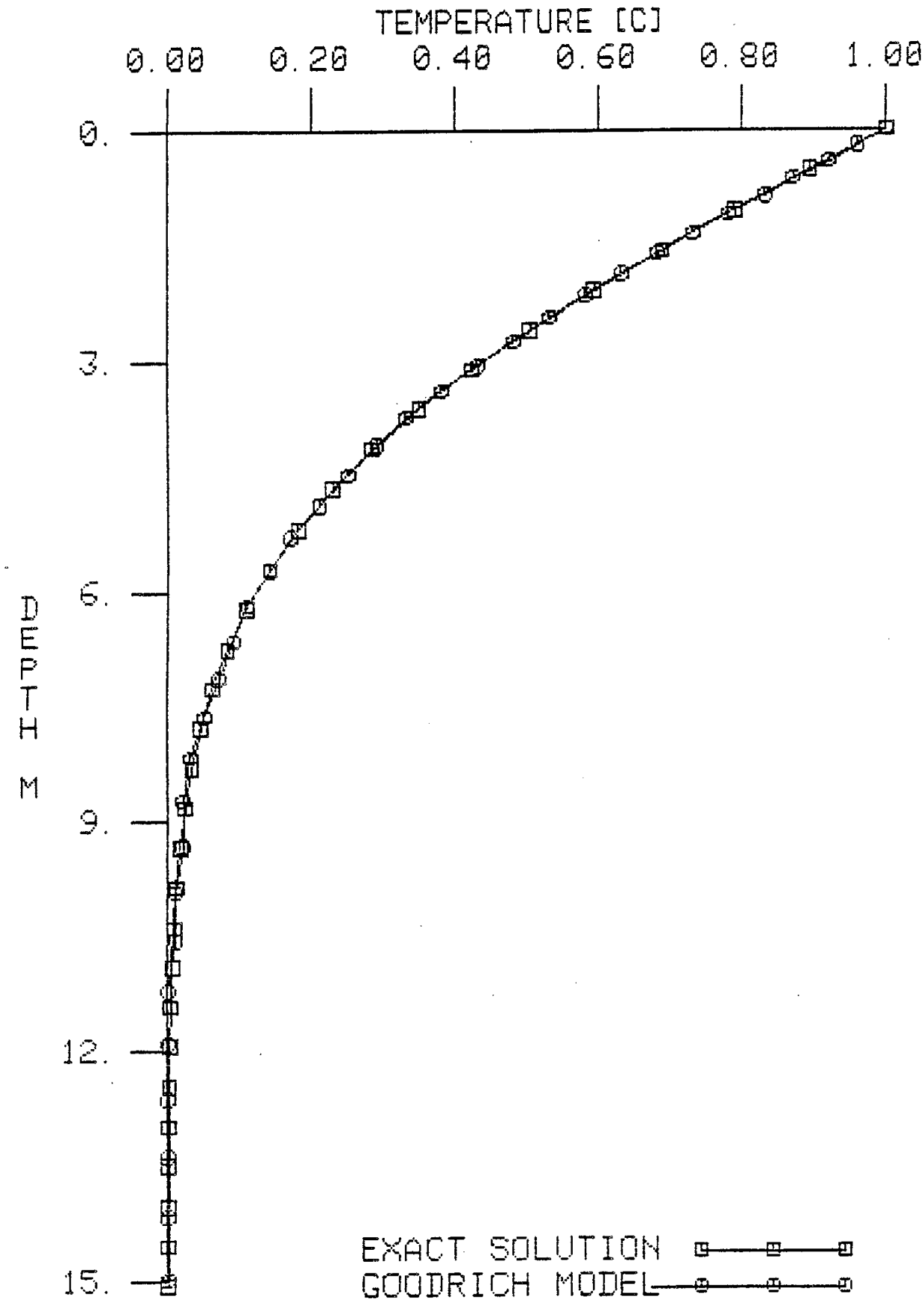

Figure 23. Comparison of exact and calculated (Goodrich model) temperatures for test case 4 after one year.

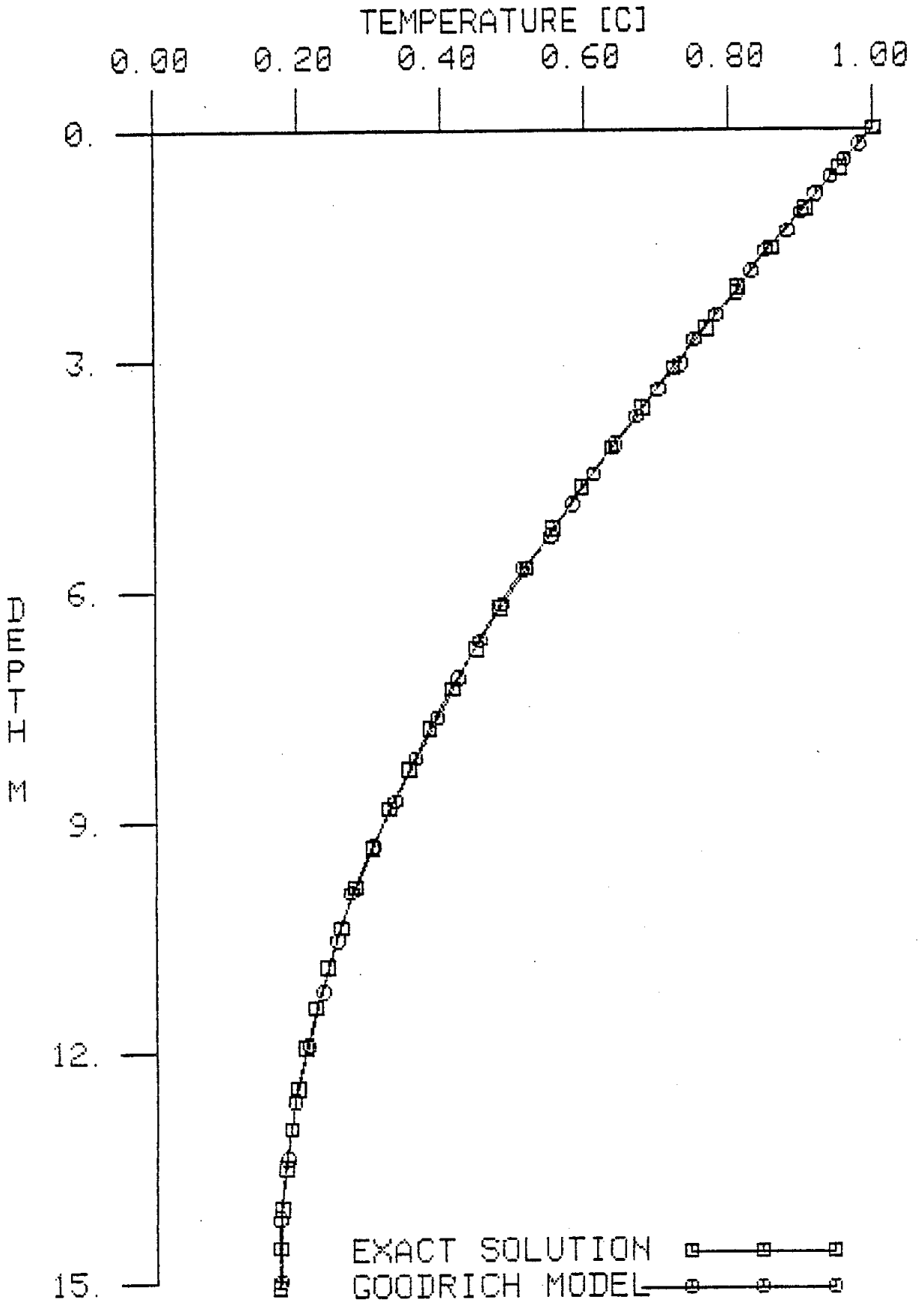

Figure 24. Comparison of exact and calculated (Goodrich model) temperatures for test case 4 after five years.

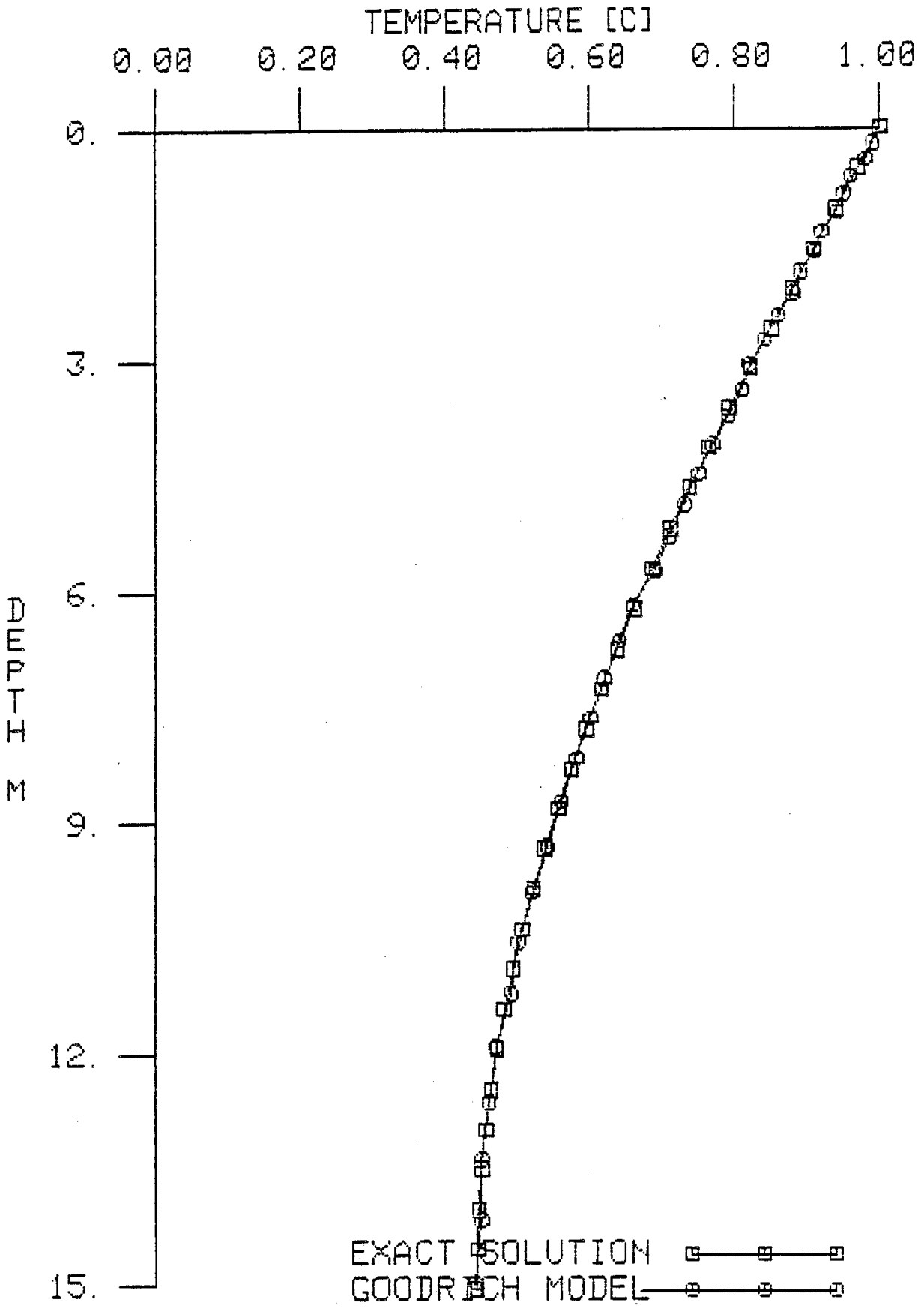

Figure 25. Comparison of exact and calculated (Goodrich model) temperatures for test case 4 after ten years.

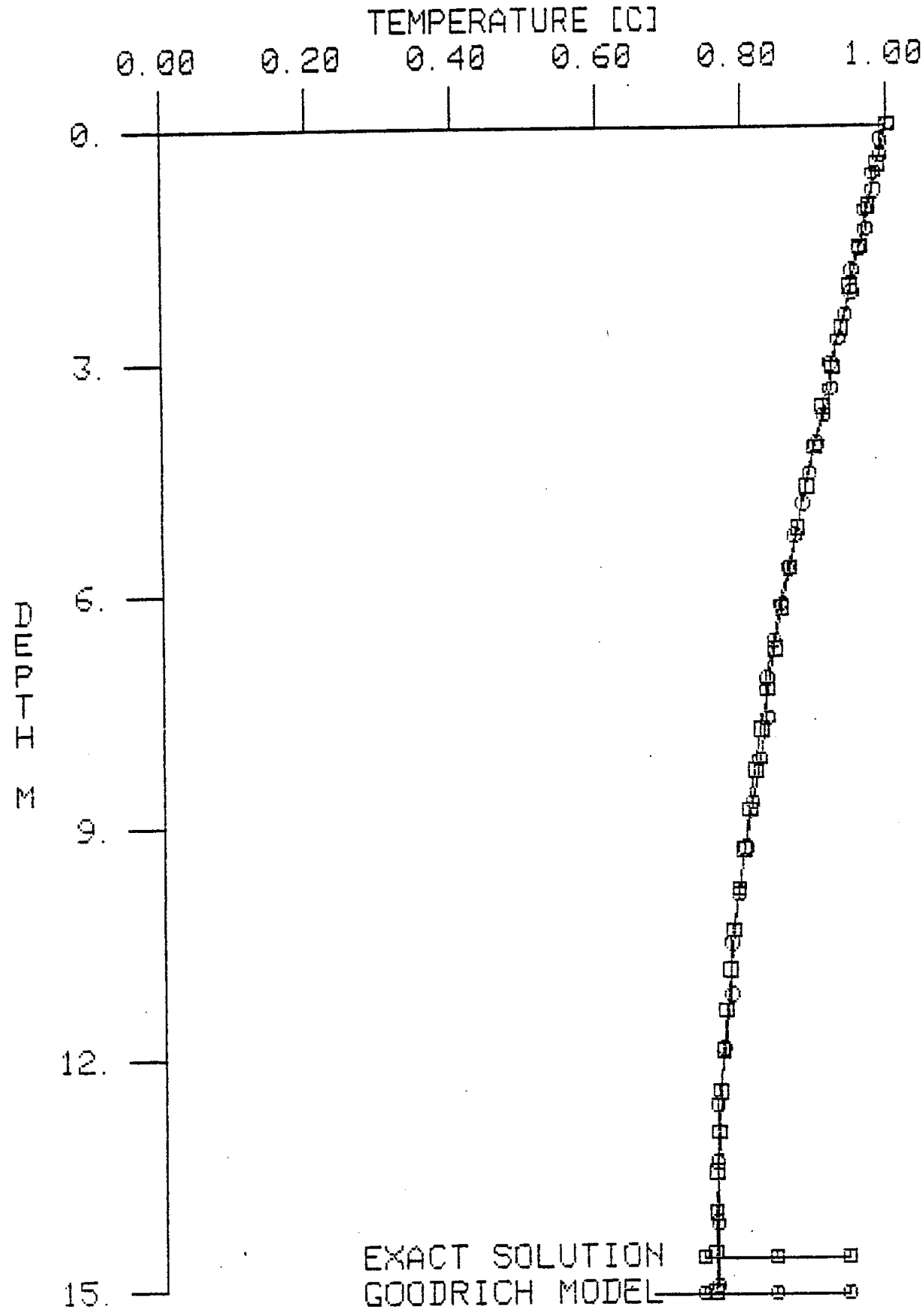

Figure 26. Comparison of exact and calculated (Goodrich model) temperatures for test case 4 after twenty years.

The calculated and analytic temperatures after six years are shown in Figure 27. Plots of the temperature distributions for 5.25, 10.5 and 19.75 years are not presented, since the solution is virtually identical with the analytic solution at all times. In fact, the Goodrich model automatically ceases calculation after 6 years and prints "Periodic steady state reached" when the analytic solution is reached within 5.0×10^{-6}. (Convergence to within 5.0×10^{-3} was within one year).

Test Case 6

This test case (the Stefan problem for sandy gravels) demonstrates the progression of a freeze front from a sudden cooling at the surface and is identical to Test Case 3 for the Guymon model. However, the simplest soil parameters were chosen i.e., constant soil diffusivities, conductivities and specific heats in the thawed and frozen layers identical to the parameters in the Stefan solution.

The calculated and analytic temperatures after one, five, ten and twenty years are shown in Figures 28, 29, 30 and 31, respectively. The calculated temperatures accurately model the analytic temperatures for the entire simulation period. The small deviation at the freeze front position after one year (Figure 28) is due to averaging between two depths in the plotting routine rather than to a real disagreement. After twenty years (Figure 31) heat flux from the bottom in the Stefan solution has begun to increase temperatures above the calculated ones. This is expected since the assumed bottom boundary condition for the calculations is zero flux. In this instance bottom temperatures are very close to the analytic solution due to the fact that soil parameters are identical with those defined in the Stefan solution.

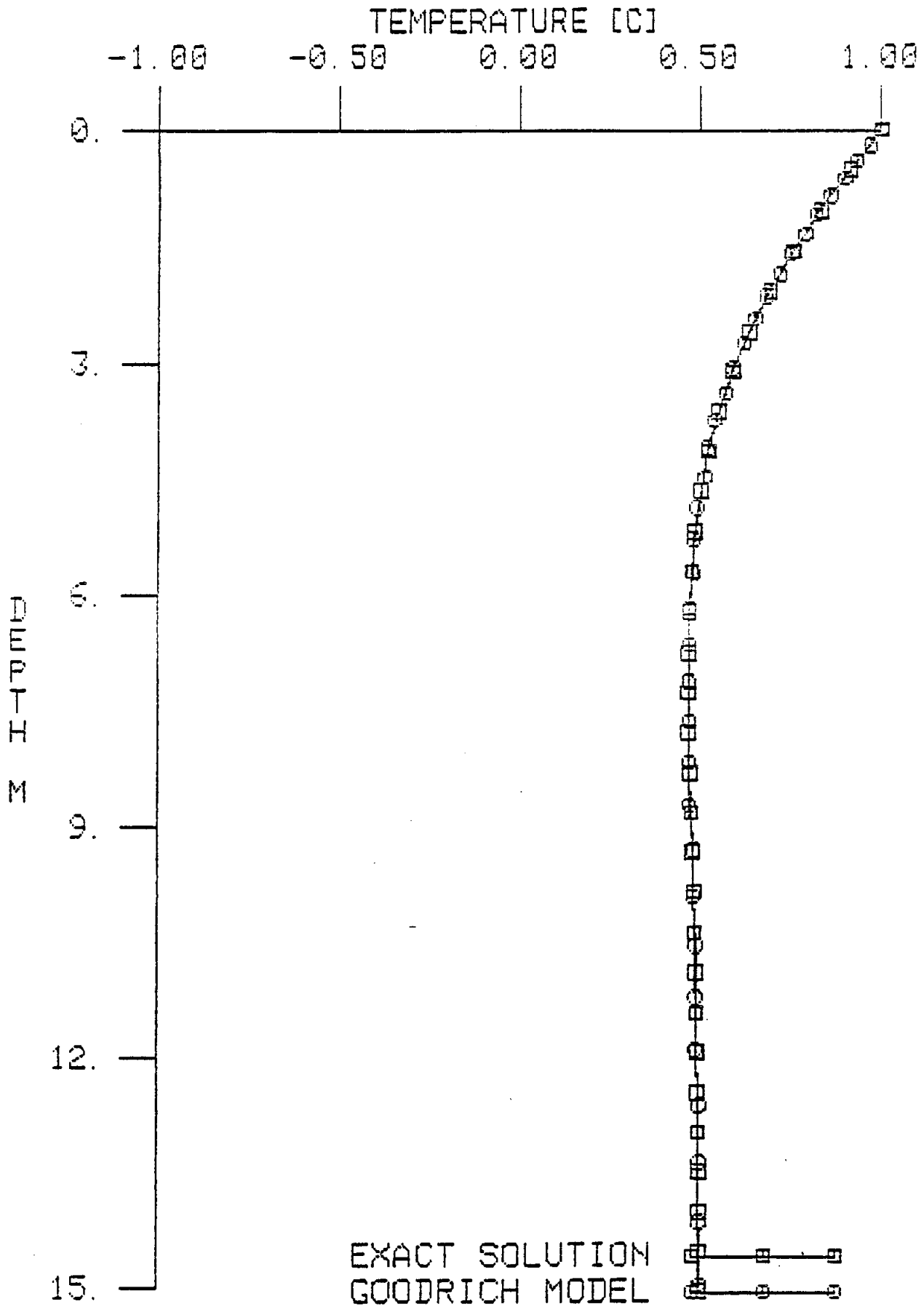

Figure 27. Comparison of exact and calculated (Goodrich model) temperatures for test case 5 after six years.

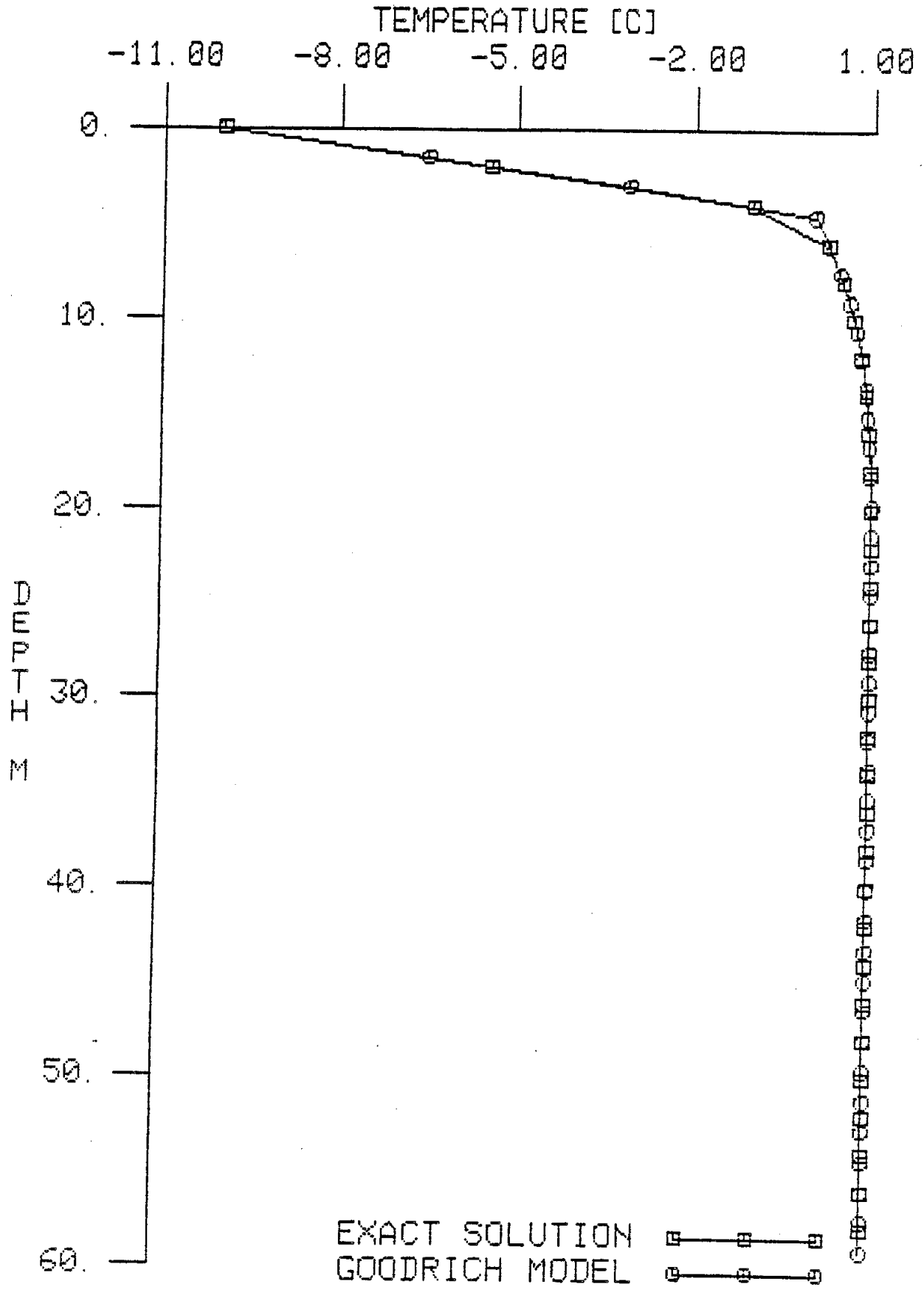

Figure 28. Comparison of exact and calculated (Goodrich model) temperatures for test case 6 after one year.

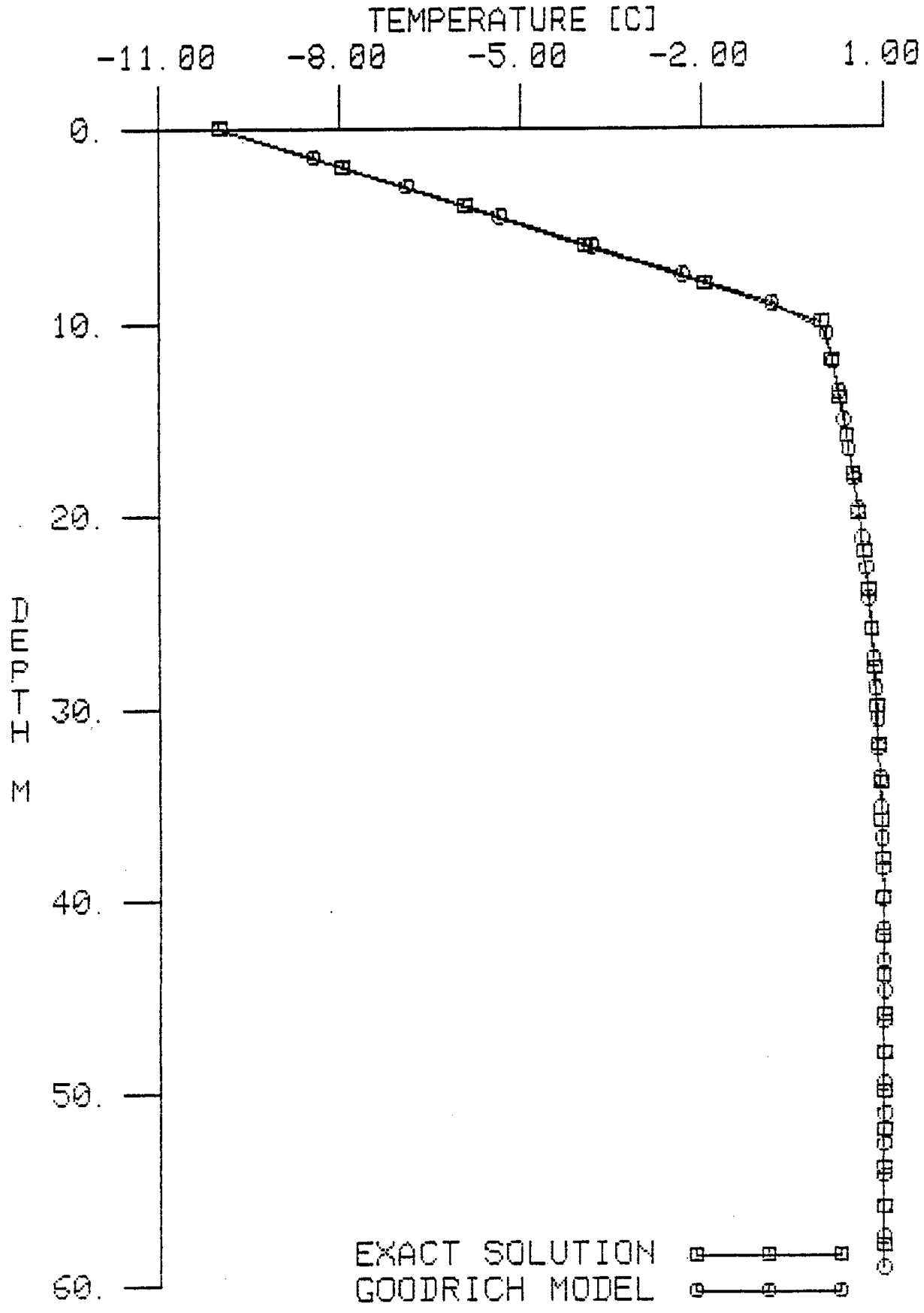

Figure 29. Comparison of exact and calculated (Goodrich model) temperatures for test case 6 after five years.

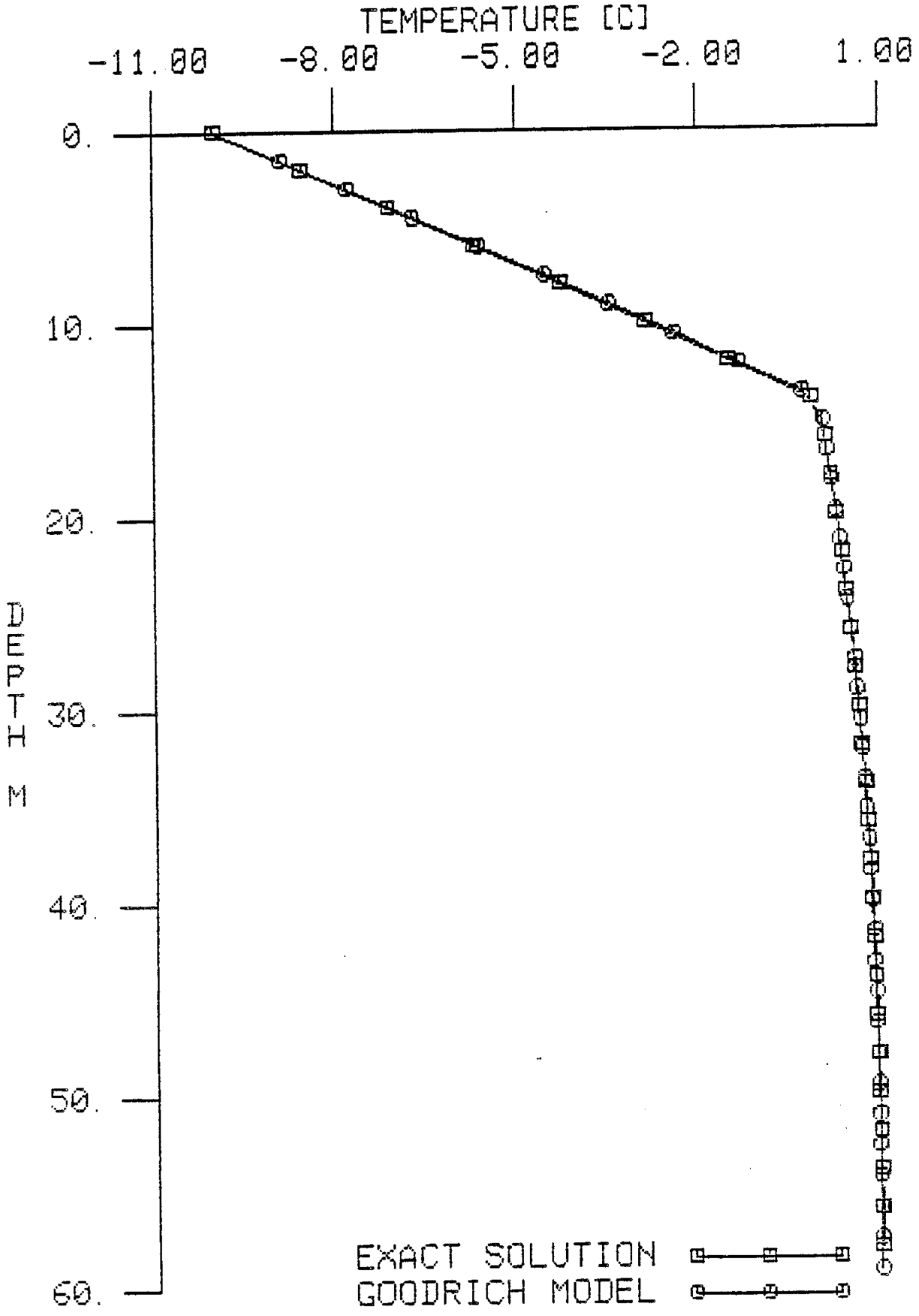

Figure 30. Comparison of exact and calculated (Goodrich model) temperatures for test case 6 after ten years.

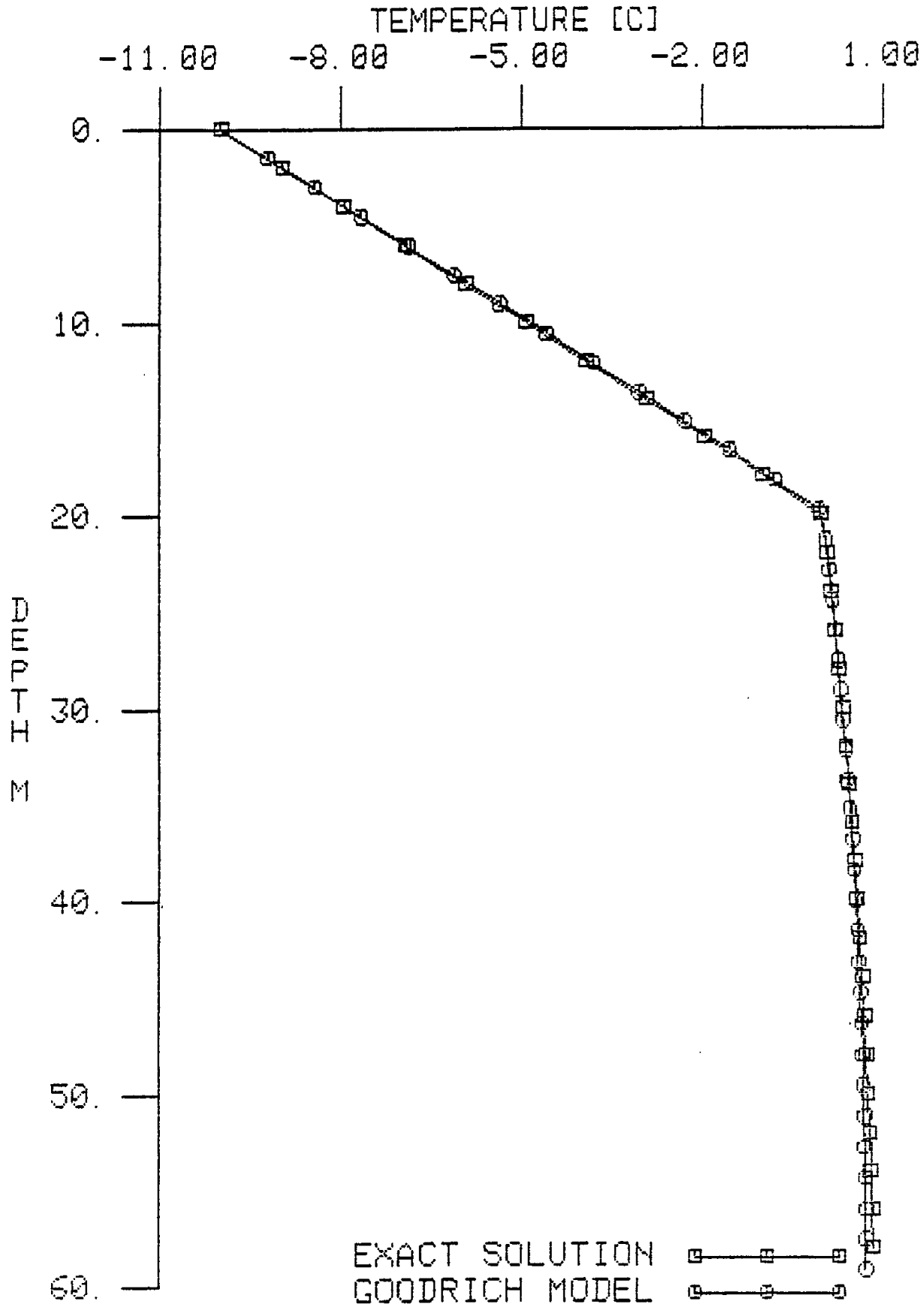

Figure 31. Comparison of exact and calculated (Goodrich model) temperatures for test case 6 after twenty years.

Test Case 7

A final test case was developed to compare the predictions of the Guymon model with actual field data. A set of ground temperature measurements was obtained from Esch (unpublished data, 1986) for the CRREL study site on Farmer's Loop Road north of Fairbanks. These data consist of temperature measurements at depths between 1 and 30 feet taken during 1981 and 1982. Of the 22 available profiles, 20 were judged to represent acceptable data. The remaining two temperature profiles contained serious inconsistencies and reversals which could not represent ground temperature in the Fairbanks area. The twenty acceptable temperature profiles are presented in Figures 32, 33, 34, 35 and 36. The symbol, date and Julian day for each profile is given in Table 1. The measured ground temperatures at one foot depth (30.48 cm) have been plotted in Figure 37. This figure demonstrates the cyclic pattern of ground temperature as it responds to air temperature.

Meteorological data for the Fairbanks Airport were obtained from the meteorological data base on the VAX computer system at the Geophysical Institute. Air temperature maximums and minimums are presented in Figure 38. The cyclic pattern for air temperatures can be discerned, and deviations from a standard sinusoidal function are of particular interest. It should be expected that the maximum discrepancies between model predictions and measured ground temperatures will be associated with these deviations, since temperature boundary conditions at the ground surface are specified in the Guymon model by means of a simple sinusoidal function. Particular occurrences of these deviations and their effect on ground temperature can be seen by superimposing the graphs of ground temperatures at 1 ft. depth (Figure 37) and air temperatures (Figure 38). For example, the extremely cold air temperature near day 48 is reflected in abnormally cold ground

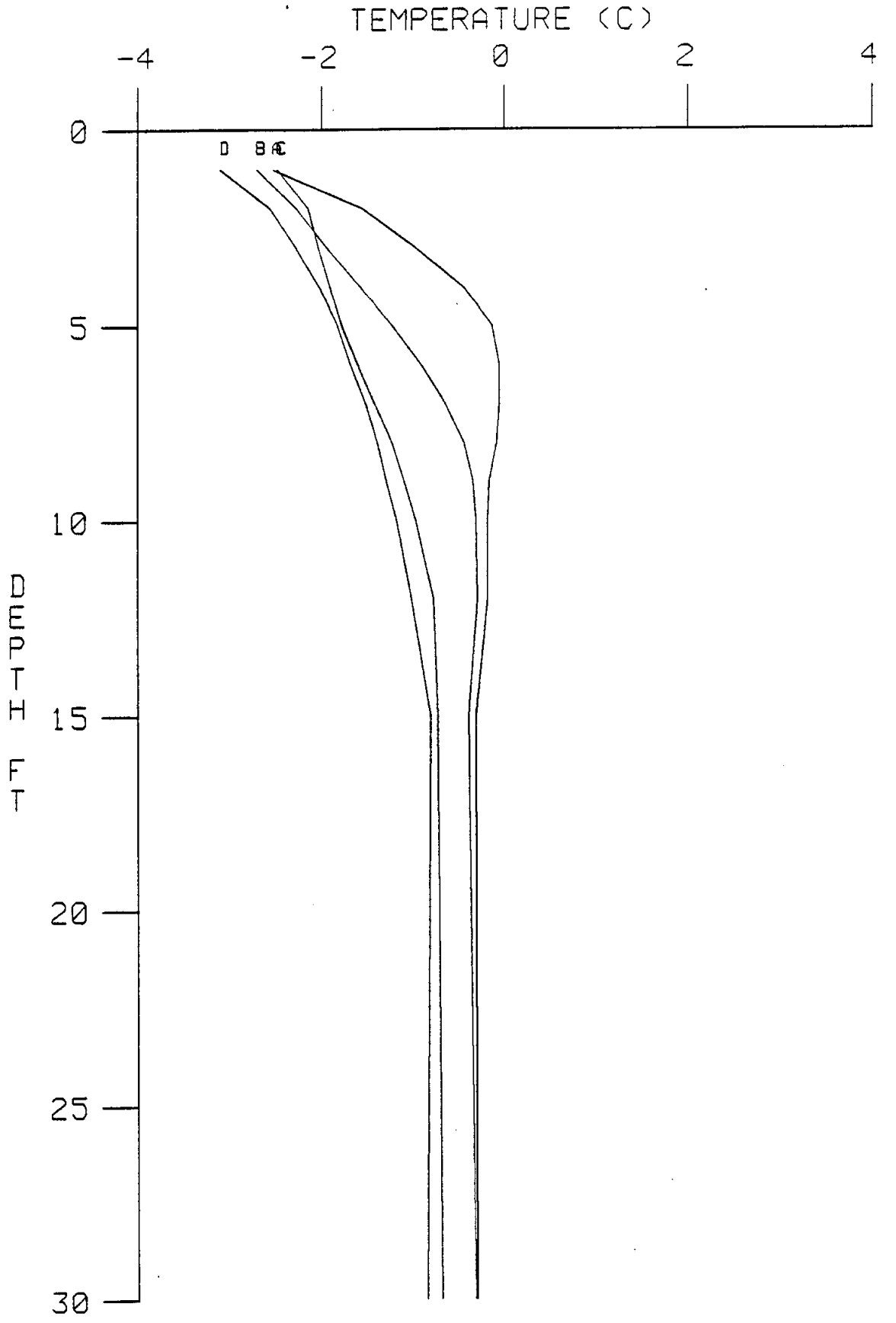

Figure 32. Measured temperature profiles for the CRREL study site near Fairbanks. A, January 8, 1981; B, March 4, 1981; C, March 23, 1981; D, April 16, 1981.

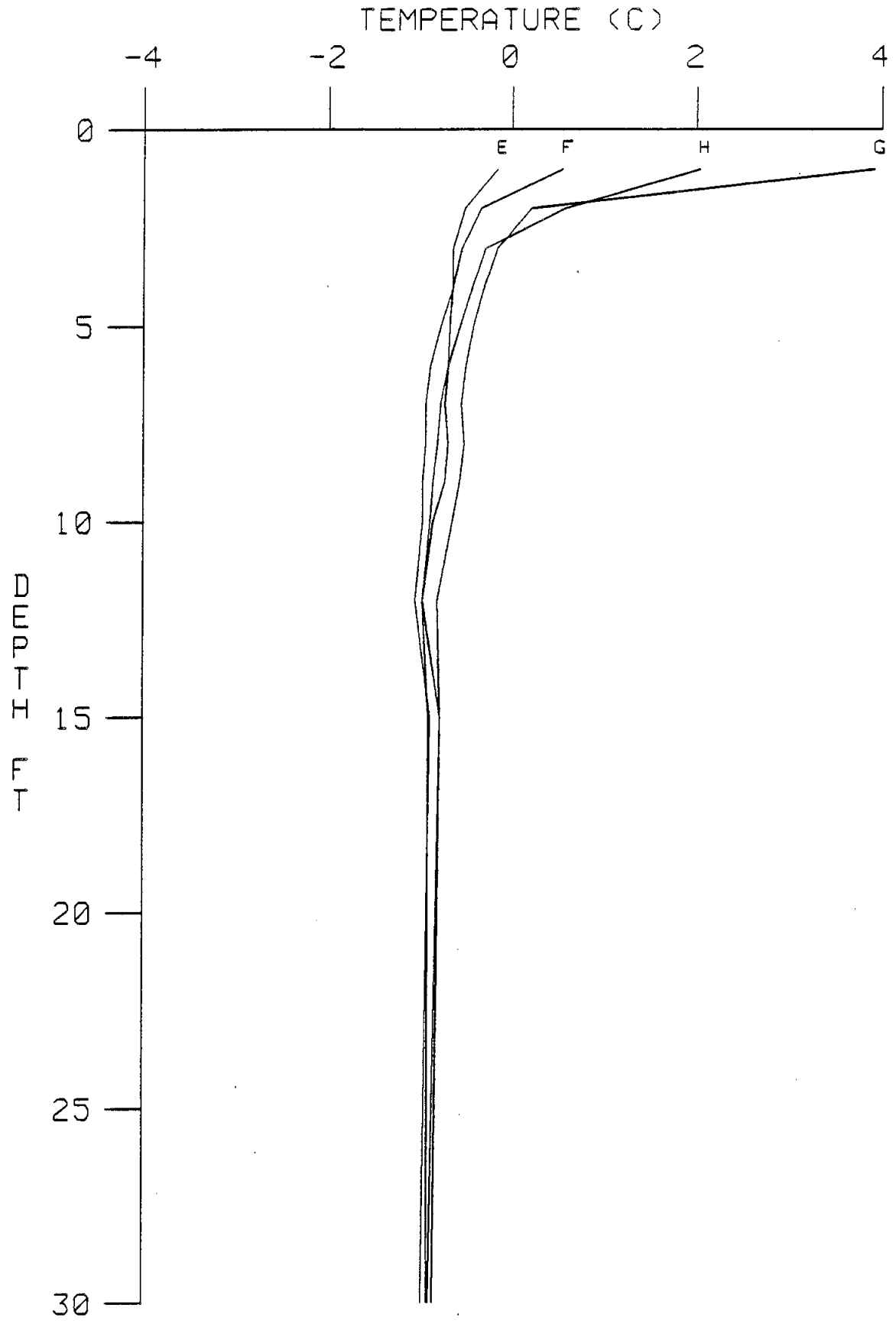

Figure 33. Measured temperature profiles for the CRREL study site near Fairbanks. E, May 12, 1981; F, June 16, 1981; G, July 13, 1981; H, August 24, 1981.

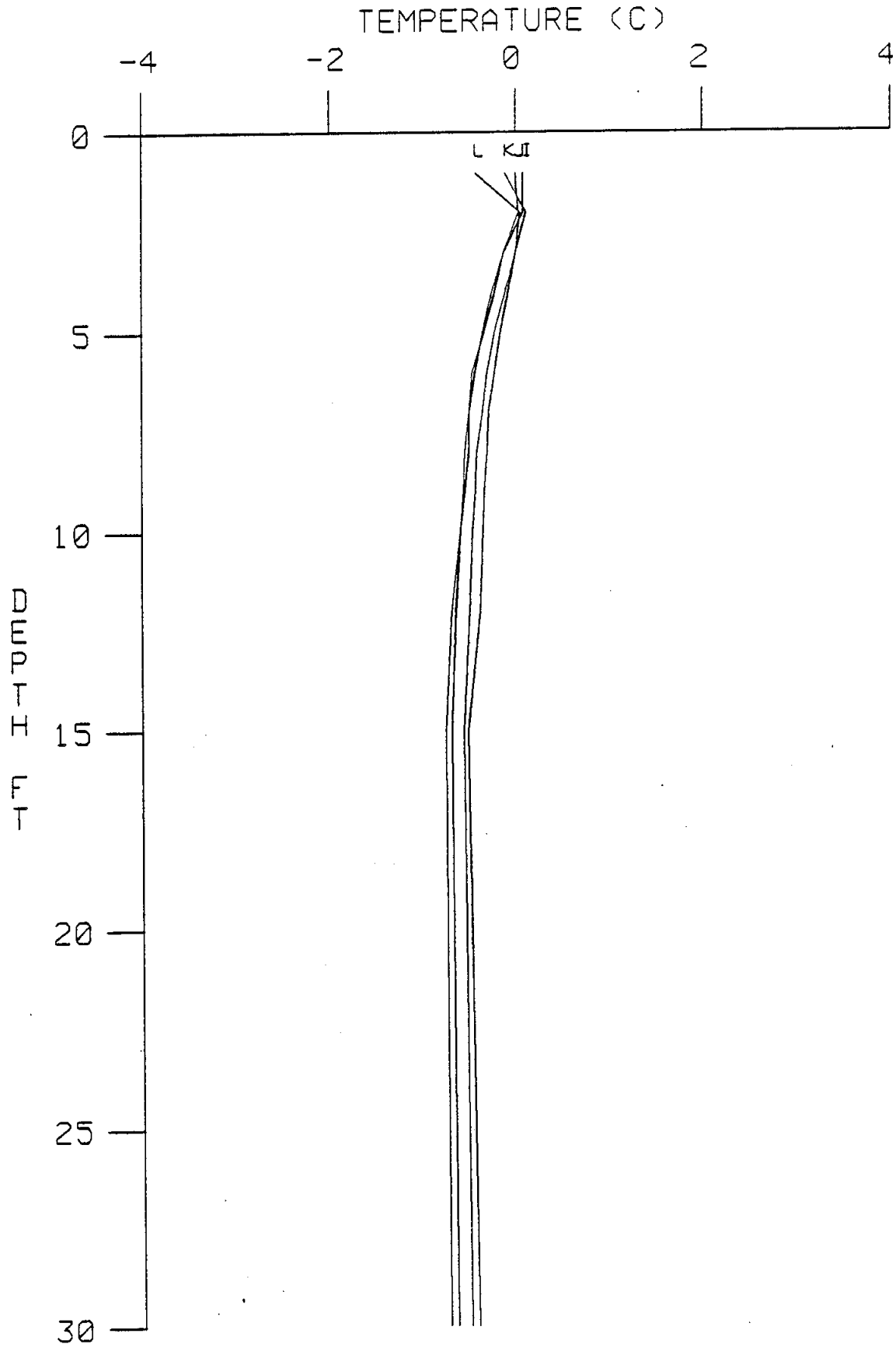

Figure 34. Measured temperature profiles for the CRREL study site near Fairbanks. I, September 30, 1981; J, October 28, 1981; K, November 19, 1981; L, January 21, 1982.

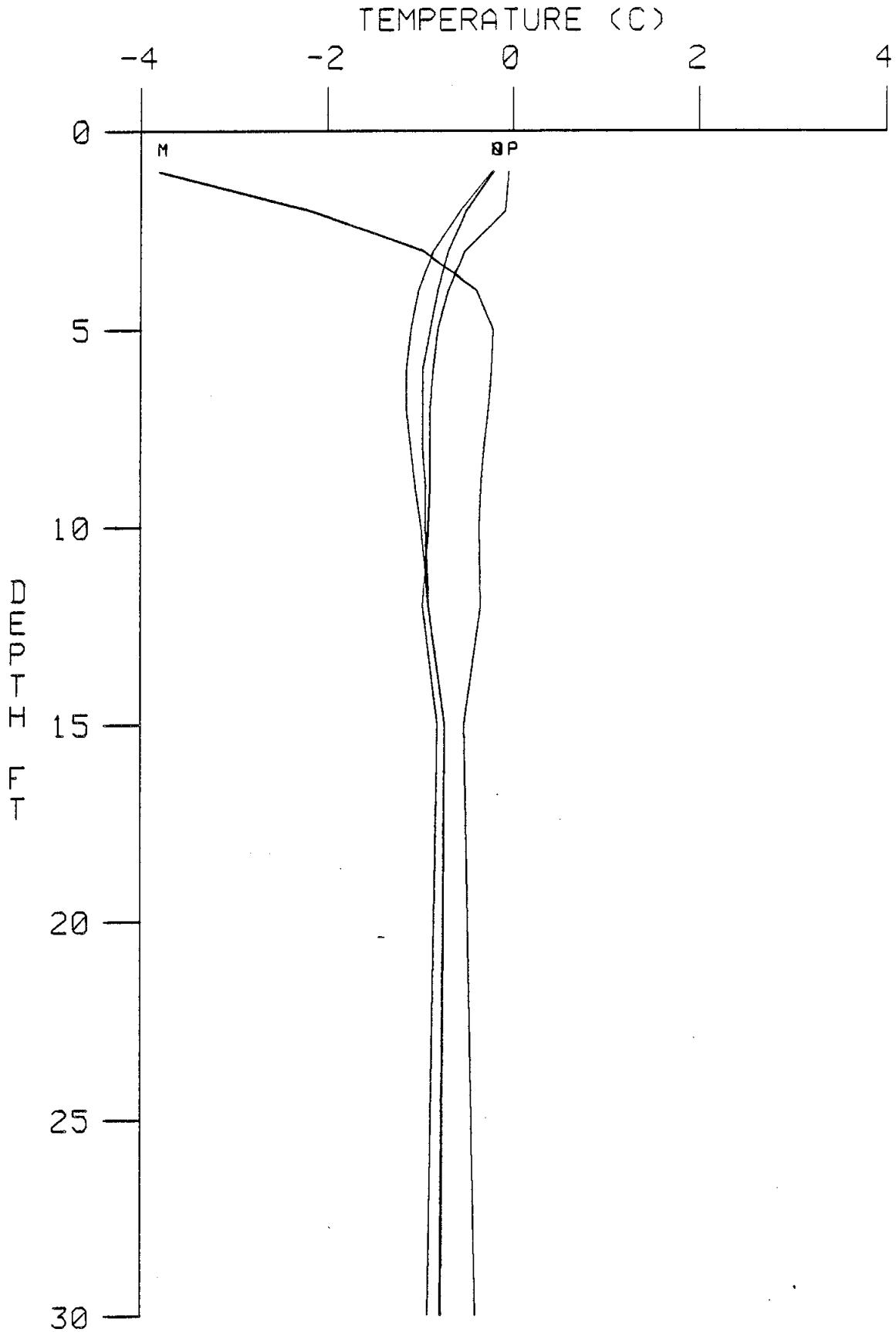

Figure 35. Measured temperature profiles for the CRREL study site near Fairbanks. M, February 25, 1982; N, May 11, 1982; O, May 21, 1982; P, June 4, 1982.

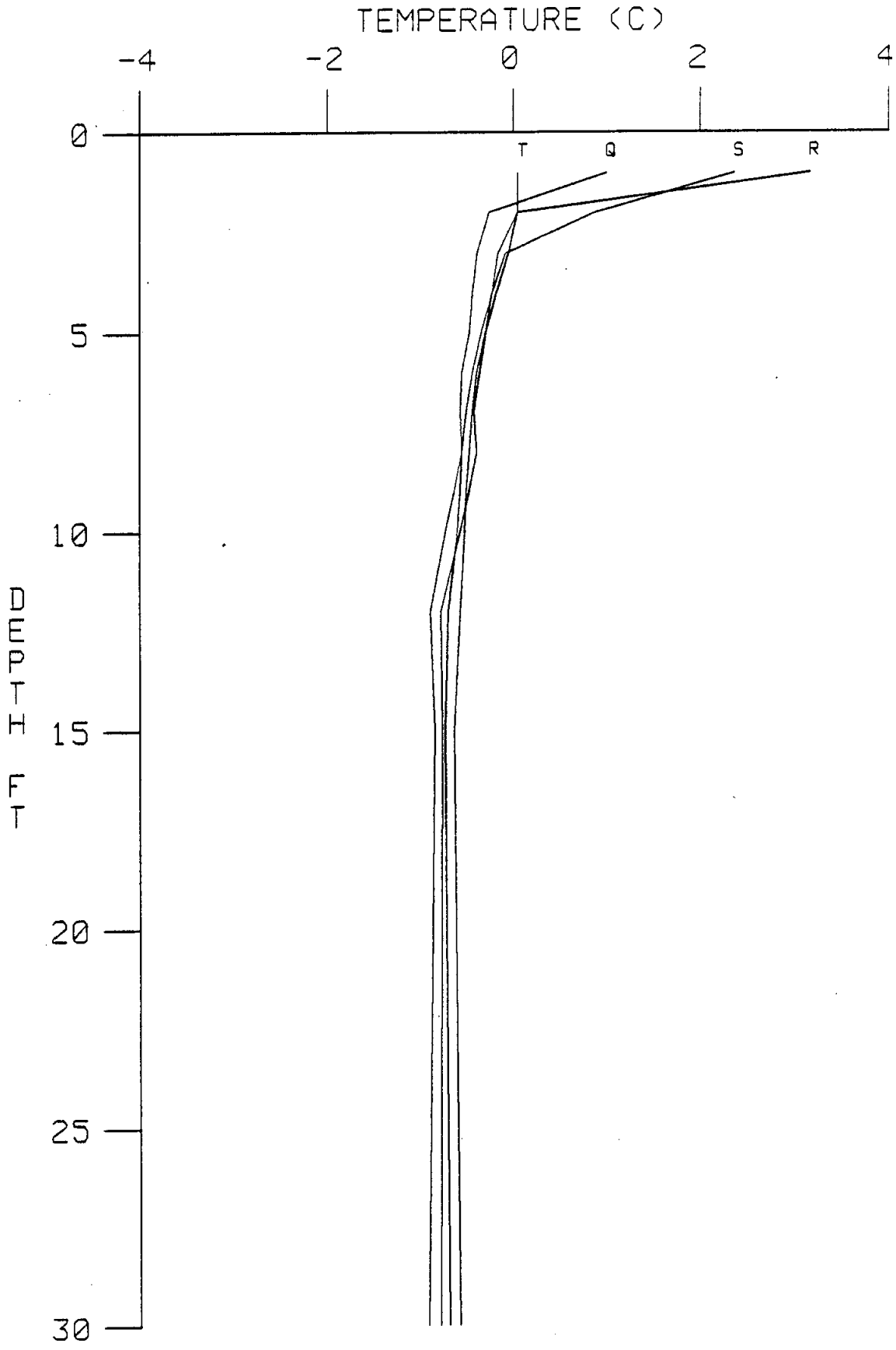

Figure 36. Measured temperature profiles for the CRREL study site near Fairbanks. Q, June 24, 1982; R, July 19, 1982; S, September 20, 1982; T, October 19, 1982.

Table 1

Dates of temperature measurements

Date	Symbol	Julian Day	Date of calculated temperatures
1/8/81	A	8	
3/4/81	B	64	3/4/81
3/23/81	C	83	
4/16/81	D	107	4/13/81
5/12/81	E	133	5/15/81
6/16/81	F	168	6/16/81
7/13/81	G	205	7/26/81
8/24/81	H	237	8/27/81
9/30/81	I	274	9/28/81
10/28/81	J	302	10/30/81
11/19/81	K	324	11/15/81
1/21/82	L	387	1/18/82
2/25/82	M	422	2/27/82
5/11/82	N	497	5/10/82
5/21/82	O	507	5/18/82
6/4/82	P	521	6/3/82
6/24/82	Q	541	6/27/82
7/19/82	R	566	7/21/82
9/20/82	S	629	9/23/82
10/19/82	T	658	10/17/82

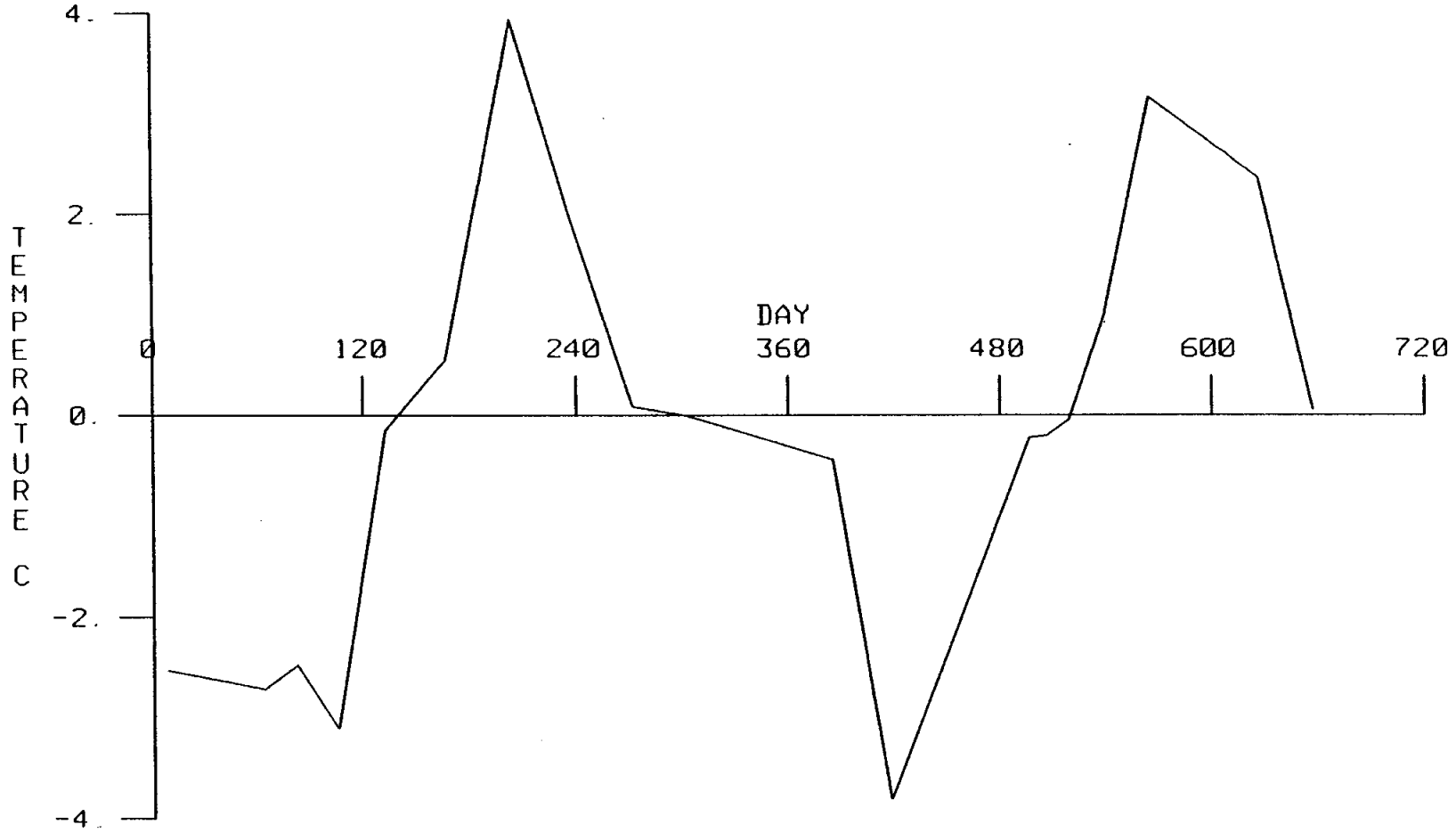

Figure 37. Measured temperatures at the one foot depth for the CRREL study site near Fairbanks. Time is measured from January 1, 1981.

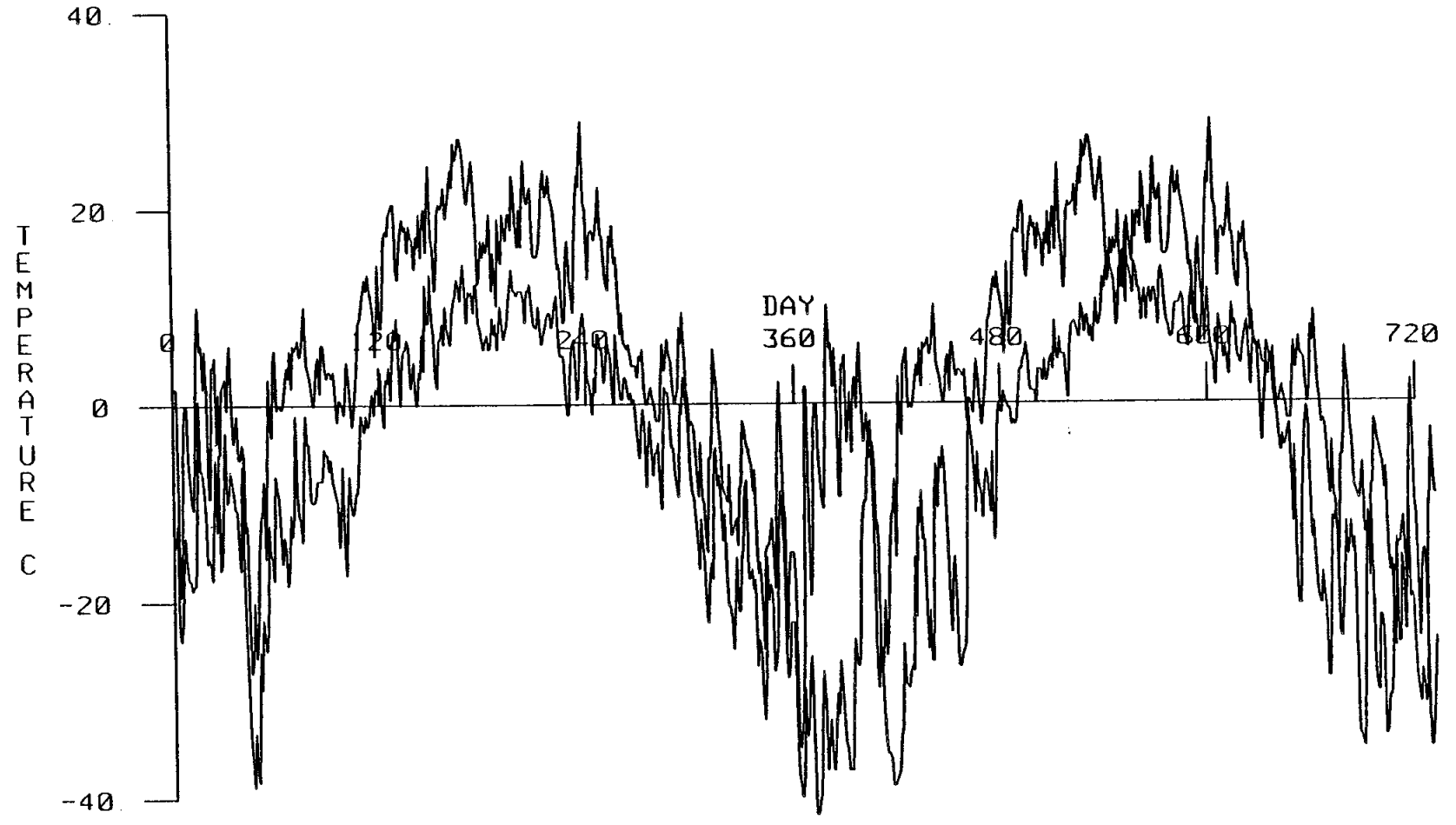

Figure 38. Measured maximum and minimum air temperatures at Fairbanks Airport from January 1, 1981 through December 31, 1982.

temperature near day 85. Another example is given by the unseasonably warm air temperatures near day 380. The measured ground temperatures show a "shoulder" of abnormally warm conditions lasting until about day 380. Near day 385, the air temperatures return to a more normal low followed by a rapid drop in surface ground temperature.

To establish the surface temperature boundary condition, both the measured ground temperature at the foot depth (Figure 37) and the measured air temperatures (Figure 38) were used. The magnitude of the imposed surface temperature was estimated from the one foot ground temperatures, and the phase from the air temperatures. In particular, the assumed surface boundary condition was:

$$T_s = -0.5 + 3.5 \sin [2\pi(t-130)/360]$$

where t is time in days.

The initial temperature condition is the initial measured temperature profile denoted by A in Figure 32. Soil properties were established from the data listed in Appendix B appropriate for Fairbanks silt. These are listed below:

K_H = 0.042 cm/hr (hydraulic conductivity)

n_k = 1.559 (pressure exponent in hydraulic conductivity expression)

A_k = 0.0583 $\cdot$ 10^{-2} (pressure coefficient in hydraulic conductivity expression)

θ_o = 0.407 (porosity)

n_θ = 0.782 (pressure exponent in soil moisture expression)

A_θ = 0.505 $\cdot$ 10^{-2} (pressure coefficient in soil moisture expression)

In addition to the soil properties found in Appendix B, two additional parameters, the residual unfrozen water content, r, and the hydraulic

conductivity attentuation factor, E, must be specified by the model user. A value of E = 10.0 was selected based on the numerical experimentation in the earlier sections of this report and on the calibrations in a report by Guymon et al., (1981) where E was determined to be 8.0 for Fairbanks silt. Varying E between 5.0 and 10.0 had little effect on the predicted temperatures over the relatively short calculation period (22 months). This is in contrast to the earlier calculations involving E. However, those test cases involved a five year calculation period with constant freezing surface temperature. The effect of E of ground temperatures increases with time, and may not be apparent in short term calculations.

The residual water content is the unfrozen volume of water per unit volume of soil remaining in the soil after freezing. In a laboratory study (Guymon et al., 1981), it was found to be about 0.045 for Fairbanks silt. Calculations were attempted with r = 0.04 and r = 0.05. This variation affected the temperature predictions, particularly at depth. When the smaller residual water content was used, the calculated temperature distribution at depth remained uniform, with T(y) = 0.0 for depths greater than about 5 meters. This temperature distribution was due to the slightly greater amount of available water in the soil. That is, the available water is equal to θ_o - r, and when the smaller residual water content was used, more water was available for phase change. Temperatures do not decrease below 0.0°C in the Guymon model until all the available water (greater than r) is frozen. This observation may provide a technique for "tuning" the model. When the unfrozen water content is not known, but detailed temperature distributions are available, variations in r will most significantly affect the deeper temperatures.

Both a pressure profile and an ice content profile must be specified as initial conditions in the Guymon mondel. However, this information was not available in the data, which consisted solely of measured temperatures. In addition, it was necessary to specify pressure boundary conditions throughout the calculation period. An initial water content profile is not specified in the Guymon model. Since the initial conditions (profile A in Figure 32) represent measured temperatures on January 8, 1981, it was assumed that no unfrozen water greater than r was present in the soil. Furthermore, it was assumed that the ice content was uniform at that time. This implies that the initial ice content (volumetric) was given by

$$\theta_i = \rho_w (\theta_o - r)/\rho_i = 1.09 (0.407-0.05) = 0.389$$

where ρ_w and ρ_i are the densities of water and ice, respectively. This proved to be an inappropriate assumption, resulting in errors which will be discussed subsequently.

The initial ice distribution was used to determine the initial pressure profile by the following procedure. When the soil is freezing, the relationship between pore pressure and water content in the Guymon model is specified by the Gardner expression:

$$\theta = \frac{\theta_o}{A_\theta \Psi^n \theta + 1}$$

where Ψ is the absolute value of the pressure or the soil tension and θ is moisture content. For a known soil moisture content, the above expression can be inverted to determine soil tension. When all available moisture is frozen and $\theta = r$, then $\Psi = \Psi_{max}$; Ψ_{max} was the initial value of soil tension

prescribed in this test case. For times greater than zero, it was assumed that the pressure gradient boundary condition at 15 m depth was zero. This is equivalent to the assumption of zero moisture flux at the bottom boundary.

The grid for the present example is similar to that in Figure 1. Therefore, as in the earlier test cases, three temperature values are computed at each depth. Some variation of these three temperatures appears in the calculated profiles, particularly near the phase front.

The comparisons between calculated and measured temperatures are presented in Figures 39-56. The first three figures, 39, 40 and 41, contain the greatest error and should be considered together. Figure 39 displays measured and calculated temperatures for March 4, 1981. Figure 40 displays measured temperatures on April 16, 1981 and calculated temperatures for April 13th. (Calculation output was set at every 8 days). Figure 41 presents measured temperatures for May 12, 1981 and calculated temperatures for May 15th. Calculated temperatures, especially at depth, are substantially below measured temperatures. We believe that this is due to the initial assumption of no available unfrozen water ($\theta - r = 0.0$). Heat loss from the soil could only result in a temperature reduction, since no latent heat was available. We expect that if the actual initial values of θ and/or θ_i were known, that the agreement between calculated and measured temperatures would substantially improve. The cold temperatures measured near the soil surface on April 16 (Figure 40) probably reflect the cold air temperatures recorded in late February (see Figure 38). The assumption of a simple sinusoidal boundary temperature has been violated by the cold February and March air temperatures. It should be noted that altering the model to admit general boundary temperatures is a relatively minor project.

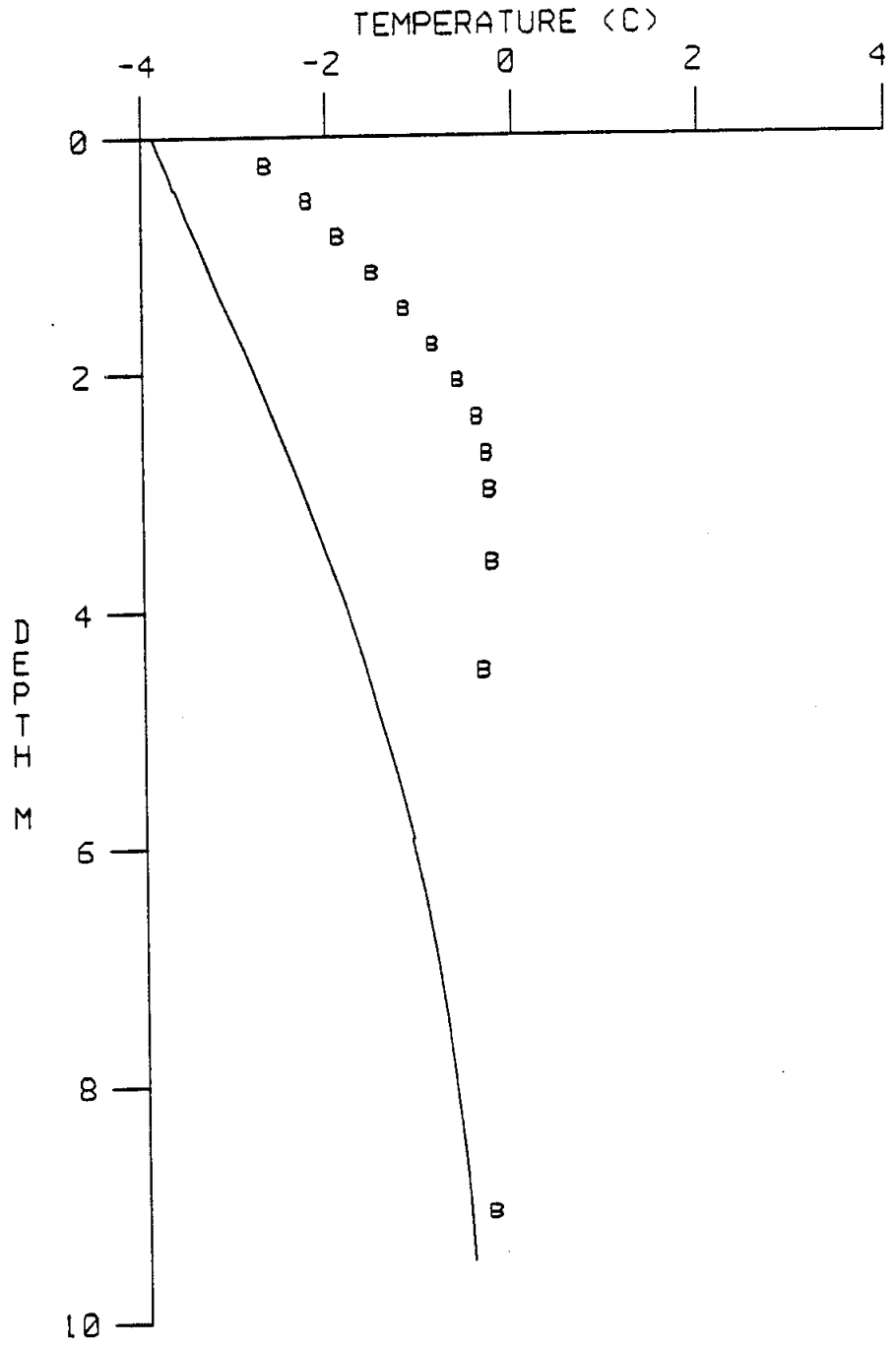

Figure 39. Comparison of measured and calculated (Guymon model) temperatures for March 4, 1981.

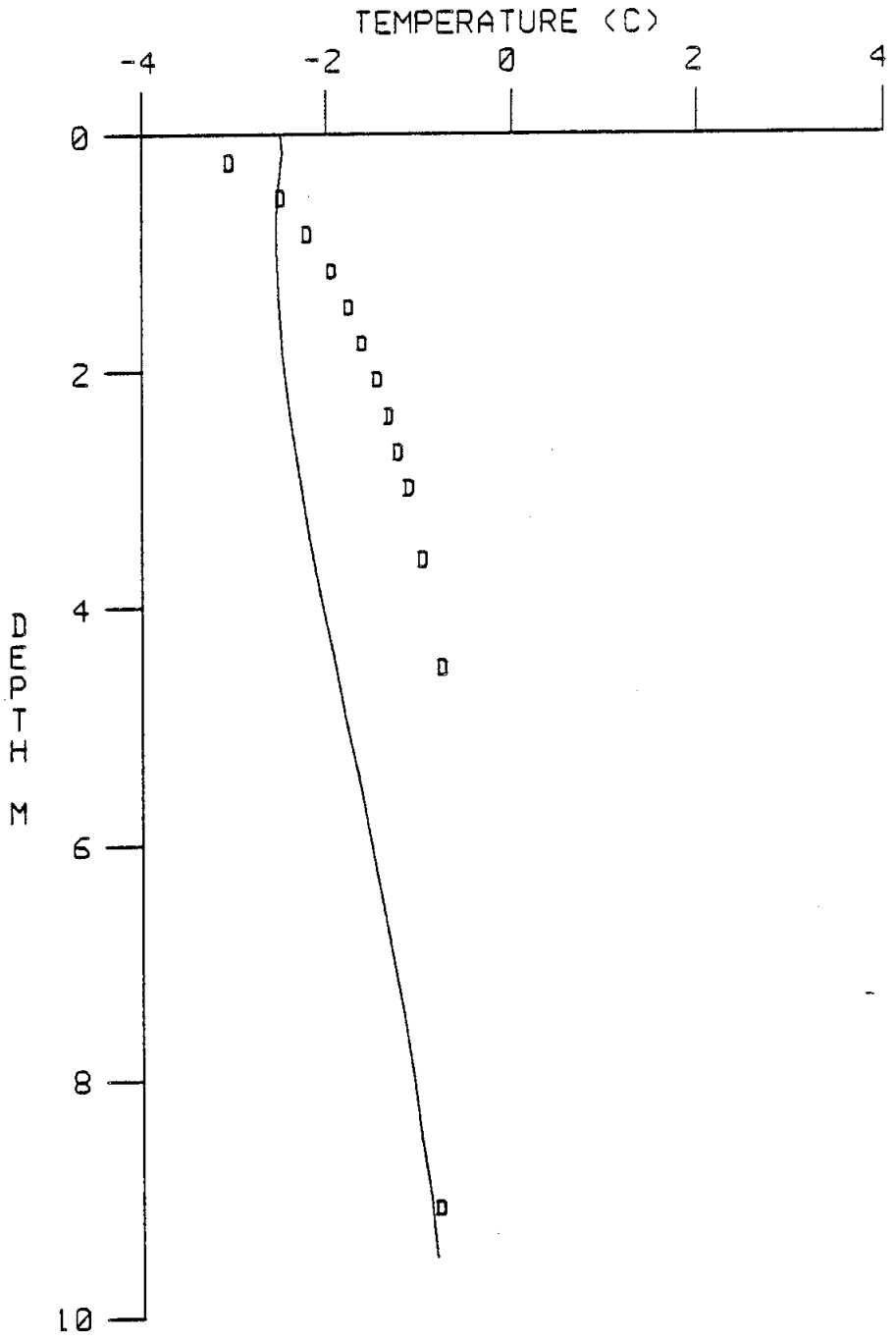

Figure 40. Comparison of measured and calculated (Guymon model) temperatures for April 16, 1981.

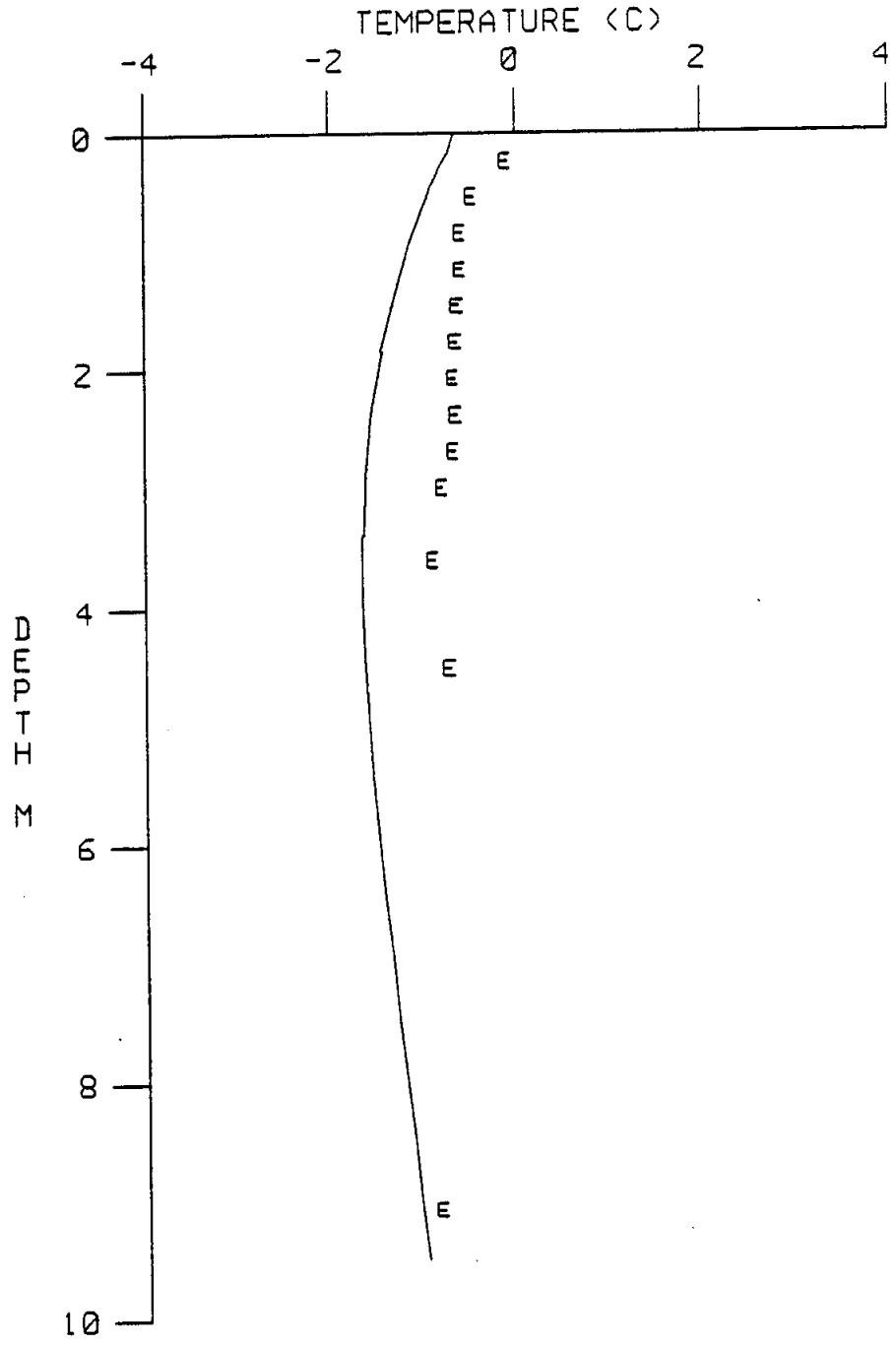

Figure 41. Comparison of measured and calculated (Guymon model) temperatures for May 12, 1981.

The calculated and measured temperatures for June 16, 1981 are presented in Figure 42. Here the agreement is substantially improved. Air temperatures (see Figure 38) for the most part followed a sinusoidal curve from about day 120 (May 1, 1981) to day 360 (December 26, 1981), implying that the assumed boundary condition was reasonable. In fact, all profiles for this period, Figures 42-47, with exception of Figure 45, indicate good agreement between predicted and measured temperatures. Figures 43 and 44 compare predicted and measured temperatures near days 205 (July 23rd) and 237 (August 24th), respectively. The agreement is better for day 205 (Figure 43). The soil was a little cooler than predicted on day 237 (Figure 44). This might be due to the slight lowering of the minimum air temperatures near day 230 (see Figure 38). By day 274 (September 30th) both maximum and minimum air temperatures are somewhat below a standard sinusoidal curve. Consequently, the match between predicted and measured temperatures is poor for September 30, 1981 (see Figure 45). The position of the freeze front is significantly overpredicted at about 1.2 m vs. the actual 0.6 m. On days 302 (October 28, 1981) and 324 (November 19, 1981), shown in Figures 46 and 47, respectively, the agreement between measured and calculated temperatures is again quite good. Note that the maximum temperature deviation at depth on day 302 is about 0.25°C.

The agreement between measured and predicted temperatures for days 382 (January 21, 1982) and 422 (February 25, 1982), shown in Figures 48 and 49, respectively, is very poor. Presumably the period of abnormally warm maximum air temperatures between about day 360 and day 460 (see Figure 38) has decreased soil freezing substantially. Note that the superposition of Figures 48 and 49 demonstrate that the predicted temperatures for January 21, 1982 match reasonably well with the measured temperatures for February

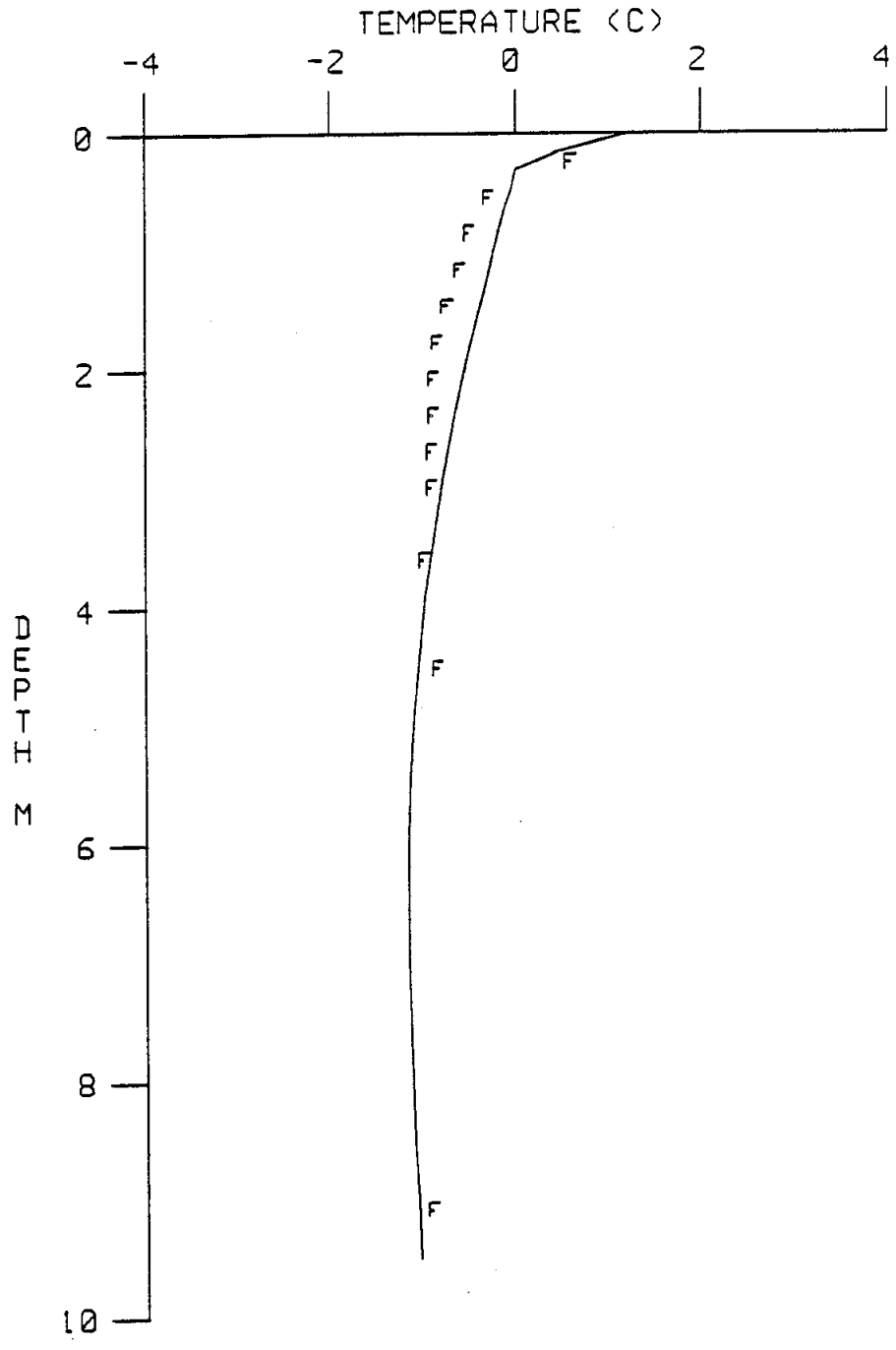

Figure 42. Comparison of measured and calculated (Guymon model) temperatures for June 16, 1981.

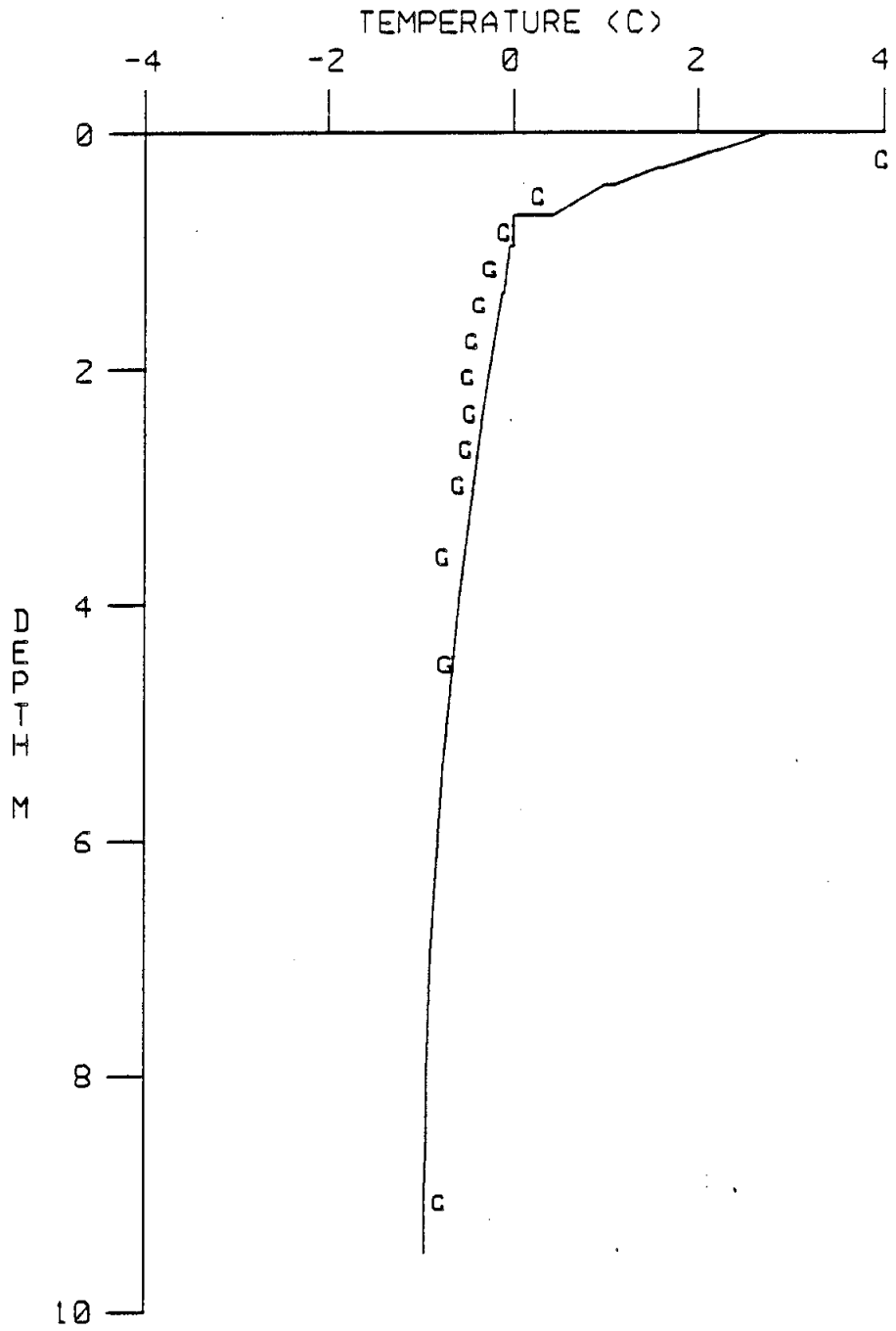

Figure 43. Comparison of measured and calculated (Guymon model) temperatures for July 23, 1981.

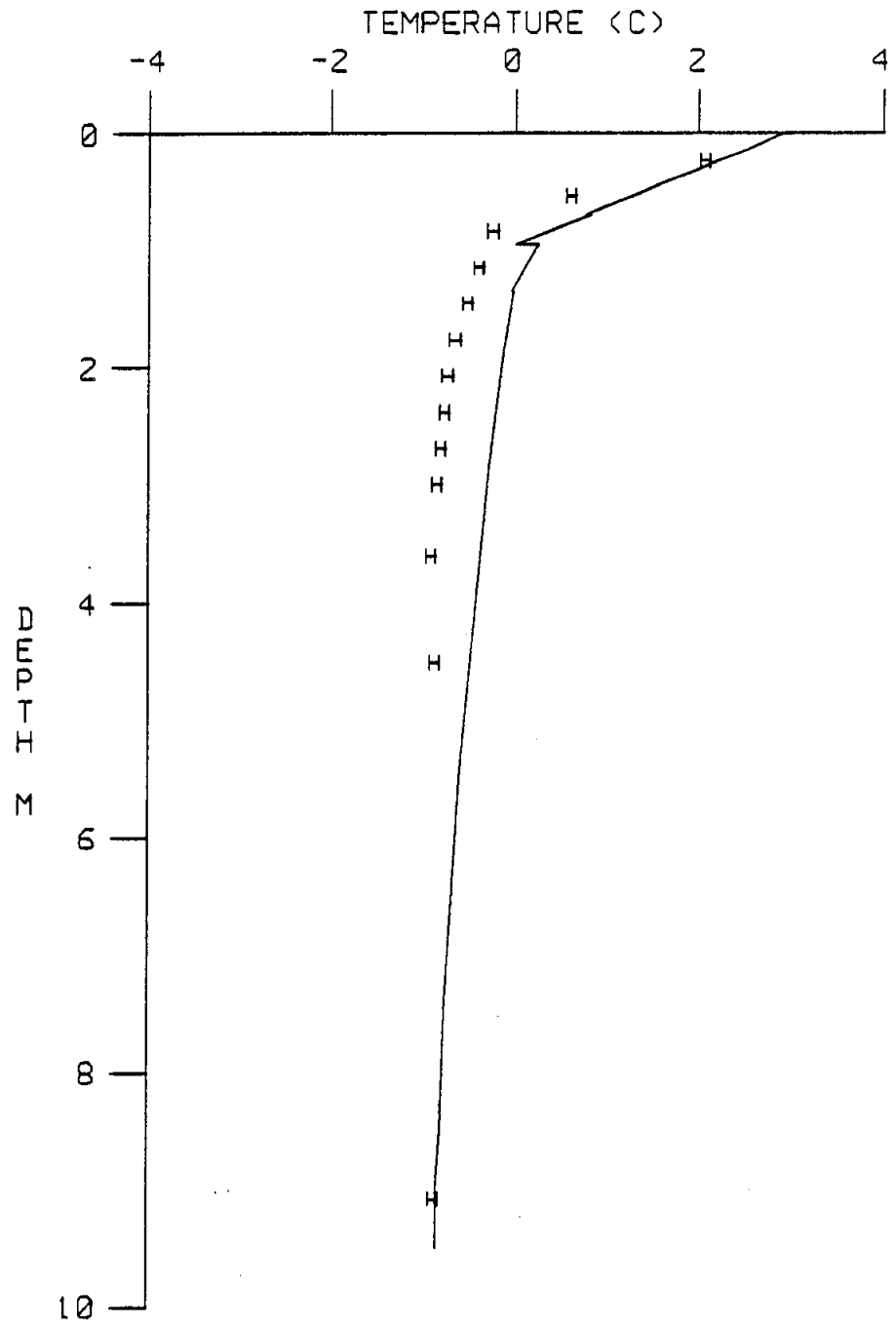

Figure 44. Comparison of measured and calculated (Guymon model) temperatures for August 24, 1981.

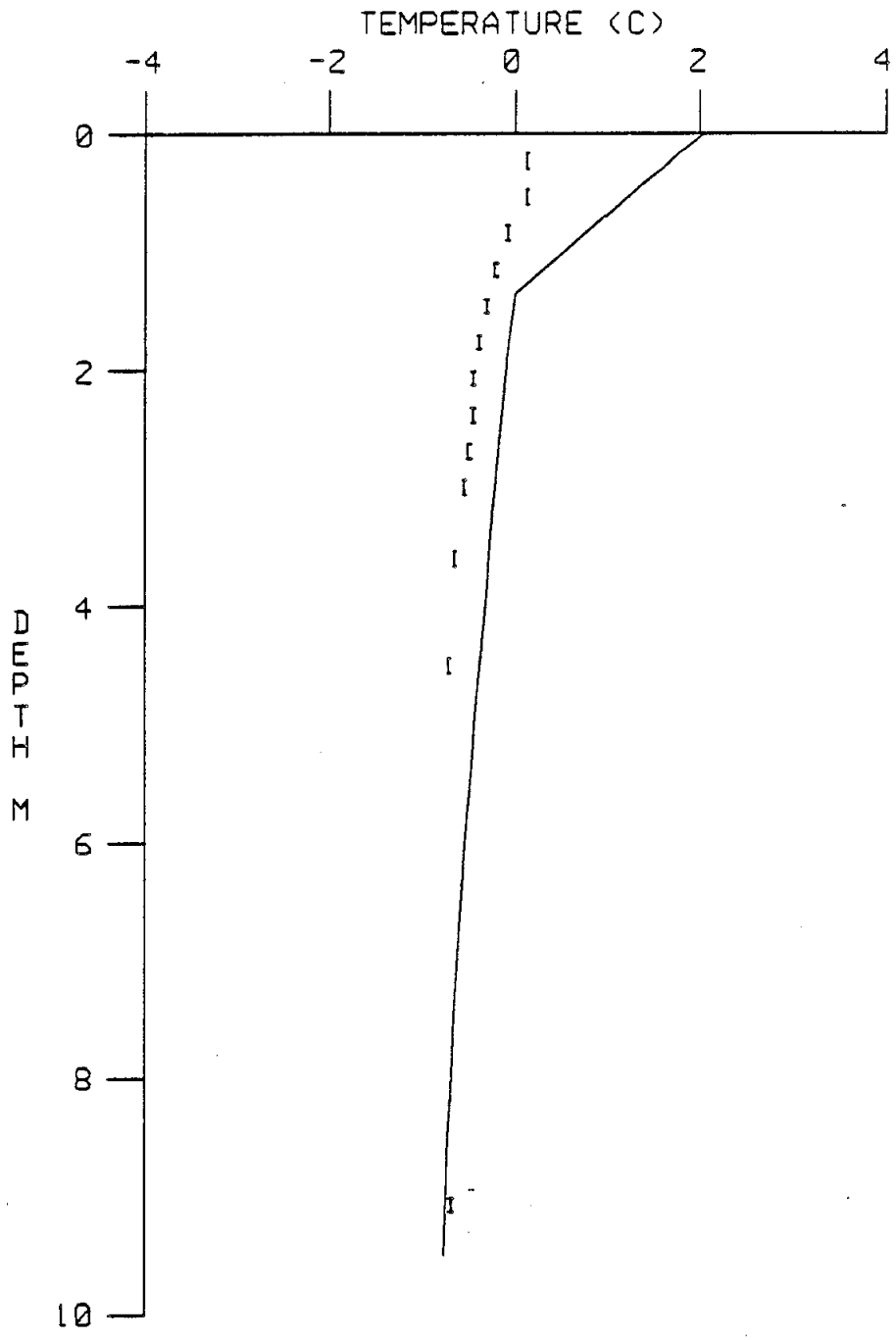

Figure 45. Comparison of measured and calculated (Guymon model) temperatures for September 30, 1981.

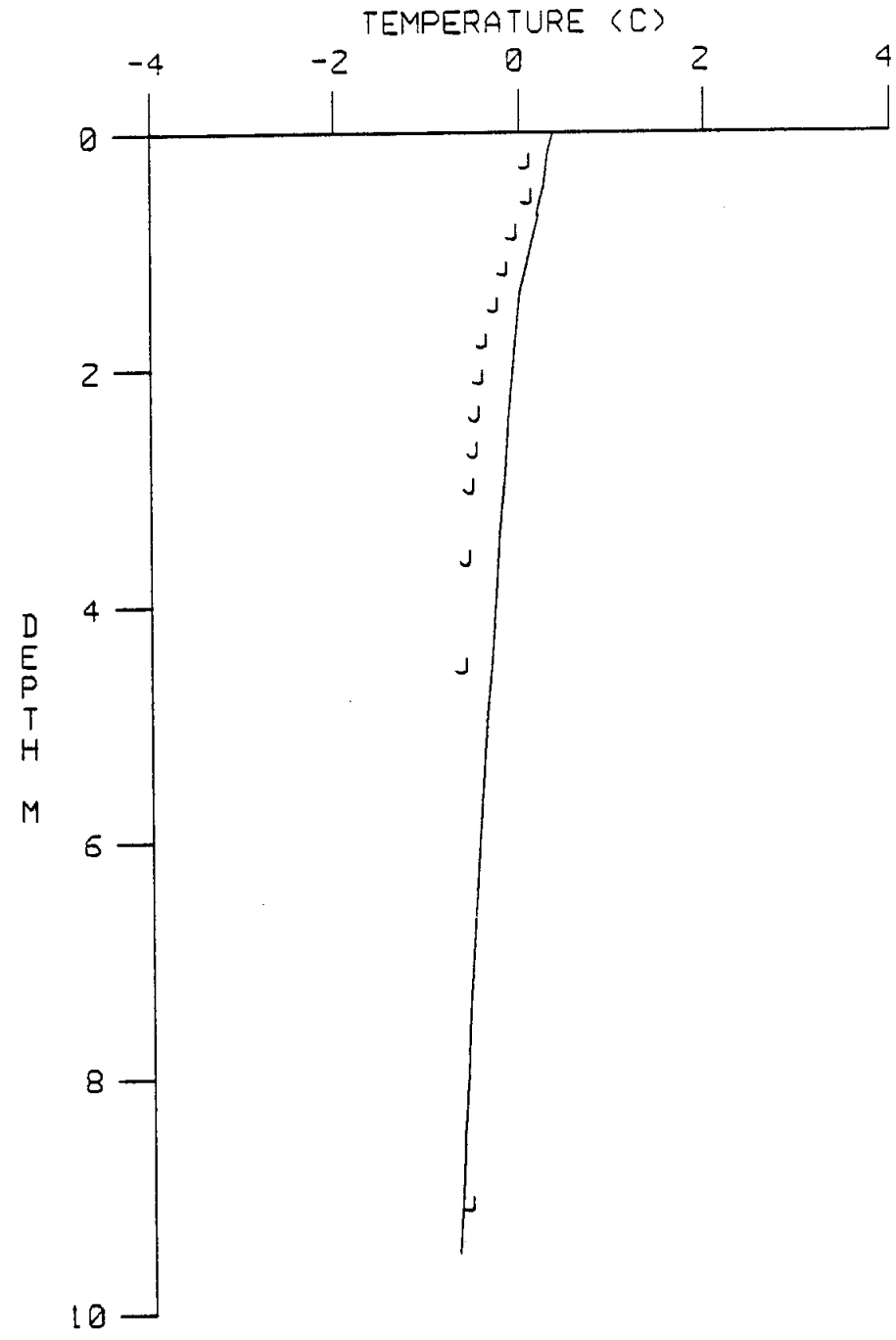

Figure 46. Comparison of measured and calculated (Guymon model) temperatures for October 28, 1981.

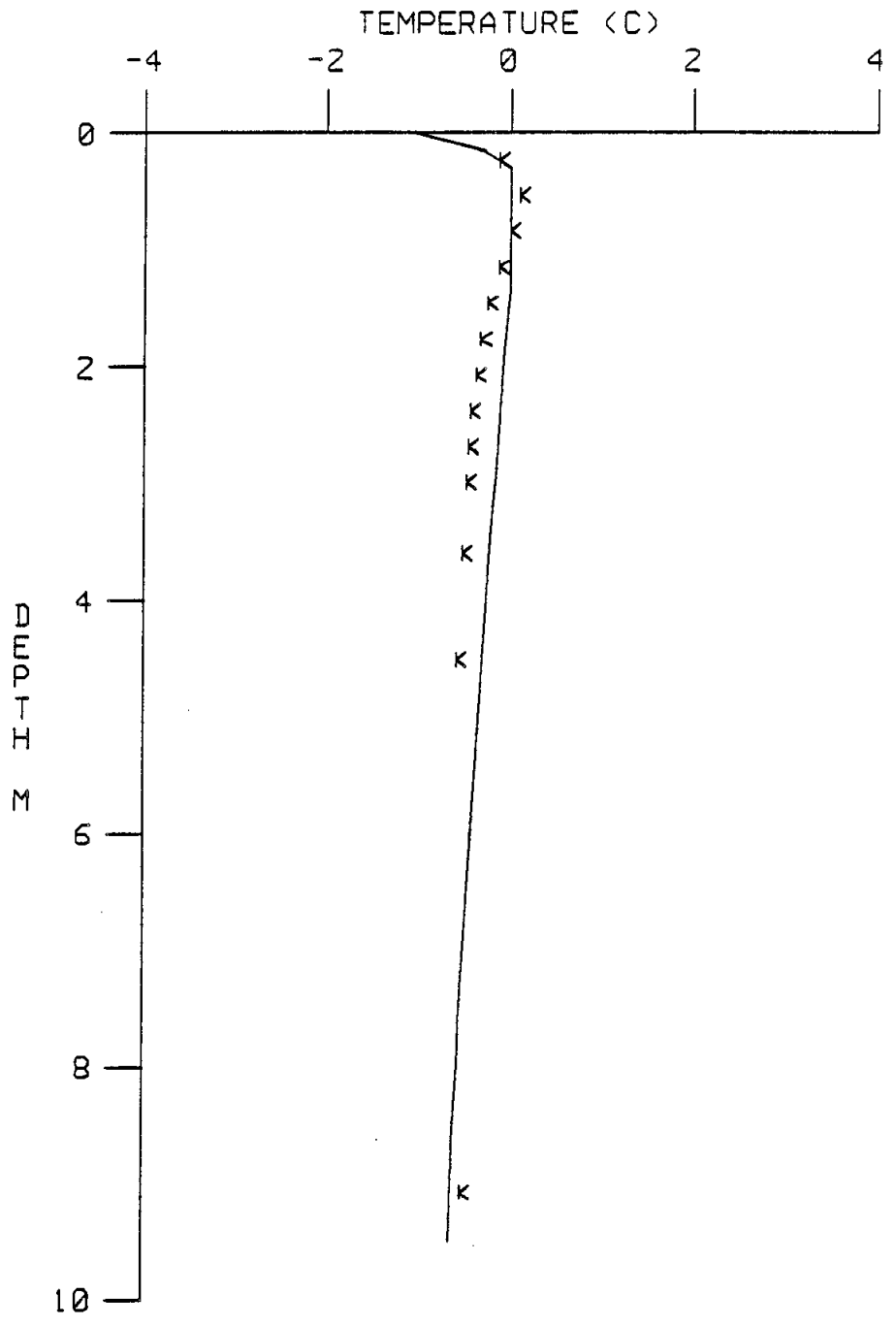

Figure 47. Comparison of measured and calculated (Guymon model) temperatures for November 19, 1981.

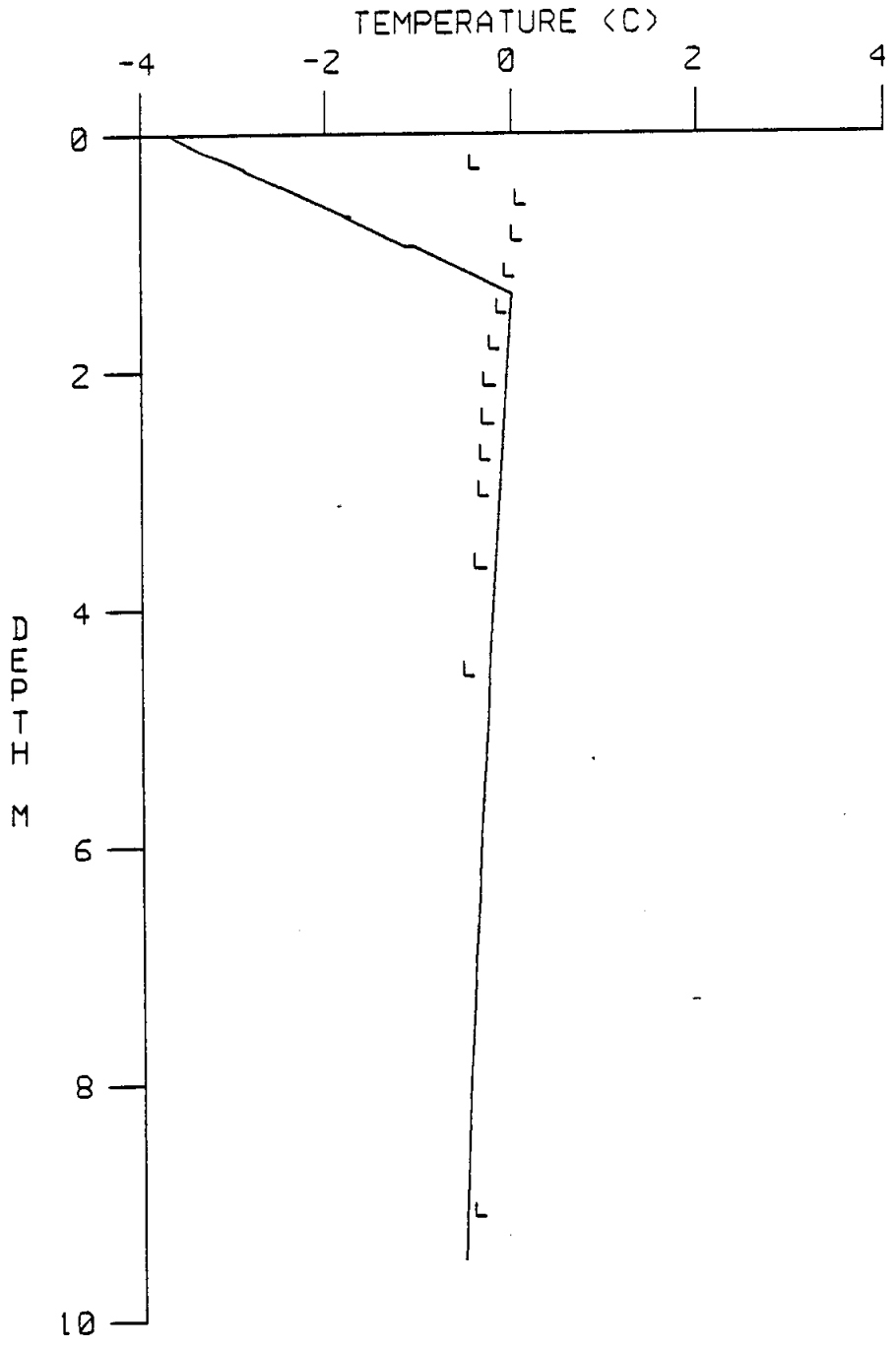

Figure 48. Comparison of measured and calculated (Guymon model) temperatures for January 21, 1982.

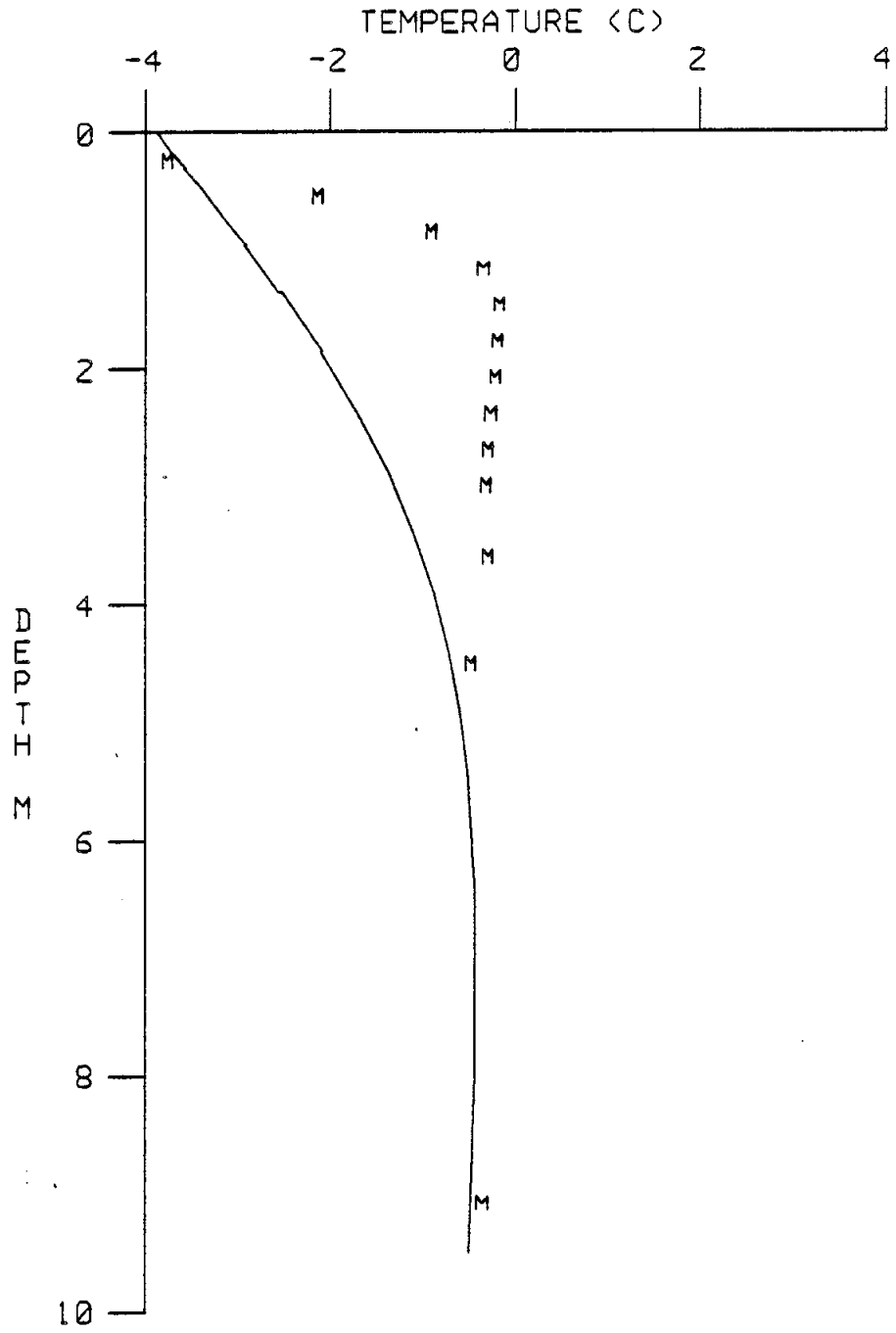

Figure 49. Comparison of measured and calculated (Guymon model) temperatures for February 25, 1982.

25, 1982, indicating soil freezing has been delayed almost a whole month by the warmer air temperatures.

Air temperatures tend to approximate a standard sinusoidal curve between day 470 and day 650 (see Figure 38). During this period the agreement between predicted and measured soil temperatures is quite good. This time period includes the remaining profiles: day 497 (May 11, 1982) on Figure 50, day 507 (May 21, 1982) on Figure 51, day 521 (June 4, 1982) on Figure 52, day 541 (June 24, 1982) on Figure 53, day 566 (July 19, 1982) on Figure 54, day 629 (September 20, 1982) on Figure 55, and day 658 (October 19, 1982) on Figure 56.

The first profile of the above group, day 497 on Figure 50, shows the persistence of the cooler calculated soil temperatures from the previous months. As indicated earlier, the disagreement between measured and calculated temperatures is almost certainly due to the inadequacy of the sinusoidal surface boundary condition. On day 507 (Figure 51) predicted temperatures begin to approach the measured values, although there is still substantial (about 0.5°C) difference at depth. Calculated temperatures on days 521, 541 and 566 on Figures 52, 53 and 54, respectively, are in very good agreement with measurements. These three figures demonstrate the variability of the calculated temperatures at the same depth. For example, in Figure 52 the computer solution at the 0.15 m depth produced temperatures ranging between 0.0°C and 0.5°C. The location of this type of perturbation appears to be consistently just above the freeze front position and is probably associated with the very sensitive moisture content calculation and its dependence upon pore pressure.

In Figures 54 and 55, the position of the freeze front has been overestimated by about 0.4 m. Note that the freeze front position for summer

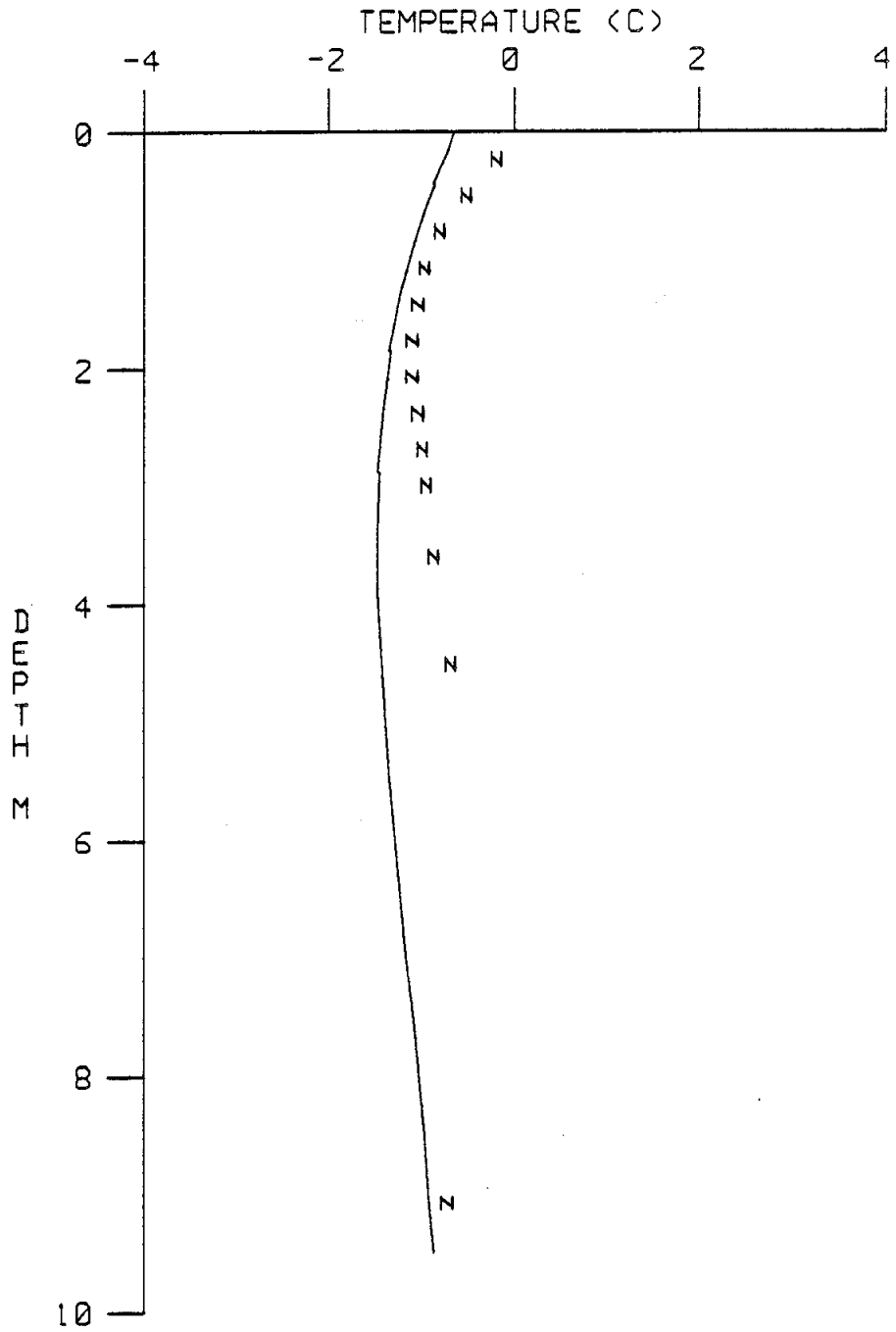

Figure 50. Comparison of measured and calculated (Guymon model) temperatures for May 11, 1982.

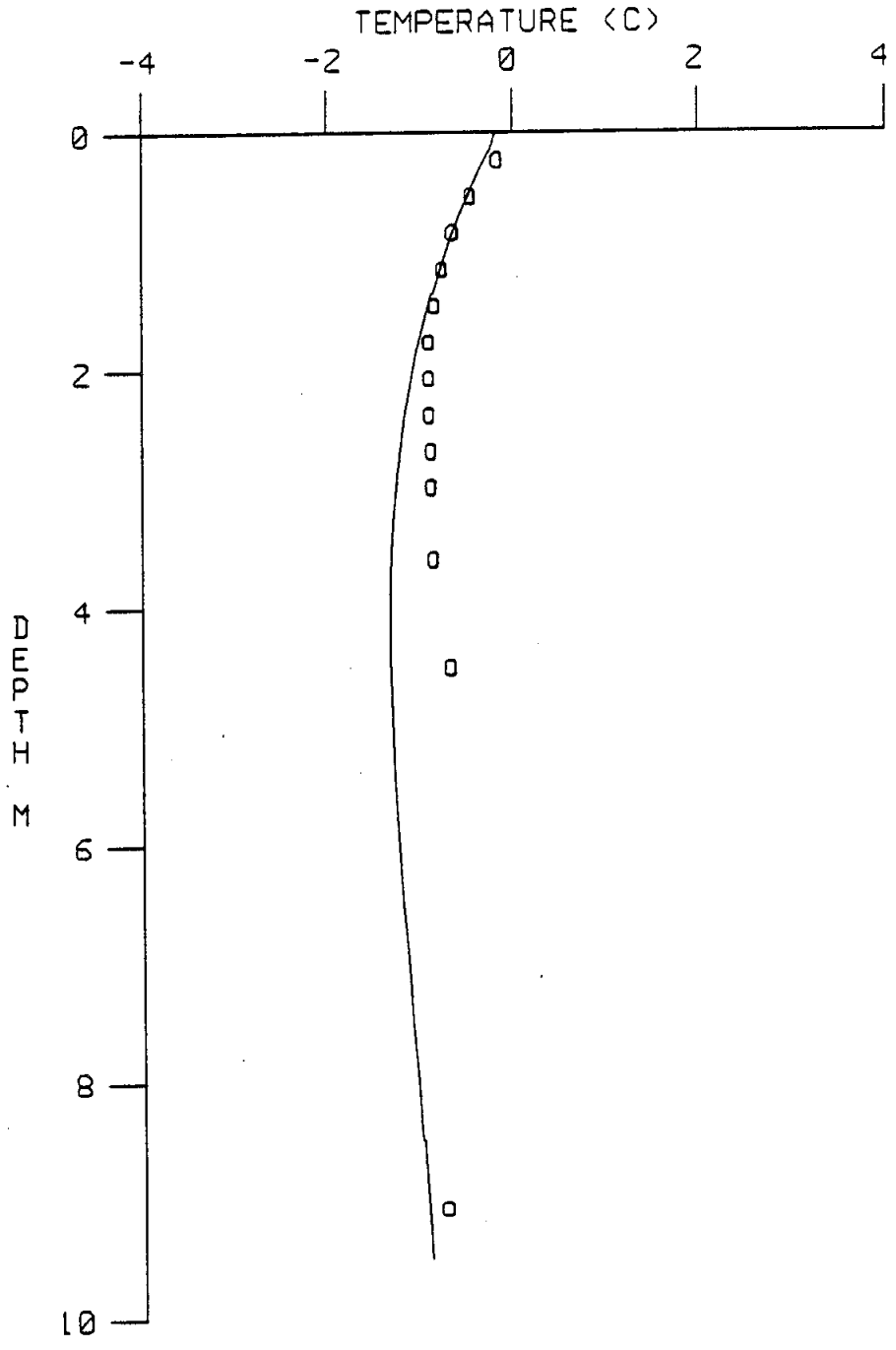

Figure 51. Comparison of measured and calculated (Guymon model) temperatures for May 21, 1982.

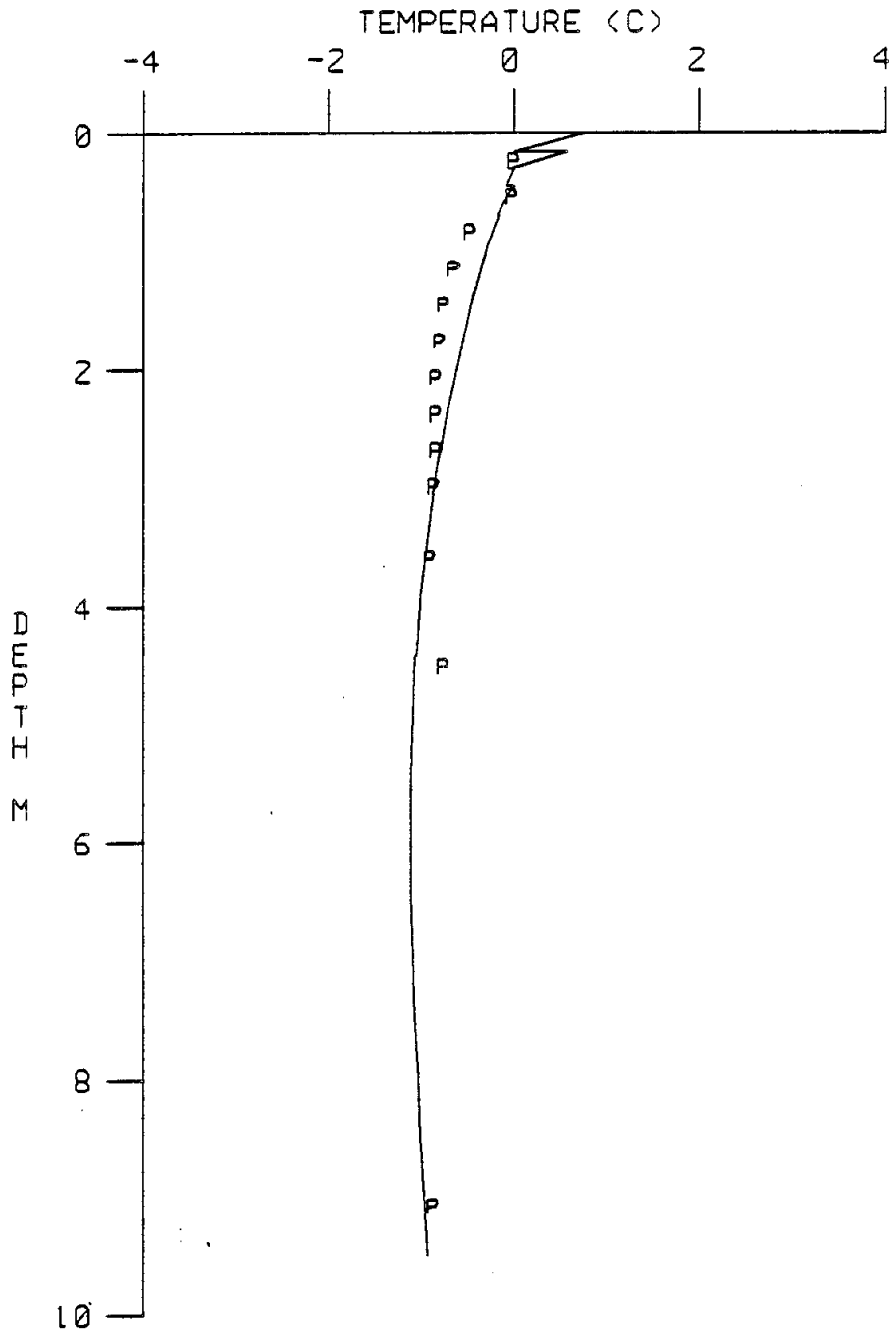

Figure 52. Comparison of measured and calculated (Guymon model) temperatures for June 4, 1982.

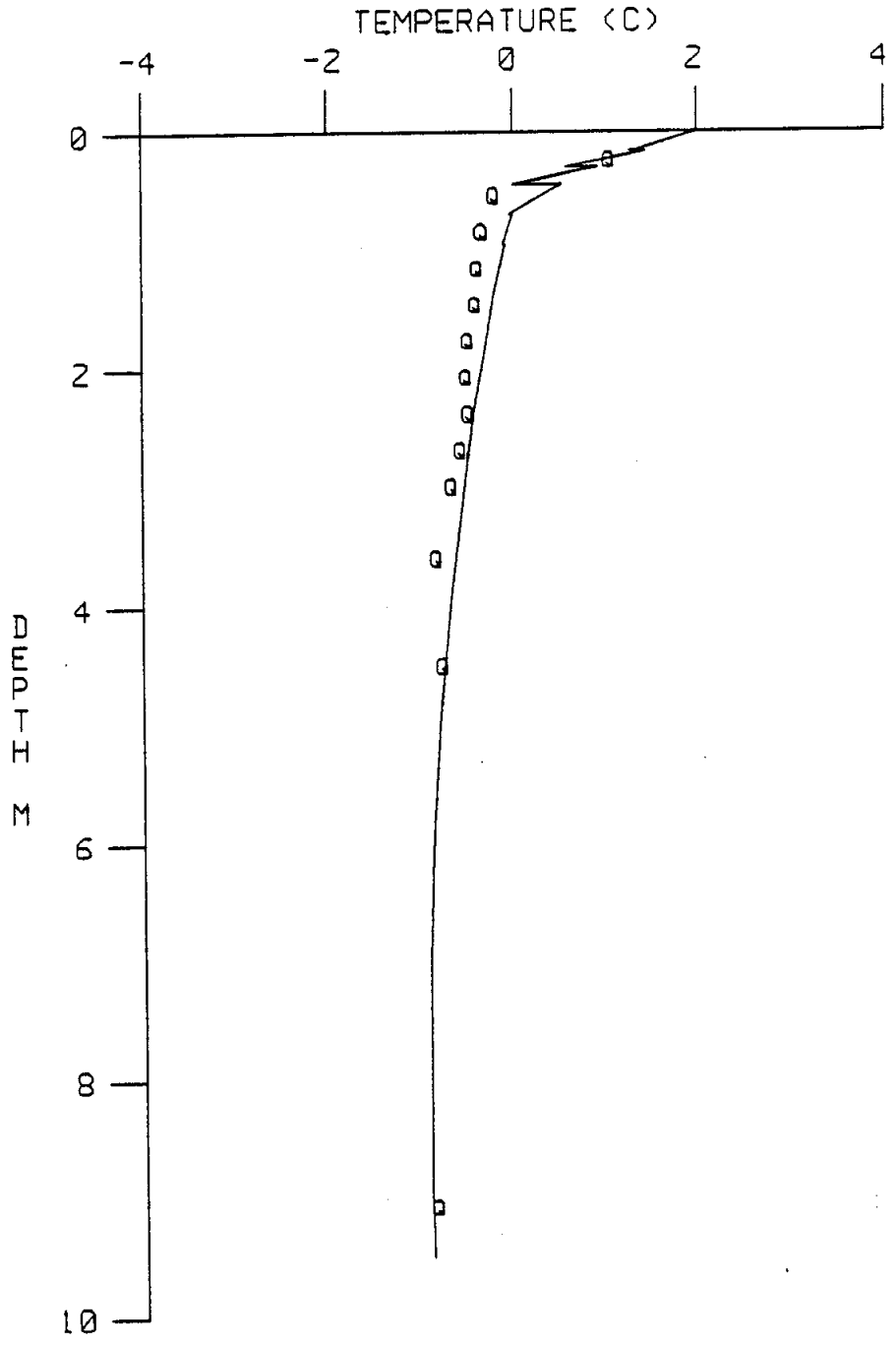

Figure 53. Comparison of measured and calculated (Guymon model) temperatures for June 24, 1982.

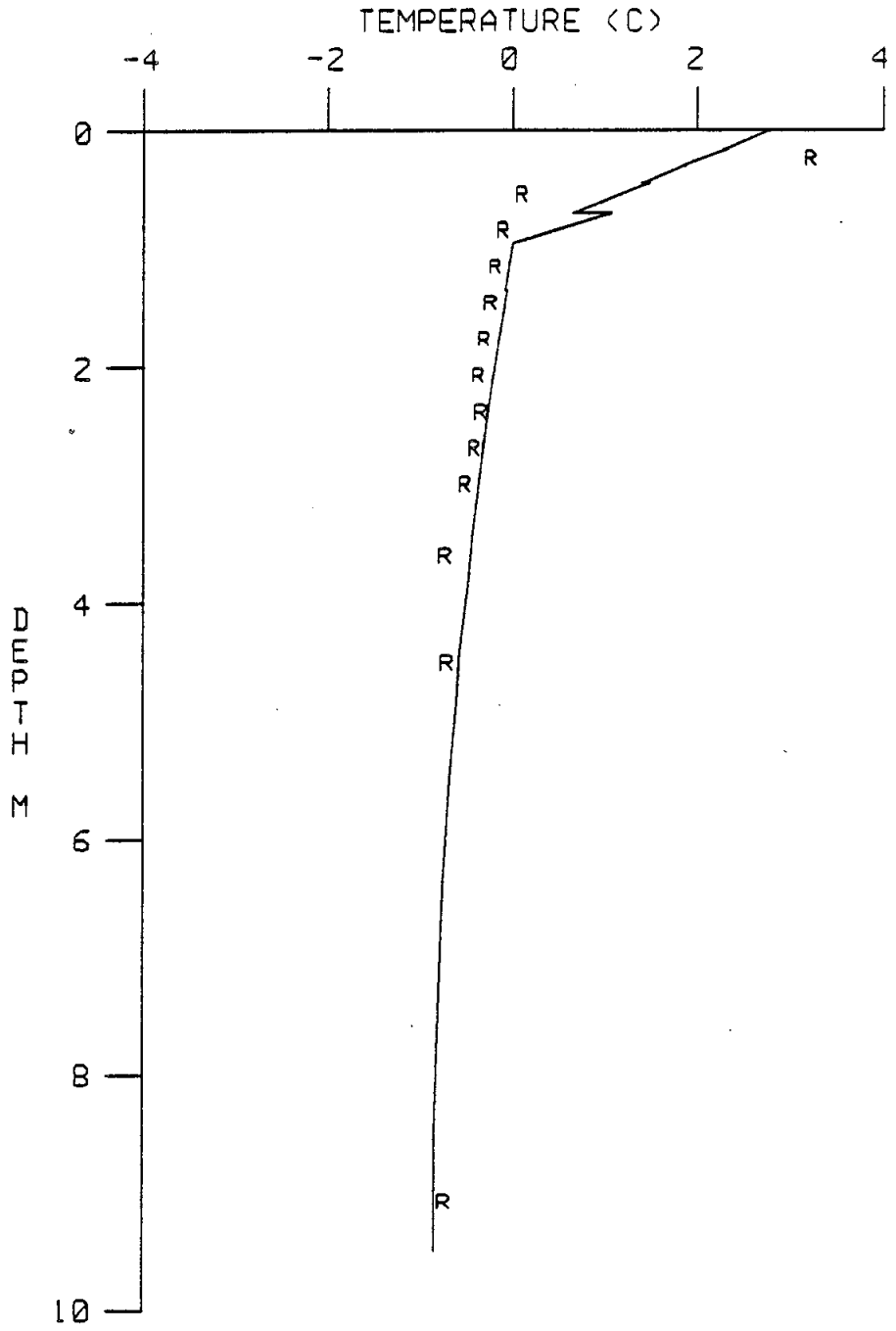

Figure 54. Comparison of measured and calculated (Guymon model) temperatures for July 19, 1982.

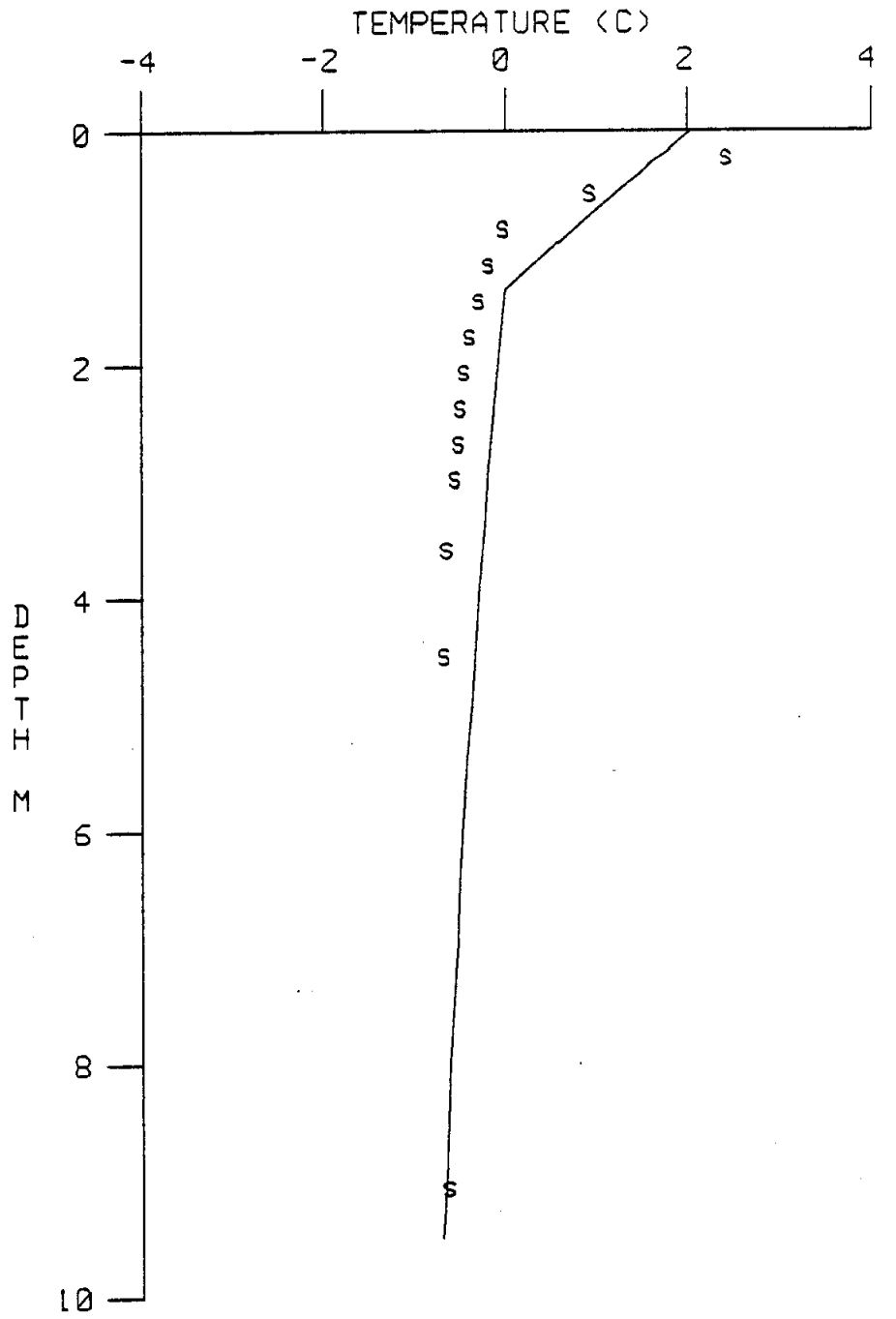

Figure 55. Comparison of measured and calculated (Guymon model) temperatures for September 20, 1982.

and late summer was also overestimated during the previous year (see Figures 44, 45 and 46). This may be due to an inappropriately high maximum temperature assumption for the surface boundary condition.

Figure 56 presents the comparison between measured and calculated temperatures on day 658 (October 19, 1982). The agreement is quite good with a maximum deviation of about 0.25°C.

In summary, the agreement between predicted and measured temperatures was generally good when the air temperatures appeared to follow a standard sinusoidal curve. When air temperature deviated substantially from this curve, the agreement between predicted and measured soil temperatures was very poor. This observation clearly demonstrates the need to include a variable surface condition into the Guymon model. The simplest and most convenient format appears to be a functional dependence on air temperatures, e.g., via n-values or a simplified surface flux balance. A reasonable next step would be to attempt to model the present data set with an air-temperature dependent boundary condition. However, the difficulty associated with an unknown initial ice content profile should not be overlooked. If a complete data set is to be assembled for model testing and verification, it must contain not only soil temperatures and meteorological data, but also soil ice content, and those soil properties defined in Appendix B of the report.

Summary and Conclusions

Both the Goodrich and the Guymon/Hromadka models have limitations which require resolution before use as a general purpose engineering design tool. The Goodrich model is severely limited by the fact that it is one-dimensional; effectively this precludes its use for engineering design involving two-dimensional problems. Furthermore, the Goodrich model solves

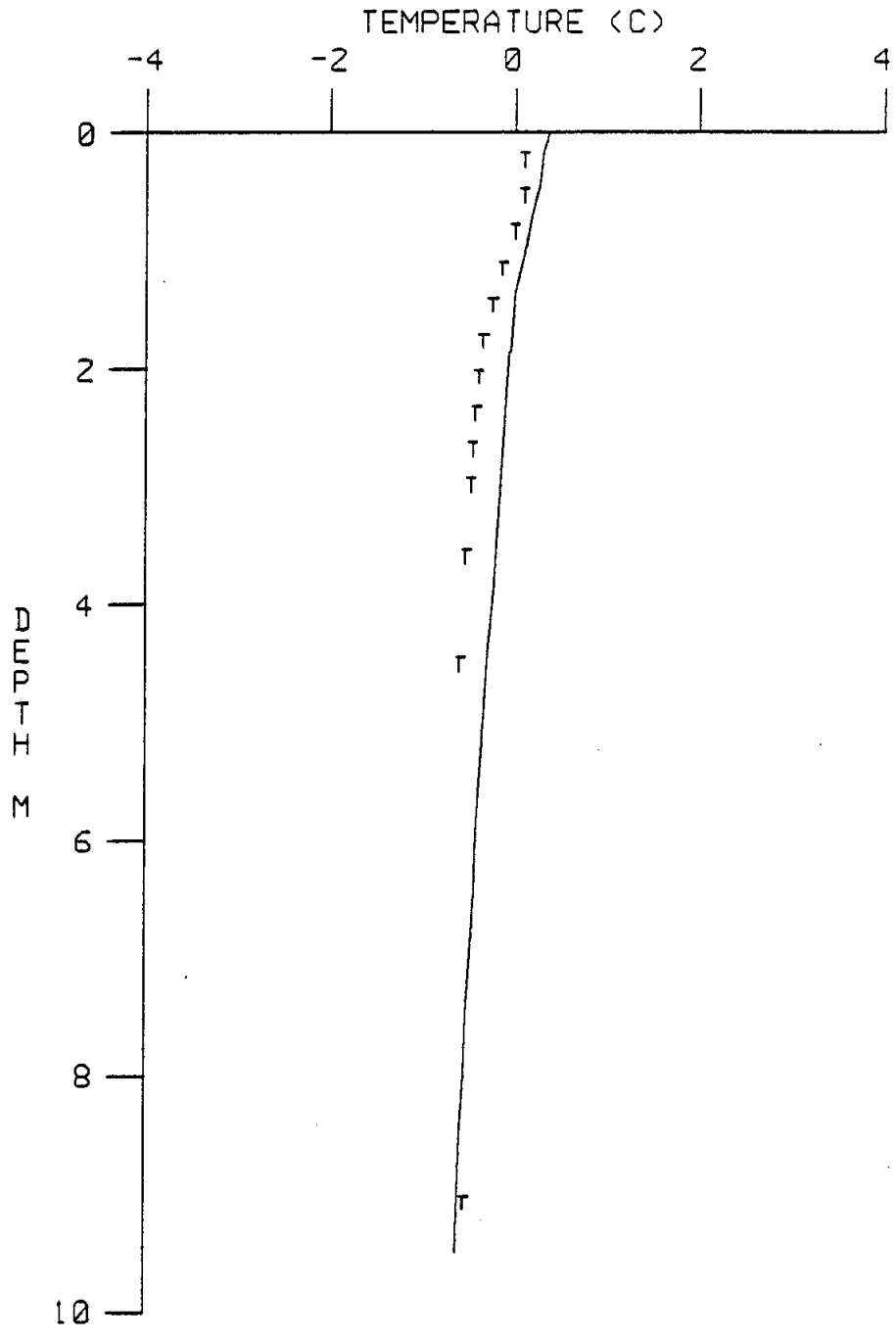

Figure 56. Comparison of measured and calculated (Guymon model) temperatures for October 19, 1982.

only the heat transport equation, permitting variations in soil moisture and other parameters via empirical formulas such as those given by DeVries, Kersten and Anderson. However, this model is particularly versatile with respect to choice of empirical expressions for soil moisture terms, surface flux and heat balance, snow conductivity formulations, internal mesh generation, and simplicity of application.

In contrast, the Guymon/Hromadka model solves both the heat transport equation and the soil water potential equation, employing a generalized Gardner-type formulation of hydraulic conductivity and soil moisture. The versatility comes in the form of the selection of coefficients and exponents in the Gardner expressions. There is an undeniable advantage in the inclusion of a soil pressure head or potential equation, in that rates of change of soil potential are calculated independently, but coupled to, rates of change of soil temperature. This implies that regions with severe moisture gradients will not inevitably produce anomalous behavior in temperature gradients (Hromadka, Guymon and Berg, 1981). In addition, the separation of the two variables, pressure head or moisture and temperature allows distinct and separate boundary conditions to be specified for each of the variables.

Both the Goodrich and the Guymon/Hromadka numerical schemes are convergent, stable over long simulations and relatively efficient. Both employ direct matrix solution techniques, eliminating errors due to convergence which are characteristic of iterative techniques. There is a real need to determine the long-term performance of models with iterative solution techniques such as Geodyn.

The Guymon/Hromadka model does lack a feature useful for simulating Alaskan soils, i.e., surface heat flux balance or specified non-zero heat flux. The model can be modified to include this feature without extensive

change. Furthermore, use of the Guymon/Hromadka model requires specification of five or six empirical coefficients. These coefficients are only imprecisely defined, thereby making application of the model complex. However, this approach, the "second method", involving solution of separate partial differential equations for heat and moisture transport, has the greatest potential for the solution of a wide range of problems including saturated and unsaturated soils, the presence of overburden, seepage and a moving freezing front. In ending, we note some detailed comments on the Guymon/Hromadka model are included in Appendix A which will allow straightforward implementation of the model by a user.

REFERENCES

Anderson, D. M. and N. R. Morgenstern, 1973. Physics, chemistry and mechanics of frozen ground, Proceedings of the Second International Conference on Permafrost, Yakutsk, U.S.S.R., p. 257-288, July 13-28, 1973.

Anderson, D. M. and A. R. Tice, 1972. Predicting unfrozen water contents in frozen soils from surface area measurements, Highway Research Record No. 393, National Acad. of Science - National Research Council, Washington, D.C. pp. 12-18.

Carslaw, H. S. and J. C. Jaeger, 1959. Conduction of heat in solids, 2nd edition, Clarendon Press, Oxford.

DeVries, D. A., 1952. Het Warmtegeleidingsvermejen van Grond (The thermal conductivity of soil). Madedelingen van de Landouwhogeschool te Wageningen, Vol. 52, No. 1, pp. 1-73, Transl. U.K., DSIR, Building Research Station Library Communication 759.

Gardner, W. R., 1958. Some steady-state solutions of the unsaturated moisture flow equation with application to evaporation from a water table, Soil Sci, 85, pp. 228-232.

Goodrich, T. E., 1973. Computer simulation, in Proceedings of the Second International Conference on Permafrost, Yakutak, U.S.S.R., National Acad. of Science, Washington, D.C.

Goodrich, T. E., 1978. Efficient numerical technique for one-dimensional thermal problems with phase change, Int. J. Heat and Mass Transfer, 21, pp. 615-621.

Gosink, J. P., T. E. Osterkamp and P. Hoffman, 1983. Modeling of ice covered lakes, Poster session presented at Frontiers in Hydrology Specialty Conference of ASCE, M.I.T., Cambridge, Mass.

Guymon, G. L., R. L. Berg, T. C. Johnson and T. V. Hromadka II, no date. Mathematical model of frost heave in pavements. Unpublished preliminary report prepared for Cold Regions Research and Engineering Laboratory, Hanover, N.H.

Guymon, G. T., M. E. Harr, R. T. Berg and T. V. Hromadka II, 1981. A probabilistic deterministic analysis of one-dimensional ice segregation in a freezing soil column, Cold Regions Science and Technology, 5, pp. 127-140.

Guymon, G. T. and T. V. Hromadka, II, 1977. Finite element model of transient heat conduction with isothermal phase change (two- and three-dimensional), U.S. Army Cold Regions Research and Engineering Laboratory, Special Report 77-38.

Guymon, G. T., T. V. Hromadka II, and R. J. Berg, 1980. A one-dimensional frost heave model based upon simulation of simultaneous heat and water flux, Cold Regions Sci. Technol., 3, (2+3): pp. 253-262.

Guymon, G. T. and J. N. Luthin, 1974. A coupled heat and moisture transport model for Arctic soils, Water Resources Research, 10(5), pp. 995-1001.

Hromadka II, T. V. and G. T. Guymon, 1980. Some approaches to modeling phase change in freezing soils, Cold Regions Science and Tech., 4, pp. 137-145.

Hromadka, T. V., G. L. Guymon and R. L. Berg, 1981. Some approaches to modeling phase change in freezing soils, Cold Regions Science and Tech., 4, pp. 137-145.

Jame, Y.-W., 1978. Heat and mass transfer in freezing unsaturated soil, Ph.D. dissertation, Univ. of Saskatchewan, Saskatoon, Canada.

Kawasaki, K., T. E. Osterkamp and J. P. Gosink, 1982. A preliminary evaluation of numerical models suitable for thermal analysis of roadways and airstrips, Report No. AK-RD-82-22, State of Alaska, Dept. of Transportation and Public Facilities.

Kersten, M. S., 1949. Laboratory research for the determination of the thermal properties of soils, Final Report, Eng. Exp. Station, Univ. of Minnesota, Minneapolis.

Osterkamp, T. E., 1984. Potential impact of a warmer climate on permafrost in Alaska, Proceedings of a Conference in the Potential Effects of Carbon Dioxide-induced Climate Changes in Alaska, Misc. Publ. 83-1, School of Agriculture and Land Resources Management, Univ. of Alaska, Fairbanks, Alaska.

Pinder, G. F. and W. G. Gray, 1977. Finite element simulation in surface and subsurface hydrology, Academic Press.

Smith, I. M., 1982. Programming the finite element method with application to geomechanics, John Wiley and Sons.

Taylor, G. S. and J. N. Luthin, 1978. A model for coupled heat and moisture transfer during soil freezing, Canadian Geotechnical Journal, 15, pp. 548-555.

Zarling, J. P., B. Connor and D. J. Goering, 1984. Air duct systems for roadway stabilization over permafrost areas, Final Report, State of Alaska DOTPS, Division of Planning, Fairbanks, Alaska 99701-6394.

ACKNOWLEDGEMENTS

We are grateful to G. Guymon of the University of California, Irvine and L. Goodrich of the Division of Buildings Research, National Research Council, Canada, for providing us copies of their programs and for also providing assistance in implementing them. We are also grateful to B. Connor and D. Esch of the Research Section, Alaska Department of Transportation and Public Facilities (ADOTPF) for providing data against which the analytical and numerical models were checked. This work was supported by ADOTPF under Agreement 82IP361.

APPENDIX A

APPENDIX A

Informal comments on the computer models

1. FROST2A and FROST2B

These are two versions of the same program for two-dimensional coupled heat and moisture transport in freezing soil. FROST2B is a more recent and slightly improved version, including an apparent heat capacity approximation to better define frozen and unfrozen regions. The latter alterations, less than about 10 program statements, are contained wholly in the subroutine PHASE. Other differences are minor, dealing primarily with input format. For these reasons all computer simulations were done with FROST2B.

In a general sense, FROST2B is "user-friendly". There is a fair amount of documentation in the form of comments and subroutine descriptions. The structure is modular and well-thought out, containing eight logically divided subroutines. Input and output are particularly well handled, with both input and output file assignments set internally within the program (by "open" statements), obviating the need for users to "assign" these files. However, there are several confusing aspects of the model, some minor and easily changed by the user, and others more intrinsically complex.

Probably the single most significant feature of the Guymon model is that convective moisture transport is included in the model. This feature is critical, allowing the physical thermodynamics to be more realistically simulated, and providing the capability for easily incorporating currently-accepted models of moisture migration. However, the inclusion of the moisture transport equation implies the introduction of complex input data into the numerical model.

Another problem is related to the presence of the moisture migration equation. In its present form, the Guymon model will not easily permit

solution of the heat transport equation alone with phase change and with zero moisture transport. That is, if phase change takes place, the moisture migration equation must also be solved, which implies the setting of sometimes poorly known pore pressure boundary conditions. However, the converse argument could be made. If freezing takes place, then pore pressure gradient and moisture migration are important and the equation should be solved, and, our inexact knowledge of the appropriate boundary conditions merely emphasizes the importance of further studies related to moisture transport in a freezing soil.

Another problem or deficiency with the Guymon model is its inability to handle non-zero surface or boundary flux conditions. This modification, however, can be rather easily made.

Other minor problems with the model are related to some confusing notation including:

i.) LENSIM appears to be the time extent of the simulation, but is not; instead it is the total number of updates of boundary conditions; ii.) the same symbols (XL and CAP), used for thermal conductivity and volumetric heat capacity in the heat transport equation, are also used as hydraulic conductivity and effective specific yield. Finally, it should be noted that the units used throughout the model are cal, cm, hr and C. This must be emphasized since the empirical coefficients, A_θ and A_k, are dimensional, with the precise dimensions determined by the empirically determined exponents n_θ and n_k (see eq. 4 and 5 in Guymon and Luthin, 1974).

2. PROTOØ, PROTOØA and PROTOØB

These are interactive data file preparation programs designed to compile the input files for the main programs, FROST2A and FROST2B. In brief, we do not recommend their use. However, due to the unavailability

of documentation for the main programs and for input file preparation, they do serve as useful references for input order, nomenclature, and dimension.

The PROTO* family of programs open a data file called FRST.DAT, the input data for either main program FROST2A or FROST2B. When PROTO* is run, a series of questions are asked of the user, the answers to which are ordered by PROTO* and set into the file FRST.DAT. It seems to be simpler for the user to compose FRST.DAT directly by typing the proper input. Furthermore, large input files for finite element programs are almost always put together sequentially as data becomes available. With PROTO*, if a response is not given to all questions, the complete data file may be lost, necessitating another tedious step-through PROTO*. Other advantages of directly composing FRST.DAT over using PROTO* include the fact that maximum advantage can be made of recurrent data and that some programming can be used to generate portions of the grid or initial conditions.

Because neither a test case nor data file nor data directions were available when this project began, we used the PROTO* listing extensively to clarify input data order, nomenclature and dimension. To eliminate this problem for future users of FROST2B, section 3 of this Appendix contains data directions for the composing of FRST.DAT.

3. FRST.DAT

As previously stated, FRST.DAT is assigned to FROST2B internally via "open" statements. The output file is also assigned internally by FROST2B to FRST.RES by "open" statements, allowing users to check the program results in the most recent version of FRST.RES at any time.

Data is read into FROST2B in free format, simplifying input file preparation. In the following synopsis of the input data, we will use the dollar sign ($) at the left margin to denote individual data lines rather than explanation.

$ XNETA

XNETA is a weighting factor on the capacitance matrix. (2 = Galerkin; 3.14 = subdomain integration; infinity = integrated finite difference). Galerkin, 2, is the recommended value in Hromadka and Guymon (1980) and adopted in these test cases.

$ DELT NUPDAT LENSIM NOUT

DELT is the length of a time increment in hours, e.g., 24, but should depend on how fast the boundary conditions are changing. DELT should be a small fraction of the total time period for sinusoidal boundary conditions.
NUPDAT is the number of DELT intervals until boundary conditions are updated, possibly 2-30 depending on how fast boundary conditions are changing. Note that if boundary conditions don't change at all, NUPDAT should equal the total number of hours in the simulation divided by DELT.
LENSIM is the total number of update intervals in the simulation. Therefore, LENSIM should equal the total number of hours in the simulation divided by the product of DELT and NUPDAT.
NOUT is the number of update intervals between outputs. If only a final output is desired, then NOUT should equal LENSIM.

$ NPATHI IPHASE KOLD

NPATHI controls which equations are solved. If = 0, both heat and moisture are solved. If = 1, heat transport only. If = 2, moisture transport only.
IPHASE controls phase change option. If = 1, the subroutine Phase is called and the so called "isothermal" phase change model is implemented (see Hromadka, Guymon and Berg, 1981). If = 0, no phase change can occur.
KOLD is an output directive such that if = 0, double output is printed including both old and new temperatures and pressures; if = 1, normal output is printed. KOLD = 1 is satisfactory in almost all cases.

$ TFPD CW CI TKW TKI XL

TFPD is the freezing point depression, usually 0.0 C.
CW is the volumetric heat capacity of water, and equals 1.0 cal cm^{-3} C^{-1}.
CI is volumetric heat capacity of ice, and equals 0.46 cal cm^{-3} C^{-1}.
TKW is the thermal conductivity of water, and equals 4.8 cal cm^{-1} hr^{-1} C^{-1}.
TKI is the thermal conductivity of ice, and equals 19.0 cal cm^{-1} hr^{-1} C^{-1}.
XL is the latent heat of fusion of ice, and equals 80.0 cal cm^{-3}.

$ NNBCT NNBCP

NNBCT is the number of boundary nodes which have prescribed temperatures. (This does not include those nodes with prescribed zero heat flux).
NNBCP is the number of boundary nodes with prescribed pore pressures. (This does not include those nodes with prescribed zero moisture flux).

$ NNOD NEL NEPG NNPG

NNOD is the total number of nodes.
NEL is the total number of triangular elements.

NEPG is the number of element parameter groupings, i.e., the number of groups of elements in which soil properties (including soil thermal conductivity, heat capacity, saturated hydraulic conductivity, and the so-called Gardner coefficients, - n_k, A_k and E) are constant and uniform. If these properties are uniform throughout the soil, then NEPG will equal one.
NNPG is the number of nodal parameter groupings, i.e., the number of groups of nodes at which soil moisture properties (including porosity, Gardner-type coefficients - A_θ and n_θ, residual volumetric water content, and soil heat capacity) are constant and uniform. If these properties are uniform throughout the soil, then NNPG will equal one.

```
$ PARNOD(1,1)   PARNOD(1,2)   PARNOD(1,3)   PARNOD(1,4)   PARNOD(1,5)
$ PARNOD(2,1)   PARNOD(2,2)   PARNOD(2,3)   PARNOD(2,4)   PARNOD(2,5)
$.....................................................................
$.....................................................................
```

The number of lines for PARNOD entries depends upon the available version of FROST2B. Originally FROST2B read in exactly 10 lines assuming 10 or less nodal groupings (with blanks or zeros in the unused lines). The present version was changed to read in exactly NNPG lines.
PARNOD(J,1) is the porosity or saturated volumetric moisture content of the soil in cm^3 cm^{-3}. This can be determined from the void ratio, e, listed in Appendix B since porosity = e/(1+e).
PARNOD(J,2) is A_θ, the multiplier of pressure head in Gardner's moisture function. This is listed in Appendix B.
PARNOD(J,3) is n_θ, the exponent of pressure head in Gardner's moisture function. This is listed in Appendix B.
PARNOD(J,4) is the residual volumetric water content or the fraction of water which is not available for phase change. When the moisture transport equation is solved (if NPATHI = 0 or 2), PARNOD(J,4) must not equal 0.0, but it may be set to some very small number.
PARNOD(J,5) is the volumetric heat capacity of the dry soil in cal $cm^{-3}C^{-1}$.

```
$ PARELE(1,1)   PARELE(1,2)   PARELE(1,3)   PARELE(1,4)   PARELE(1,5)   PARELE(1,6)
$ PARELE(2,1)   PARELE(2,2)   PARELE(2,3)   PARELE(2,4)   PARELE(2,5)   PARELE(2,6)
$.....................................................................
$.....................................................................
```

The number of lines for PARELE entries depends upon the available version of FROST2B. Originally FROST2B read in exactly 10 lines assuming 10 or less element groupings (with blanks or zeros in the unused lines). The present version was changed to read in exactly NEPG lines.
PARELE(J,1) is the dry soil thermal conductivity in cal hr^{-1} cm^{-1} C^{-1}.
PARELE(J,2) is the volumetric heat capacity of dry soil in cal $cm^{-3}C^{-1}$. This entry may be numerically the same as PARNOD(J,5), or it may permit a heat capacity variation to occur at this element position.
PARELE(J,3) is the saturated hydraulic conductivity in cm hr^{-1}. This is listed in Appendix B for various soils.
PARELE(J,4) is n_k, the exponent of pressure head in Gardner's function for hydraulic conductivity. This is listed in Appendix B.
PARELE(J,5) is A_k, the coefficient of pressure head in Gardner's function for hydraulic conductivity. This is listed in Appendix B.
PARELE(J,6) is E, the hydraulic conductivity adjustment factor for ice formation (see eq. 8 in Guymon, Berg, Johnson and Hromadka). This parameter must be obtained by model calibration.

```
$ DATNOD(1,1)   DATNOD(1,2)   DATNOD(1,3)
$ DATNOD(2,1)   DATNOD(2,2)   DATNOD(2,3)
$.....
$.....
```

The number of lines for DATNOD entries depends upon the available version of FROST2B. Originally FROST2B always read in 90 lines of DATNOD (the maximum node dimension). The present version was changed to read in precisely NNOD lines.
DATNOD(J,1) is the x location of node J (in cm)
DATNOD(J,2) is the y location of node J (in cm)
Note that y normally should increase in the opposite direction from pore pressure; consequently, the bottom-most soil boundary should be defined as y = 0, with y increasing upward.
DATNOD(J,3) is the nodal parameter group number - a particular group of nodes with uniform soil moisture properties.

```
$ IDTELE(1,1)   IDTELE(1,2)   IDTELE(1,3)   IDTELE(1,4)
$ IDTELE(2,1)   IDTELE(2,2)   IDTELE(2,3)   IDTELE(2,4)
$.....
$.....
```

The number of lines for IDTELE entries depends upon the available version of FROST2B. Originally FROST2B always read in 150 lines of IDTELE (the maximum element dimension). The present version was changed to read in exactly NEL lines.
IDTELE(J,1) is a node number of any node in the Jth element.
IDTELE(J,2) is the next node number of the Jth element, progressing counterclockwise.
IDTELE(J,3) is the final node number of the Jth element, progressing counterclockwise.
IDTELE(J,4) is the element parameter group number - a particular group of elements with the same soil properties.

```
$ TOLD(1)   POLD(1)   XICEOL(1)
$ TOLD(2)   POLD(2)   XICEOL(2)
$.....
$.....
```

These are the initial conditions at each node. Again, the older version of FROST2B reads 90 lines, while the modified version reads exactly NNOD lines.
TOLD(J) is the initial temperature array in C.
POLD(J) is the initial pore pressure array in cm. For example, for level, saturated soil with no overburden, the value of POLD would equal the depth.
XICEOL(J) is the initial volumetric ice content array in $cm^3\ cm^{-3}$.

```
$ NBCT(1)  BCT(1,1)  BCT(1,2)  BCT(1,3)  BCT(1,4)
$ NBCT(2)  BCT(2,1)  BCT(2,2)  BCT(2,3)  BCT(2,4)
$.....
$.....
```

These are the temperature boundary conditions. There will be either 35 or NBCT lines, depending on the FROST2B version.
NBCT(J) is the node number for a prescribed temperature. The temperature is prescribed as a sinusoidal function of time according to the formula
$T = (A+B)/2 + ((A-B)/2)\ \sin(2\pi(t+\theta)/TP)$;
BCT(J,1) = A = maximum temperature on the sine curve in C.
BCT(J,2) = B = minimum temperature on the sine curve in C.

BCT(J,3) = TP = period in hours of the temperature cycle.
BCT(J,4) = θ = phase shift in hours of the temperature cycle.
Note: 1) BCT(J,3) must not be set to zero, even if constant boundary temperatures are prescribed, 2) if a constant temperature is needed, simply set A = B.

```
$ NBCP(1)   BCP(1,1)   BCP(1,2)   BCP(1,3)   BCP(1,4)
$ NBCP(2)   BCP(2,1)   BCP(2,2)   BCP(2,3)   BCP(2,4)
$.....
$.....
```

These are the pore pressure boundary conditions. There will be either 35 or NBCP lines, depending on the FROST2B version. NBCP(J) is the node number for a prescribed pressure. The pressure is prescribed as a sinusoidal function of time according to the formula $P = (A+B)/2 + ((A-B)/2)\sin(2\pi(t+\theta)/TP)$;
BCP(J,1) = A = maximum pore pressure on the sine curve in cm.
BCP(J,2) = B = minimum pore pressure on the sine curve in cm.
BCP(J,3) = TP = period in hours of the pore pressure cycle.
BCP(J,4) = θ = phase shift in hours of the pore pressure cycle.
Note: 1) BCP(J,3) must not be set to zero, 2) if a constant pore pressure is needed, simply set A = B.

A P P E N D I X B

SOIL NUMBER	MOISTURE CHARACTERISTICS A	n	R	AVERAGE ABSOLUTE ERROR	UNSATURATED HYDRAULIC CONDUCTIVITY A	n	R	AVERAGE ABSOLUTE ERROR
GRAVELS								
DGS-HP	0.883E-02	0.665	0.998	0.002				
DGS-1	0.717	0.195	0.924	0.005				
DGS-2	1.321	0.166	0.956	0.003	2.681	1.026	0.997	0.000+
ASE-A1	0.171	0.255	0.969	0.003	0.404E-01	2.200	0.934	0.015
WLMH-1	0.668E-01	0.556	0.962	0.008	0.674E-04	2.861	0.989	0.008
AD-1	0.128	0.486	0.985	0.004	0.843E-03	2.462	0.969	0.011
SANDS & SILTY SANDS								
MFS-1	0.1411E-01	0.959	0.943	0.018				
MFS-2	0.289E-02	1.262	0.930	0.024				
MFS-3	0.449E-01	0.886	0.961	0.015	0.108E-03	3.576	0.994	0.026
SPLC-1	0.373E-04	1.548	0.976	0.014				
SPLC-2	0.693E-03	1.188	0.852	0.025				
SPLC-3	0.401E-03	1.283	0.951	0.023				
SPLC-4	0.318E-03	1.353	0.933	0.030				
SPLC-5	0.101E-02	1.200	0.929	0.026				
SPLC-6	0.189E-02	0.971	0.986	0.016				
SBI-HP	0.291E-02	0.618	0.846	0.014				
SBI-1	0.276E-02	0.824	0.967	0.011				
SBI-2	0.786E-01	0.576	0.973	0.006	0.598E-03	3.085	0.966	0.012
SBI-3	0.693E-02	0.667	0.962	0.006	0.184E-03	2.772	0.969	0.004
GSS-HP	0.392E-02	0.824	0.922	0.036				
GSS-1	0.307E-03	1.259	0.920	0.032				
GSS-2	0.353E-04	1.748	0.929	0.037	0.810E-03	2.536	0.940	0.061
HYS-HP	0.597E-03	1.292	0.859	0.040				
HYS-1	0.455E-02	1.123	0.961	0.017				
HYS-2	0.329E-03	1.728	0.972	0.023	0.521E-04	3.709	0.983	0.204
HBS-HP	0.751E-01	0.965	0.948	0.022				
HBS-1	0.345E-01	0.748	0.975	0.008				
HBS-2	0.594E-01	0.696	0.895	0.023	0.582E-05	5.591	0.977	0.121

DVI-1-B	0.7851-02	0.665	0.962	0.013				
DVI19-24	0.1261-01	0.559	0.979	0.007				
DVI21-9	0.1161-03	1.287	0.992	0.004				
DVI21-0	0.2181-04	1.708	0.979	0.015				
LNBS-HP	0.1051-01	0.851	0.864	0.043				
LNBS-1	0.1111-02	1.422	0.947	0.025				
ASG-B1	0.1751-02	1.236	0.874	0.035	0.843E-03	2.777	0.989	0.014
IKI-HP	0.4261-02	0.939	0.946	0.027				
IKI-1	0.1711-03	1.654	0.942	0.024				
IKI-2	0.2421-04	2.013	0.985	0.010	0.1061-07	4.059	0.941	0.045
CH-A	0.1491-03	1.063	0.978	0.014				
CH-B	0.3441-04	1.605	0.972	0.029				
CH-C	0.5461-05	1.856	0.959	0.019				
WR-A	0.7641-03	1.191	0.887	0.036				
WR-B	0.3691-01	0.520	0.998	0.002				
WR-C	0..0bE-01	0.794	0.994	0.002				
IGK B-1	0.1521-02	1.307	0.923	0.017				
IGK B-2	0.3641-02	1.109	0.784	0.034				

CARDNER COEFFICIENTS FOR SOILS

CIS-1	0.699E-03	1.263	0.953	0.029				
CRG-1	0.780E-01	0.641	0.944	0.012				
DV32-23	0.197E-02	1.147	0.961	0.023				
DV32-33	0.139E-02	1.168	0.976	0.013				
DV32-16	0.312E-03	1.452	0.699	0.050				
DV32-8	0.190E-01	0.735	0.971	0.023				
DV31-6-1	0.121E-01	0.689	0.984	0.016				
DV32-6-2	0.462E-02	0.818	0.961	0.025				
LNH-SB	0.720E-01	0.631	0.998	0.002				
LNH-SG	0.119E-04	1.861	0.968	0.021				
STS	0.263E-02	1.007	0.960	0.015				
			SILTS					
NHS-1	0.461E-06	2.351	0.935	0.039				
NHS-2	0.352E-04	1.649	0.976	0.018				
NHS-3	0.693E-06	2.206	0.951	0.022				
NHS-4	0.860E-06	2.122	0.947	0.021				
NHS-5	0.297E-03	1.263	0.969	0.020				
NHS-6	0.558E-06	2.192	0.962	0.020	0.248E-06	3.015	0.921	0.036
FORKS-UP	0.402E-02	0.711	0.962	0.025				
FORKS-1	0.933E-04	1.449	0.986	0.012				
FORKS-2	0.547E-02	0.744	0.996	0.004				
FORKS-3	0.505E-02	0.782	0.990	0.006	0.583E-02	1.559	0.965	0.002

MPS-HP	0.172E-02	0.866	0.989	0.020				
MPS-1	0.947E-06	2.089	0.978	0.015				
MPS-2	0.927E-06	1.888	0.848	0.039				
MPS-3	0.209E-05	1.644	0.741	0.044				
MPS-4	0.987E-06	1.814	0.857	0.038				
MPS-5	0.420E-06	2.116	0.872	0.039	0.926E-07	2.996	0.847	0.035
DVT19-5	0.575E-03	1.224	0.965	0.027				
DVT10-3	0.368E-02	0.940	0.948	0.028				
DVT10-24	0.139E-02	1.142	0.960	0.022				
DVT17-18	0.668E-02	0.636	0.995	0.003				
DVT17-0	0.246E-01	0.529	0.999	0.001				
DVT17-6	0.135E-01	0.537	0.996	0.003				
AVM	0.515E-01	0.356	0.986	0.005				
CS7-1	0.452E-03	1.219	0.827	0.041				
CS7-2	0.113E-04	1.779	0.991	0.015				
CS7-3	0.186E-04	1.726	0.978	0.021				
CS8-1	0.503E-03	1.114	0.798	0.047				
CS8-2	0.333E-03	1.212	0.986	0.011				
CS8-3	0.636E-05	1.907	0.970	0.033				
CS9-1	0.390E-03	1.223	0.991	0.008				
CS9-2	0.290E-03	1.267	0.994	0.008				
CS9-3	0.452E-03	1.256	0.992	0.013				
CHSS-HP	0.353E-04	1.219	0.945	0.032				
CHSS-1	0.166E-04	1.532	0.991	0.010				
CHSS-2	0.485E-05	1.684	0.964	0.008				
CHSS-3	0.274E-05	1.737	0.893	0.013	0.145E-03	1.046	0.962	0.001
CHSS-4	0.679E-05	1.739	0.995	0.011	0.973E-03	1.835	0.945	0.005
CHSS-5	0.115E-05	2.082	0.933	0.014	0.104E-03	2.224	0.964	0.005

OMS-1	0.134E-03	1.423	0.996	0.007				
OMS-2	0.151E-04	1.697	0.989	0.009				
HNVS-1	0.977E-04	1.550	0.975	0.027				
HNVS-2	0.983E-06	2.180	0.928	0.036				
HNVS-3	0.52HE-05	1.860	0.975	0.018				
HNVS-4	0.605E-04	1.399	0.996	0.006				
JSS-1	0.306E-04	1.730	0.929	0.044				
JSS-2	0.117E-04	1.837	0.945	0.038				
JSS-3	0.345E-05	1.940	0.954	0.026				
JSS-4	0.767E-05	1.749	0.965	0.017				
DV32-12	0.174E-04	1.863	0.913	0.067				
DV32-5	0.540E-02	0.901	0.954	0.036				
SSS	0.382E-03	1.205	0.820	0.031				

CLAYS

BHD-12	0.497E-02	0.779	0.990	0.009				
BHD-5	0.316E-02	0.928	0.989	0.012				
AVM-10	0.165E-01	0.597	0.986	0.009				
AVM-24	0.403E-01	0.465	0.999	0.001				
MCL-HP	0.250E-02	0.608	0.974	0.013				
MCL-1	0.460E-04	1.206	0.978	0.005				
MCL-2	0.500E-03	0.966	0.992	0.003	0.145E-02	1.760	0.987	0.000
SL 11-0	0.154E-01	0.435	0.935	0.038				

SL 11-10	0.484E-01	0.332	0.971	0.006
SL 11-24	0.194E-01	0.435	0.977	0.007
SL 12-24	0.331E-02	0.779	0.964	0.012
SL 12-29	0.664E-03	1.012	0.944	0.017
SL 12-8	0.216E-02	0.681	0.985	0.006
SL 12-13	0.983E-02	0.483	0.868	0.012
SL 12-19	0.261E-01	0.458	0.995	0.004
DC0-7	0.762E-01	0.257	0.884	0.010
DC0-14	0.660E-01	0.258	0.975	0.005
DC0-0	0.226E-01	0.526	0.987	0.008
DC0-5	0.219E-02	0.786	0.971	0.009
DC0-6	0.879E-03	0.779	0.965	0.006
DC0-14	0.909E-02	0.490	0.979	0.003
DC0-24	0.200E-01	0.432	0.997	0.001
DC0-34	0.997E-02	0.469	0.984	0.002

GARDNER COEFFICIENTS FOR SOILS

NOTES: GARDNER COEFFICIENTS IN Y=P/(A*X**n+1)

WHERE P=POROSITY OR SATURATED PERMEABILITY(cm/hr)

X=PORE WATER PRESSURE(TENSION)(cm of H20)

Y=VOLUMETRIC WATER CONTENT(decimal fraction) OR HYDRAULIC CONDUCTIVITY(cm/hr)

REGRESSIONS ARE FOR DRYING CURVES

HP=HIGH PRESSURE CELL

R=REGRESSION COEFFICIENT

AVERAGE ABSOLUTE ERROR=SUM(ABS(Yglven-Ycomputed))/(NUMBER OF DATA POINTS)

SUMMARY OF SOIL PROPERTIES

SOIL NUMBER	MATERIAL & SOURCE	PROCEDURE USED	MAX. SIZE MM	D60	D10	PERCENT PASSING INDICATED SIEVE 4.76 MM	0.42 MM	.074 MM	.02 MM	.01 MM	.005 MM	CU	G	UNIF. SOIL SYM.	FROST SUSC. CLASS	FROST GROUP	DRY UNIT WT.	VOID RATIO E	PERM SAT. CM/H
GRAVELS																			
S-1	DENSE GRAD STONE	V.P.	13	5	.19	56	17	9	6	5	3	50	2.60	GW	L-M	F-1	1.94	.443	
S-2	MASS.	P.P.															1.86	.506	5.5
B-A1	SUB-BASE A N.Y.	P.P.	50	2.0	.04	70	37	11	8	7	5	70	2.72	GM	L-M	F-1	2.16	.259	2.8
NH-1	DIRTY GRAV LEB. NH	P.P.	19	6	.0-	15	25	11	5	3	2	100	2.75	GM	VL-M	F-1	1.99	.382	.46
-1	BASE A CR STONE NY.	P.P.	4.	10	.03	18	26	12	9	7	4	333	2.71	GP	L-M	F-1	2.16	.255	1.1
SAND & SILTY-SAND																			
S-1	FINE SAND MANCH. NH	T.C.	.6	.21	.083	100	91	3	0	0	0	2.5	2.69	SP	NFS.	0	1.56	.712	
S-2		V.P.															1.55	.736	
S-3		P.P.															1.48	.810	18.3
EC-1	SPECIAL TEST SAND	T.C.	13	.35	.017	95	64	32	12	7	2	20.6	2.72	SM	VL-M	F-2	1.60	.700	
EC-2	HANOVER	T.C.															1.68	.619	
EC-3	N.H.	T.C.															1.76	.546	
EC-4		T.C.															1.84	.479	
EC-5		T.C.															1.92	.417	
EC-6		V.P.															1.84	.479	
T-1	SILTY TILL MASS	V.P.	13	.26	.001	9	75	41	24	20	15	200	2.75	SM	L-M	F-4	1.97	.396	
T-2	GLACIAL TILL	P.P.															1.89	.455	1.5
T-3		P.P.															2.07	.328	.24
S-1	GRAVELS SILTY SAND	V.P.	2	.12	.015	100	99	44	14	8	5	9.2	2.73	SM	VL-M	F-2	1.58	.728	
S-2	MASS.	P.P.															1.49	.832	1.92
S-1	HYANNIS SAND	V.P.	5	.25	.005	97	76	21	4	1	0	7.1	2.67	SM	M-H	F-2	1.65	.619	
S-2	MASS.	P.P.															1.49	.580	1.3

S-1	HART BROS. SANDS MASS.	V.P. P.P.	5	.18	.07	99	91	25	4	3	2	2.7	2.78	SM	VL-M	F-2	1.76 1.75	.580 .607	4.0
T 1-C	DANVILLE VT.	V.P.	2	.30	.023	93	65	32	8	[illegible]	3	13.0	2.74	SM	VL-M	F-2	1.25	1.192	
T19-24	DANVILLE VT.	V.P.	2	.21	.018	100	70	41	12	[illegible]	3	11.7	2.75	SM	VL-M	F-2	1.84	.495	
T21-9	DANVILLE VT.	V.P.	2	.11	.02	100	99	48	10	4	2	5	2.78	SM	VL-M	F-2	1.68	.655	
T21-0	DANVILLE VT.	V.P.	2	.25	.03	100	89	29	6	3	2	6.7	2.76	SM	N-M	F-2	1.61	.715	
HS-1	BANK RUN SAND LEB.	V.P.	2	.18	.07	100	86	12	3	2	1	2.6	2.73	SW-SM	N-M	F-2	1.54	.773	
G-P1	SUB GRADE B ALBANY NY	P.P.	2	.15	.06	100	99	14	3	1	0	2.5	2.71	SM	N-M	F-2	1.67	.623	2.4
E-1 L-2	IKELANIAN SAND MASS.	V.P. P.P.	3	.15	.032	100	87	34	6	2	1	4.7	2.66	SM	N-M	F-2	1.61 1.70	.664 .577	.77
-A	CHARLTON A HANOVER NH	T.C.	5	.15	.006	99	74	47	25	15	8	25	2.63	SM	VL-M	F-3	1.3	1.024	.13
-B	CHARLTON B HANOVER NH	T.C.	5	.17	.008	99	74	46	22	13	7	21	2.64	SM	VL-M	F-3	1.30	1.070	2.8
-C	CHARLTON C HANOVER NH	T.C.	5	.20	.005	100	72	42	20	11	6	22	2.70	SM	VL-M	F-3	1.57	.720	.6
-A	WINDSOR A LEB NH	T.C.	2	.34	.044	100	69	14	5	3	2	7.7	2.63	SM	N-M	F-2	1.54	.707	.14
-B	WINDSOR B LEB. NH	T.C.	2	.41	.05	100	62	15	4	2	1	8	2.64	SM	N-M	F-2	1.47	.831	18

-C	LINDSOR C LEB. NH	T.C.	2	.18	.036	100	82	32	4	2	1	5.3	2.73	SM	N-H	F-2	1.43	.909 18
P-1	INIGOK BORROW ALASKA	T.C.	.7	.17	.07	100	99	11	3	2	1	2.4	2.66	SP-SM	N-L	F-2	1.69	.574
B-2		T.C.															1.68	.583
1-1	INIGOK BORROW ALASKA	T.C.	.05	.23	.098	100	94	5	1	1	0	2.3	2.66	SP	NFS		1.67	.593
1-2		T.C.															1.68	.583
S-1	CHENA TOP SOIL AK	T.C.	15	.18	.012	56	88	36	13	6	3	15	2.65	SP	VL-H	F-2	1.54	.721
G-1	CHENA GRA. ALASKA	T.C.	4.8	.55	.056	100	68	13	4	3	2	6.3	2.71	SM	N-H	F-2	1.75	.548
32-33	W DOVER VT.	T.C.	30	.15	.078	96	84	41	7	4	2	5.4	2.78	SM	N-H	F-2	1.53	.818
32-33	W DOVER VT.	T.C.	25	.22	.03	94	77	27	5	3	2	7.3	2.79	SM	N-H	F-2	1.80	.550
32-16	W DOVER VT.	T.C.	7	.13	.018	98	88	44	11	7	4	7.2	2.75	SM	VL-H	F-2	1.29	1.132
32-8	W DOVER VT.	T.C.	4.8	.11	.02	99	91	48	13	7	4	5.5	2.64	SM	VL-H	F-2	.61	2.196
1-6-1	W DOVER VT.	T.C.	4.8	.12	.014	100	94	46	13	6	2	7.5	2.66	SM	VL-H	F-2	.84	2.16
1-6-2		T.C.															.69	2.85
-SB	LEB AIRPORT SUB BASE	T.C.	40	1	.1	85	28	5	2	2	1	5.6	2.76	SW	NFS	0	1.78	.551
-SG	LEB AIRPORT SUB GRADE	T.C.	5	.4	.036	95	62	35	14	10	5	44	2.74	SM	L-H	F-4	1.90	.442
	SIERRETT TOP SOIL	V.P.	3	.15	.015	100	96	39	25	16	8	30	2.65	SM-SC	L-H	F-4	1.60	.656

SILT

	MANCHESTER		.15	.015	.006	104	100	58	52	21	8	4.2	2.73	ML	L-VH	F-A	1.36 1.015
S-1	N.H.	T.C.															1.44 .902
S-2	SILT	T.C.															1.52 .802
S-3		T.C.															1.60 .712
S-4		T.C.															1.30 1.10
S-5		V.P.															1.45 .883 .32
S-6		P.P.															
	FAIRBANKS		.47	.038	.0042	100	99	94	33	15	11	9.0	2.73	ML	L-M	F-A	1.56 .751
KS-1	SILT	T.C.															1.69 .615
KS-2	FAIRBANKS	V.P.															1.62 .686 .042
KS-3	ALASKA	P.P.															
	MOULTON		.08	.016	.0039	100	100	99	74	40	18	8.4	2.62	ML	L-VH	F-A	1.33 1.067
S-1	PIT SILT	T.C.															1.49 .845
S-2	LEB NH	T.C.															1.55 .774
S-3		T.C.															1.50 .880
S-4		V.P.															1.35 1.037 .28
S-5		P.P.															
	DANVILLE		2	.07	.02	100	91	60	10	4	1	3.5	2.69	ML	VL-H	F-A	1.16 1.139
T19-5	VT.	V.P.															
	DANVILLE		2	.10	.02	100	92	48	13	2	0	5	2.59	ML-OL	VL-H	F-A	.95 1.721
T10-3	VT.	V.P.															
	DANVILLE		2	.10	.02	100	92	51	10	4	2	5	2.62	ML	VL-H	F-A	1.33 1.119
T10-24	VT.	V.P.															
	DANVILLE		15	.11	.02	97	82	53	13	5	4	5.5	2.74	ML	VL-H	F-A	1.43 .689
T17-18	VT.	V.P.															
	DANVILLE		10	.07	.02	97	85	55	14	7	2	5.5	2.61	ML	VL-H	F-A	1.02 1.550
T17-0	VT.	V.P.															
	DANVILLE		9	.01	.02	98	84	57	13	4	3	4	2.71	ML	VL-H	F-A	1.12 1.421
T17-6	VT.	V.P.															
	APPLE VAL-		2	.03	.005	100	94	84	43	28	18	10	2.59	OL	L-H	F-A	1.16 1.252
H-2	LEY NH	V.P.															
	CRREL SILT		5	.04	.007	100	94	78	25	13	7	6.9	2.65	ML	L-H	F-A	1.43 .880
T-1	HANOVER NH	T.C.															1.59 .935
T-2		T.C.															1.57 .964
T-3		V.P.															

-1	CARLL SILT HANOVER NH	T.C.	2	.05	.004	100	96	81	21	12	5	5.6	2.70	ML	L-H	F-4	1.48	.825
-2		I.C.															1.48	.825
-3		V.P.															1.42	.901
	CAREL SILT		2	.047	.01	100	96	81	21	10	4	4.7	2.71	ML	L-H	F-4		
-1	HANOVER NH	T.C.															1.45	.869
-2		I.C.															1.48	.831
-3		V.P.															1.38	.964
	CHENA HOT		.2	.027	.005	100	100	92	39	20	12	5.4	2.68	ML	L-VH	F-4		
S-1	SPRINGS	T.C.															1.57	.783	
S-2	AK SILT	V.P.															1.59	.761	
S-3		P.P.															1.62	.729	.017
S-4		P.P.															1.54	.817	.063
S-5		P.P.															1.49	.879	.07
	NW STANDARD		2	.03	.005	100	99	98	38	17	10	6	2.65	ML	L-VH	F-4		
-1	SILT AK	P.P.															1.42	.866	.26
	OTTAWA SAND		.15	.038	.0028	100	100	91	37	25	15	13.6	2.66	ML	L-H	F-4		
S-1		T.C.															1.40	.858	
S-2		T.C.															1.53	.700	
	HANOVER		.2	.032	.004	100	100	95	34	17	11	8	2.69	ML	L-H	F-4		
S-1	SILT	T.C.															1.30	1.07	
S-2	HANOVER NH	T.C.															1.46	.842	
S-3		T.C.															1.58	.703	
S-4		T.C.															1.67	.611	
	JENKS		.85	.018	.006	100	99	66	29	13	9	11	2.73	ML	VL-H	F-4		
-1	SANDY-SILT	T.C.															1.70	.606	
-2	VT.	T.C.															1.61	.695	
-3		T.C.															1.51	.808	
-4		T.C.															1.38	.979	
	W DOVER		5	.08	.016	99	92	57	11	7	4	4.4	2.65	ML	VL-H	F-4		
2-12	VT.	T.C.															1.15	1.304	
	W DOVER		4.8	.07	.011	103	94	62	24	19	15	76	2.72	ML	L-VH	F-4		
2-5	VT.	T.C.															.81	2.163	
	SIERRETT		.6	.19	.0005	100	97	53	45	17	30	200	2.69	ML-CL	L-VH	F-4		
5	SUB SOIL	V.P.															1.59	.692	

CLAY

	BELTSVILLE		.5	.03	.001	100	92	58	37	31	22	90	2.71	ML-CL	L-H	F-4		
012	MD.	V.P.															1.65	.642

D-5	BELTSVILLE MD.	V.P.	2	.15	.61	100	93	50	15	11	5	15	2.65	ML-CL	L-M	F-4	1.61	.645	
M-10	APPLE VALLEY MN.	V.P.	2	.023	.0022	100	96	90	50	30	17	8.7	2.64	CL	M-H	F-4	1.21	1.183	
M-24	APPLE VALLEY MN.	V.P.	5	.045	.0005	100	87	68	41	28	22	90	2.73	CL	L-H	F-4	1.53	.785	
L-1 L-2	MORIN CLAY	T.C. P.P.	.04	.0058	--	100	100	100	85	70	53	--	2.80	CL	L-H	F-3	1.74 1.56	.621 .795	.048
11-0	ST. LOUIS	T.C.	.4	.0045	--	100	100	98	85	73	61	900+	2.71	CL	L-H	F-3	1.57	.727	**
* 4.2 X (10 -4)																			4.2E-04
11-10	ST. LOUIS	T.C.	2	.02	--	100	96	77	61	51	43	900+	2.73	CL	L-H	F-3	1.53	.785	.025
11-24	ST. LOUIS	T.C.	2	.035	--	100	93	70	50	44	37	900+	2.72	CL	L-H	F-3	1.69	.61	.026
12-24	ST. LOUIS	T.C.	2	.02	.0001	100	90	78	61	41	30	200	2.72	CL	L-H	F-3	1.49	.825	.014
12-29	ST. LOUIS	T.C.	2	.04	.0002	100	93	71	50	40	31	260	2.69	CL	L-H	F-3	1.68	.601	.017
12-6	ST. LOUIS	T.C.	2	.02	--	100	97	82	69	48	36	900+	2.69	CL	L-H	F-3	1.37	.964	**
* 8.8 X (10 -4)																			
12-15	ST. LOUIS	T.C.	2	.096	--	100	99	97	90	70	56	900+	2.73	CL	L-H	F-3	1.44	.897	**
* 9.2 X (10 -4)																			
12-19	ST. LOUIS	T.C.	2	.015	--	100	98	87	69	50	37	900+	2.73	CL	L-H	F-3	1.51	.808	.054
CO-7	DEER CREEK OHIO	T.C.	2	.02	.0006	100	94	80	66	43	29	33	2.71	CL	L-H	F-3	1.67	.623	
CO-14	DEER CREEK OHIO	T.C.	5	.009	--	100	94	84	72	63	52	900+	2.72	CL	L-H	F-3	1.58	.972	

CO-0	DEER CREEK OHIO	T.C.	A	.04	.0005	100	84	71	51	38	26	60	2.67	CL	L-H	F-S	1.40	.908	
CO-3	DEER CREEK OHIO	T.C.	2	.022	.0005	100	92	76	57	41	28	44	2.67	CL	L-H	F-S	1.71	.562	
CO-6	DEER CREEK OHIO	T.C.	1*	.02	.0001	98	95	78	61	52	42	200	2.67	CL	L-H	F-S	1.57	.701	**
* 1.3 X (10 -4)																			
CO-14	DEER CREEK OHIO	T.C.	5 *	.035	.0001	100	84	72	52	44	37	350	2.73	CL	L-H	F-S	1.80	.517	.018
CO-24	DEER CREEK OHIO	T.C.	9	.09	.0007	95	76	58	41	32	23	128	2.74	CL	L-VH	F-S	1.82	.506	.05
CO-34	DEER CREEK OHIO	T.C.	19	.065	.0007	96	78	62	45	33	25	93	2.76	CL	L-VH	F-S	1.95	.415	.011

DIES:

G = SPECIFIC GRAVITY OF SOLIDS

CU = UNIFORMITY COEFFICIENT = D60/D10

D60 = GRAIN DIAMETER CORRESPONDING TO 60% FINER

D10 = GRAIN DIAMETER CORRESPONDING TO 10% FINER

UNIFIED SOIL SYMBOL = DETERMINED FROM GRAIN SIZE DISTRIBUTION AND VISUAL CLASSIFICATION ATTERBERG LIMITS NOT AVAILABLE FOR MOST SOILS

T.C. = TEMPE CELL

V.P. = VOLUMETER PLATE EXTRACTION

P.P. = PRESSURE CELL PERMEAMETER

PERM SAT. = SATURATED HYDRAULIC CONDUCTIVITY (PERMEABILITY